Subtype and pathway specific responses to anti-cancer compounds in breast cancer

Heiser, et al.

Supplementary Information

Association of growth rate and response to therapeutic agents

In general, we found that luminal subtype cell lines grew more slowly than basal or claudin-low cells (Kruskal-Wallis test $p = 0.006$, **Fig. S3A and Table S1**) and the range of doubling times was broad (18 to 300 hours). This raised the possibility that the most sensitive cell lines were those that grew most rapidly. We tested this hypothesis by assessing the effects of subtype and doubling time simultaneously with an ANCOVA (see details below) and found that 20 of 23 subtype-specific compounds had better associations with subtype than with doubling time (mean log ratio of *p*-values = 0.87, standard deviation 1.09). Moreover, 11 of 23 subtype-specific compounds were most effective in the most slowly growing luminal cell lines (**Table 1**). One agent, 5-fluorouracil, was not significant in the subtype test alone but showed strong significance in the ANCOVA model for both class and doubling time. (**Fig. S3B)**. We conclude that in most cases, the 3-day proliferation assay detects molecular signature-specific responses that are not strongly influenced by growth rate.

To assess the effects of cell line subtype and growth rate on drug sensitivity, we performed a set of 2-way analysis of covariance (ANCOVA) tests, one for each of the three cell line classification schemes: *i*) luminal vs. basal vs. claudin-low; *ii*) luminal vs. basal + claudin-low; and *iii*) $ERBB2^{AMP}$ vs. non-$ERBB2^{AMP}$. This yielded 6 sets of *p*-values (2 main effects x 3 classification schemes); we separately adjusted the two sets of main effect *p*-values for multiple comparisons. We used the R functions lm and Anova (available as part of the car package).

Integrated Pathway Analysis

Integration of copy number, gene expression and pathway interaction data was performed using the PARADIGM software(1). Briefly, this procedure infers integrated pathway levels (IPLs) for genes, complexes, and processes using pathway interactions and genomic and functional genomic data from a single cell line or patient sample. TCGA breast cancer data was obtained from the TCGA DCC on November 7, 2010. TCGA and cell line gene expression data were median probe centered within each data set separately. All of the values in each of these datasets (either the cell lines or TCGA tumor samples) were rank transformed and converted to –log10 rank ratios before supplying to PARADIGM. Pathways were obtained in BioPax Level 2 format on October 13, 2010 from http://pid.nci.nih.gov/ and included NCI-PID, Reactome, and BioCarta databases. Interactions were combined into a merged Superimposed Pathway (SuperPathway). Genes, complexes, and abstract processes (e.g. "cell cycle") were retained as pathway concepts. Before merging gene concepts, all gene identifiers were translated into HUGO nomenclature. All interactions were included and no attempt was made to resolve conflicting influences. A breadth-first undirected traversal starting from P53 (the most

connected component) was performed to build one single component. The resulting merged pathway structure contained a total of 8768 concepts representing 3491 proteins, 4757 complexes, and 520 processes. Expectation-Maximization parameters for PARADIGM were trained on the cell line data and then applied to the TCGA samples. Data from the cell lines and tumor samples were then combined into a single data matrix. Any entry without at least 1 value above 0.5 IPL in either the data from cell lines or tumor samples was removed from further analysis.

TCGA and cell line clustering

Using PARADIGM IPLs, cell lines were clustered together with TCGA tumor samples to determine if cell lines were similar to tumor samples of the same subtype. Well-studied areas of the SuperPathway contain genes with many interactions (hubs) and large signaling chains of many intermediate complexes and abstract processes for which no direct data is available. To avoid bias toward due to the presence of hubs, pathway concepts with highly correlated vectors (Pearson correlation coefficient > 0.9) across both the cell line and tumor samples were unified into a single vector prior to clustering. This unification resulted in 2351 non-redundant vectors from the original 8768 pathway concepts.

Samples were clustered using the resulting set of non-redundant concepts. The matrix of inferred pathway activities for the 46 breast cancer cell lines and 183 TCGA tumor samples was clustered using complete linkage hierarchical agglomerative clustering implemented in the Eisen Cluster software package version 3.0(2). Uncentered Pearson correlation was used as the metric for the pathway concepts and Euclidean distance was used for sample metric (**Fig. S4**).

To quantify the degree to which cell lines clustered with tumor samples of the same subtype, we compared two distributions of t-statistics derived from Pearson correlations (**Fig. S5**). Let C_s be the set of cell lines of subtype s. Similarly, let T_s be the set of TCGA tumor samples of subtype s. For example, C_{basal} and T_{basal} are the set of all basal cell lines and basal tumor samples respectively. The first distribution was made up of t-statistics derived from the Pearson correlations between every possible pair containing a cell line and tumor sample of the same subtype; i.e. for all subtypes s, every pairwise correlation t-statistic was computed between a pair (c, t) such that $c \in C_s$ and $t \in T_s$. The second distribution was made of correlation t-statistics between cell lines of different subtypes; i.e. computed over pairs (c, c') such that $c \in C_s$ and $c' \in C_{s'}$ and $s \neq s'$. We performed a Kolmogorov-Smirnov test to compare the distributions. We repeated this analysis using samples from the same source (cell line or tumor) to verify that cells of the same subtype have overall pathway activities that are more similar than cells of different subtypes. As above, the first distribution was made up of t-statistics between pairs of samples of the same subtype and the same origin (cell line or tumor). The second distribution was made of correlation t-statistics between samples of different subtypes again from the same origin.

We assessed the significance of the subpathways by comparing to subnetworks generated from a background model. Specifically, we measured how likely it would be to find the

identified subnetworks with the observed sizes by chance. To this end, we constructed a background set of subnetworks computed from 1000 simulations in which samples were randomly partitioned into two equal bins, which simulated groupings of cancer cell lines reflecting no biological relevance. Statistical Analysis of Microarrays (SAM) then was used to compute differential pathway activity scores for each concept and each random partitioning using the same thresholds as with the original subtype definitions. Histograms of the subpathway sizes obtained from the random partitions were compared against the subpathway sizes derived from the original subtypes to gauge significance. Our analysis shows that subnetworks derived from the original basal, luminal, claudin-low, and ERBB2 ^{AMP} definitions are significantly larger than those subnetworks obtained from random partitionings. This is true for both the size of the entire subpathway (total number of nodes in the graph) as well as for the largest connected component. Histograms and empirical Z-scores were collected from this random partitioning analysis (see **Fig. S6**).

Supplementary Figure and Table Legends

Figure S1. Genomic and transcriptional profiles of the breast cancer cell lines. A. Hierarchical consensus clustering matrix for 55 breast cancer cell lines showing 3 clusters (claudin-low, luminal, basal) based on gene expression signatures. For each cell line combination, color intensity is proportional to consensus. **B.** DNA copy number aberrations for 43 breast cancer cell lines are plotted with $\log_{10}$(FDR) of GISTIC analysis on the y-axis and chromosome position on the x-axis. Copy number gains are shown in red with positive $\log_{10}$(FDR) and losses are shown in green with negative $\log_{10}$(FDR).

Figure S2. GI50 calculations are highly reproducible. A. Each bar represents a count of the frequency of replicated drug/cell line combinations. Most cell lines were tested only one time against a particular compound, but some drug/cell line combinations were tested multiple times. **B.** Each boxplot represents the distribution of median absolute deviations for drug/cell line pairs with 3 or 4 replicates. **C.** Example drug response curves for HCC1395 treated with cisplatin. Data from three experiments are shown, each plotted in a unique color. Each dot represents the growth inhibition following three days of treatment with one of 10 concentrations of cisplatin. For each dose of each experiment, measurements are performed in triplicate. The x-axis represents increasing cisplatin concentration; the y-axis indicates growth inhibition following treatment. A single curve is fit to the set of 30 data points (3 untreated and 27 treated). The vertical line represents GI50, which is extrapolated from the fitted curve. Across multiple experimental replicates, the dose-response curve is highly reproducible. **D, E, F**. Example drug response curves for three other cell lines, each treated with a different compound. Convention as in C.

Figure S3. Doubling time varies across cell line subtype. A. Growth rate, computed as the median doubling time in hours, of the breast cancer cell lines subtypes are shown as box-plots. The basal and claudin-low subtypes have shorter median doubling time as

compared to luminal and ERBB2^{AMP} subtypes, Kruskal-Wallis *p* value (p = 0.006). **B.** The ANCOVA model shows strong effects of both subtype and growth rate on response to 5-FU. Luminal (black) and basal/claudin-low (red) breast cancer lines each show significant associations to growth rate but have distinct slopes.

Figure S4. Heatmap of non-redundant PARADIGM activities for both cell line and TCGA samples. Cluster dendrogram represents Euclidian distance between samples and was created using Eisen Cluster and drawn using Java Treeview. Each row represents a network feature, each column represents a sample (tumor or cell line). Colored bars below dendrogram indicate sample subtype (upper) and sample cohort (lower). Overall, cell lines and tumors are intermixed, and subtypes tend to cluster together, indicating that the tumors and cell lines share many of the same network features.

Figure S5. Inferred pathway activities are more strongly correlated within subtypes than within cohorts. A. Histogram of t-statistics derived from Pearson correlations computed between cell lines and TCGA samples of the same subtype (red) compared to t-statistics of Pearson correlations between cell lines of different subtypes (black). X-axis corresponds to the Pearson correlation t-statistic; y-axis shows the density of (cell-line, cell-line) or (cell-line, TCGA sample) pairs. K-S test ($p < 1x10^{-22}$) indicates cell lines and TCGA samples of the same subtype are more alike than cell lines of other subtypes. **B**. Pairwise Pearson correlations of cell line samples within the same subgroup (red) versus cell line samples in different subgroups (black). **C**. Pairwise correlations of TCGA breast cancer samples within the same subgroup (red) versus cell line samples in different subgroups (black).

Figure S6. **The cell line networks are highly significant.** The significance of the subpathways identified by our method was assessed by comparing the size of our subpathways to the size of the subpathways generated from a background model in which cells were randomly partitioned into groups, rather than in the original subtype definitions. The subpathway sizes were measured in two ways, the total number of nodes in the subpathway (A,C,E,G) and the number of nodes in the largest connected component of the subpathway (B,D,F,H). The luminal (A,B), ERBB2 ^{AMP} (C,D), claudin-low (E,F), and basal (G,H) subpathway sizes are shown as red dotted lines compared against the distribution of null subpathway sizes. In all cases the subpathway sizes for the true subtype partitioning are significantly larger than the subpathway sizes for the background model.

Dataset S1. Transcriptional, genomic and phenotypic characteristics of cell lines in the panel.

Dataset S2. Drug response data for each cell line tested against 77 therapeutic compounds. Data are -log10 transformed. These data were used to determine subtype specific responses.

Dataset S3. Pearson correlations between drug responses for all compound pairs.

Dataset S4. Subtype associations for all therapeutic compounds. Both raw *p*-values and FDR-corrected *q*-values are shown.

Dataset S5. Censored drug response data. GI50 values that are same as maximum experimental concentration used for different drugs were removed. Data are -log10 transformed. These data were used to identify responses associated with copy number aberrations.

Dataset S6. Non-redundant PARADIGM activities for cell lines and TCGA samples share similar subtype enrichment. Non-redundant pathway entities are along the rows, with subtype-specific SAM scores along the columns, for cell lines alone, TCGA samples alone, and the combined cell line and tumor samples ("BOTH") as shown in Figure S4. Each SAM score has been ranked within the source-specific subtype and average ranks were computed between the cell lines and TCGA samples for the same subtype (luminal, basal, claudin-low and $ERBB2^{AMP}$).

Dataset S7. Subtypes for TCGA breast tumor samples, as determined by the TCGA AWG using heirarchical clustering of an intrinsic gene list. Data were obtained from the TCGA on November 6, 2010.

Waterfall plots

Waterfall plots of breast cancer subtypes and anti-cancer compounds follow after the supplementary figures. Association of clinical subtypes of breast cancer cell lines with 74 anti-cancer compounds. Each bar represents response sensitivity for one cell line, cell lines are ordered by sensitivity ($-\log_{10}(GI_{50})$) and colored to indicate subtype.

PARADIGM Network files

Cytoscape files for the PARADIGM breast cancer cell line networks are available at: http://users.soe.ucsc.edu/~jstuart/heiser2011/

References

1. Vaske CJ, *et al.* (Inference of patient-specific pathway activities from multi-dimensional cancer genomics data using PARADIGM. *Bioinformatics* 26(12):i237-245.
2. de Hoon MJ, Imoto S, Nolan J, & Miyano S (2004) Open source clustering software. *Bioinformatics* 20(9):1453-1454.

Figure S1

A

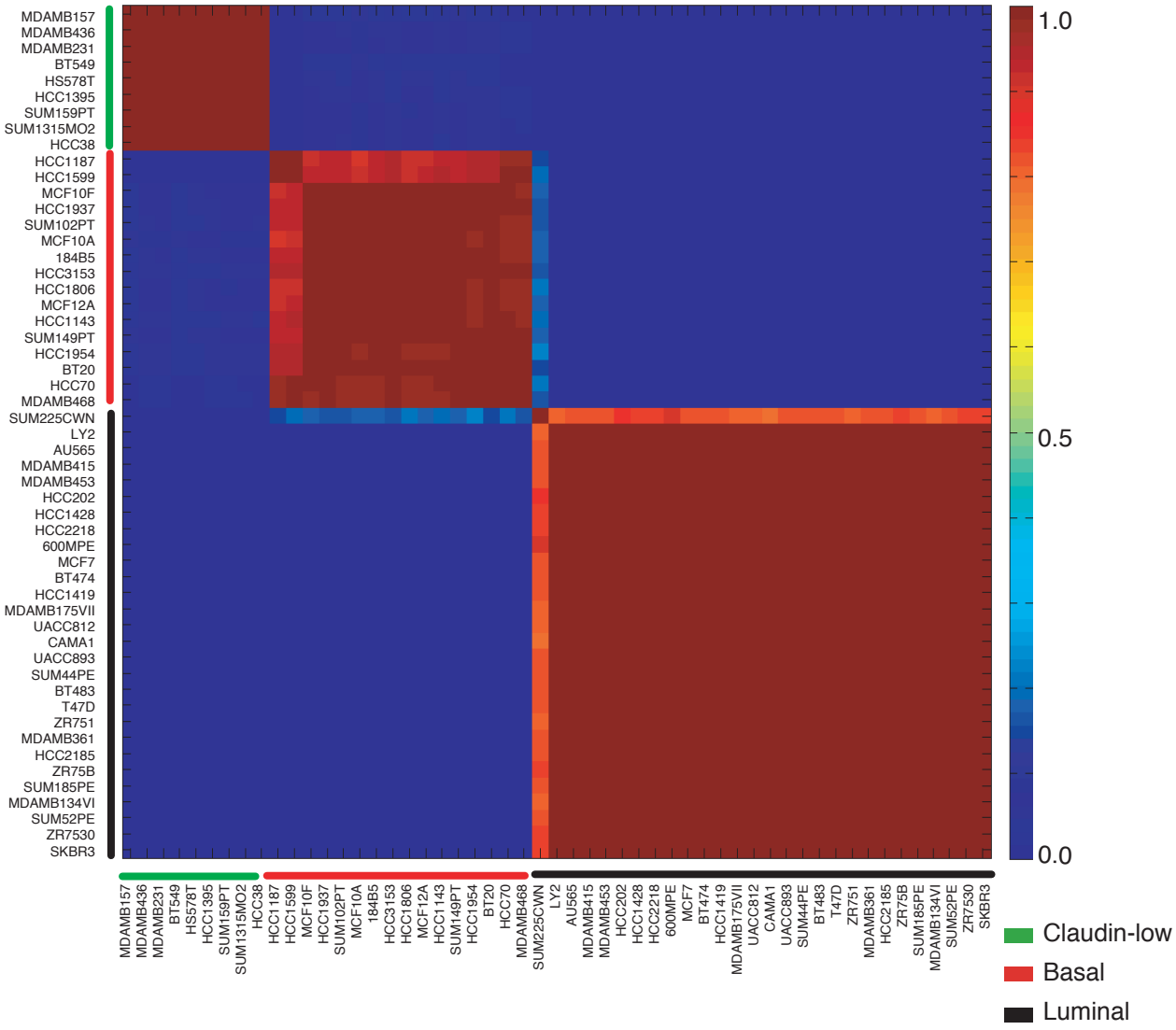
MDAMB157
MDAMB436
MDAMB231
BT549
HS578T
HCC1395
SUM159PT
SUM1315MO2
HCC38
HCC1187
HCC1599
MCF10F
HCC1937
SUM102PT
MCF10A
184B5
HCC3153
HCC1806
MCF12A
HCC1143
SUM149PT
HCC1954
BT20
HCC70
MDAMB468
SUM225CWN
LY2
AU565
MDAMB415
MDAMB453
HCC202
HCC1428
HCC2218
600MPE
MCF7
BT474
HCC1419
MDAMB175VII
UACC812
CAMA1
UACC893
SUM44PE
BT483
T47D
ZR751
MDAMB361
HCC2185
ZR75B
SUM185PE
MDAMB134VI
SUM52PE
ZR7530
SKBR3
1.0
0.5
0.0
Claudin-low
Basal
Luminal

B

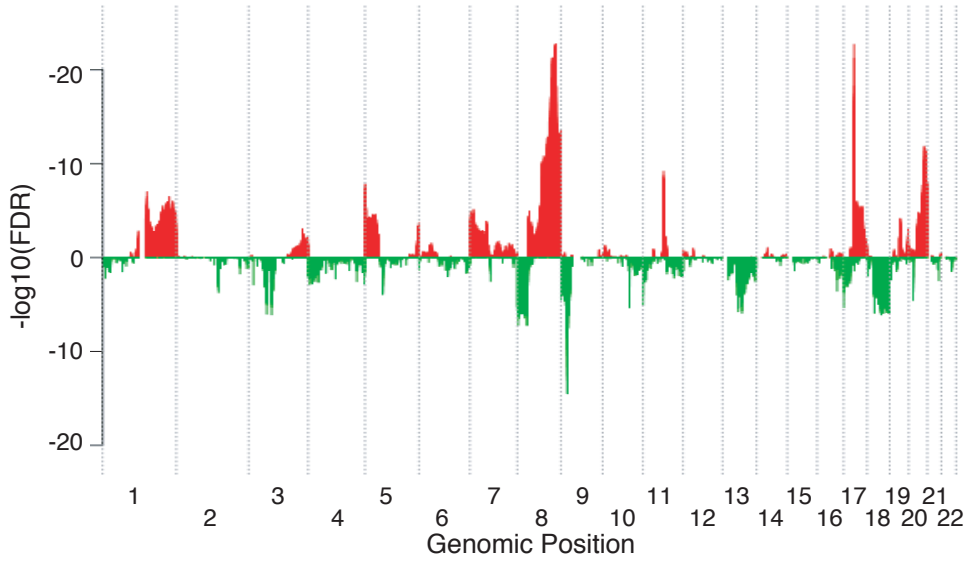
-20
-10
0
-10
-20
-log10(FDR)
1
2
3
4
5
6
7
8
9
10
11
12
13
14
15
16
17
18
19
20
21
22
Genomic Position

Figure S2

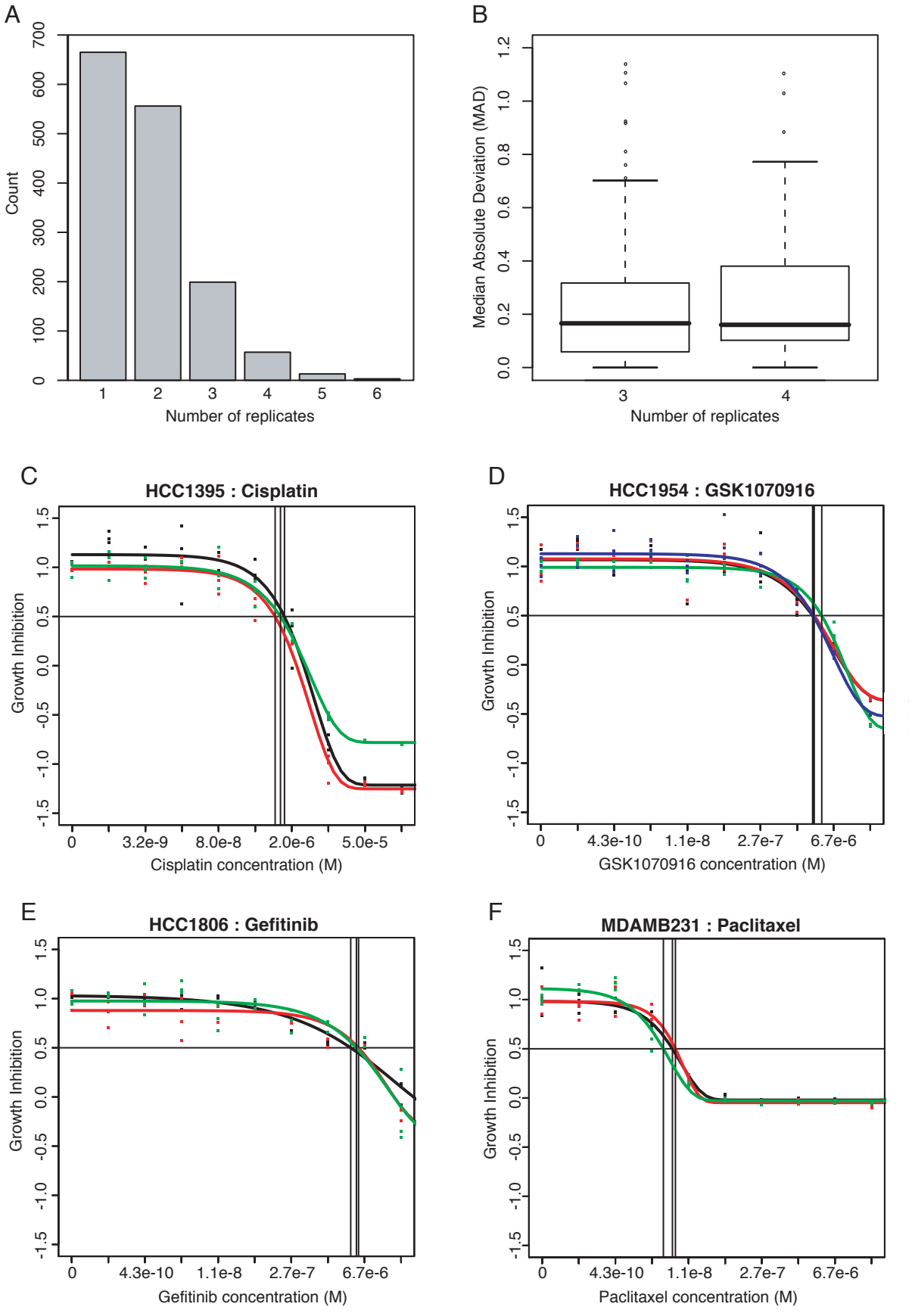
A
Count
0
100
200
300
400
500
600
700
1
2
3
4
5
6
Number of replicates
B
Median Absolute Deviation (MAD)
0.0
0.2
0.4
0.6
0.8
1.0
1.2
3
4
Number of replicates
C
HCC1395 : Cisplatin
Growth Inhibition
-1.5
-1.0
-0.5
0.0
0.5
1.0
1.5
0
3.2e-9
8.0e-8
2.0e-6
5.0e-5
Cisplatin concentration (M)
D
HCC1954 : GSK1070916
Growth Inhibition
0
4.3e-10
1.1e-8
2.7e-7
6.7e-6
GSK1070916 concentration (M)
E
HCC1806 : Gefitinib
Growth Inhibition
0
4.3e-10
1.1e-8
2.7e-7
6.7e-6
Gefitinib concentration (M)
F
MDAMB231 : Paclitaxel
Growth Inhibition
0
4.3e-10
1.1e-8
2.7e-7
6.7e-6
Paclitaxel concentration (M)

Figure S3

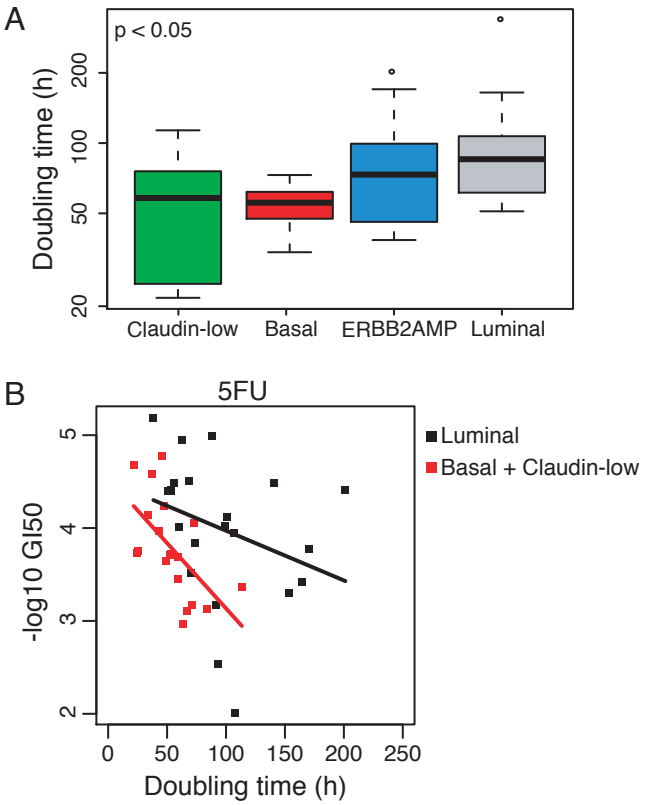
A
p < 0.05
Doubling time (h)
20
50
100
200
Claudin-low
Basal
ERBB2AMP
Luminal
B
5FU
-log10 GI50
2
3
4
5
0
50
100
150
200
250
Doubling time (h)
Luminal
Basal + Claudin-low

Figure S4

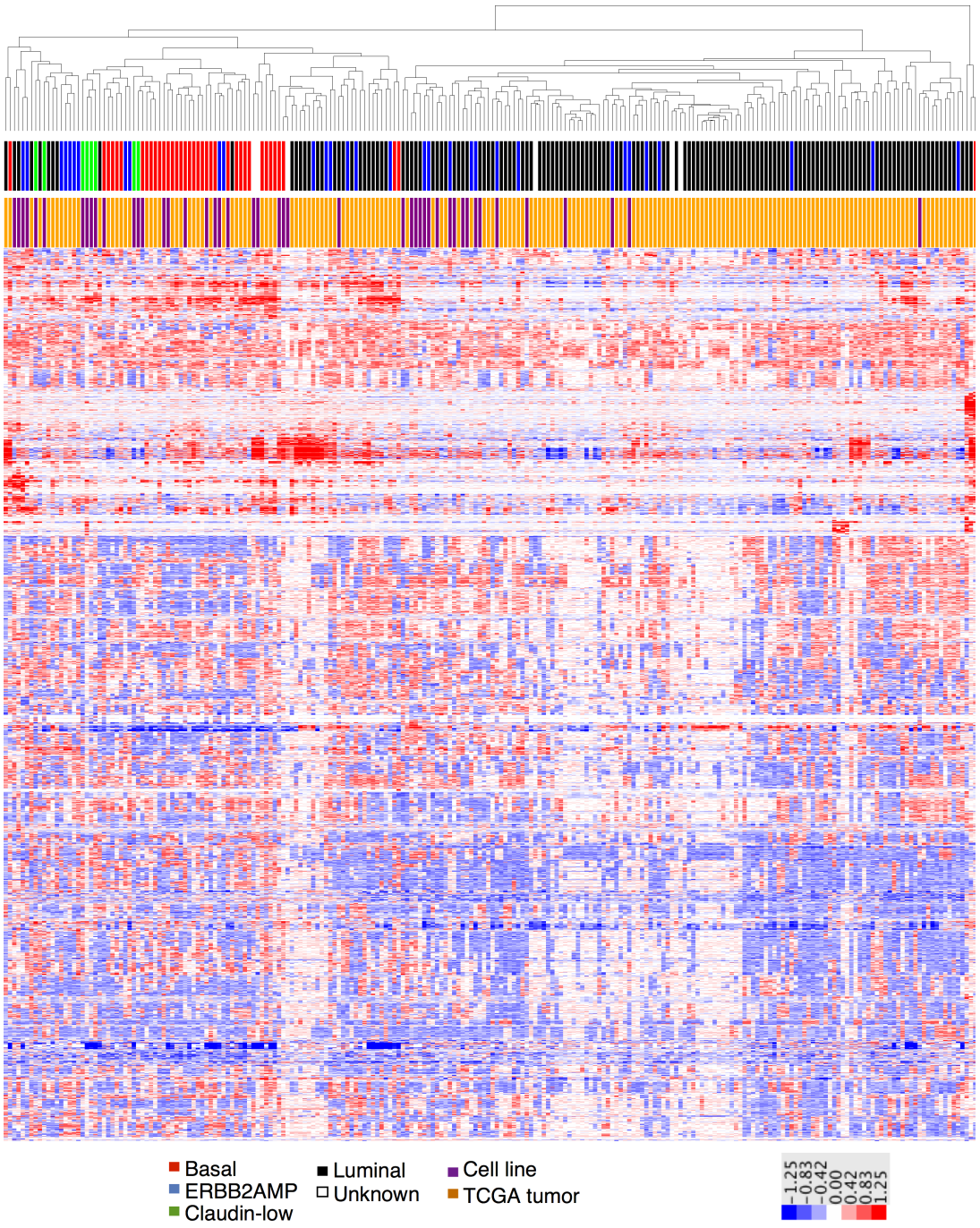
Basal
ERBB2AMP
Claudin-low
Luminal
Unknown
Cell line
TCGA tumor
-1.25
-0.83
-0.42
0.00
0.42
0.83
1.25

Figure S5

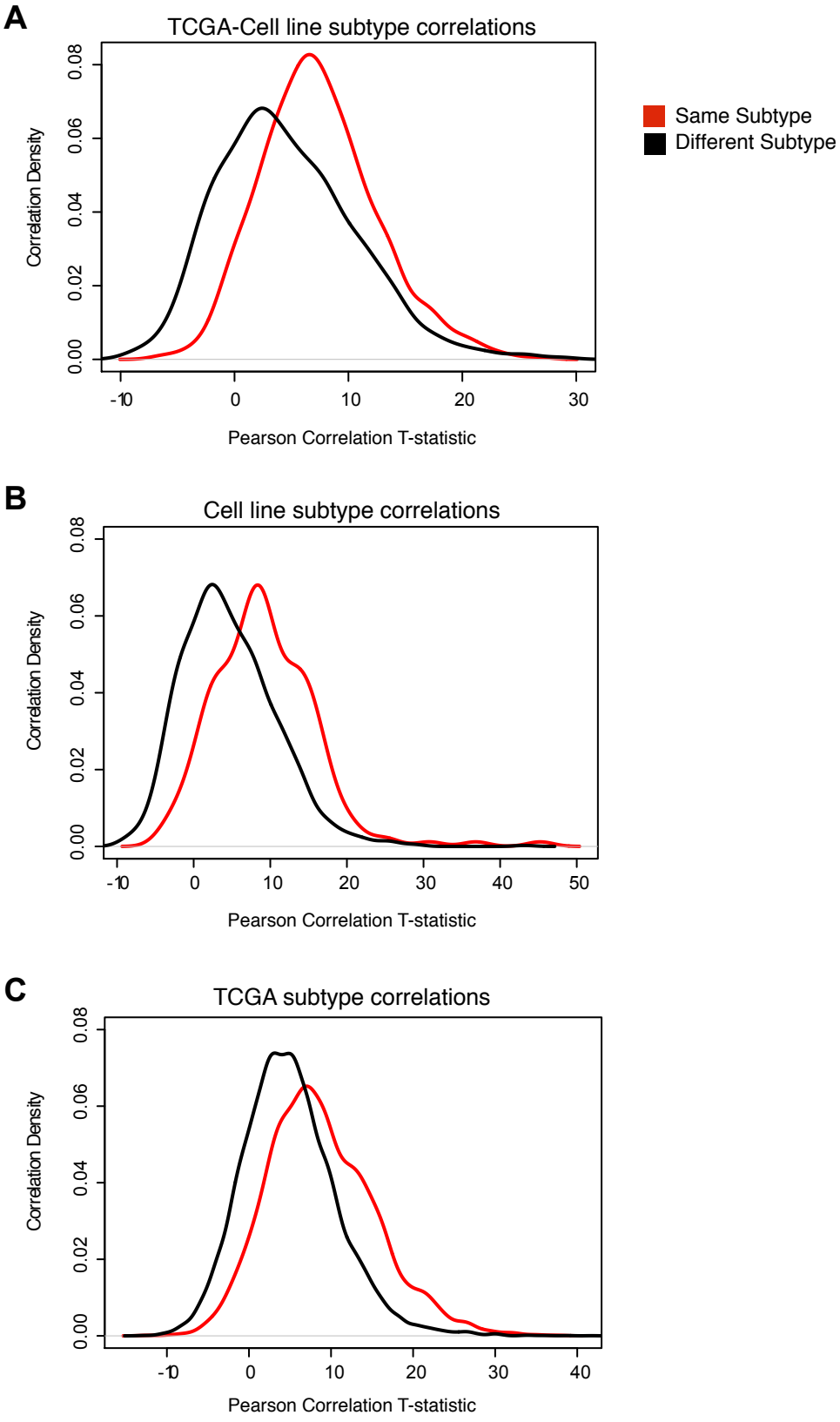
A
TCGA-Cell line subtype correlations
Correlation Density
0.00
0.02
0.04
0.06
0.08
-10
0
10
20
30
Pearson Correlation T-statistic
Same Subtype
Different Subtype
B
Cell line subtype correlations
Correlation Density
0.00
0.02
0.04
0.06
0.08
-10
0
10
20
30
40
50
Pearson Correlation T-statistic
C
TCGA subtype correlations
Correlation Density
0.00
0.02
0.04
0.06
0.08
-10
0
10
20
30
40
Pearson Correlation T-statistic

Figure S6

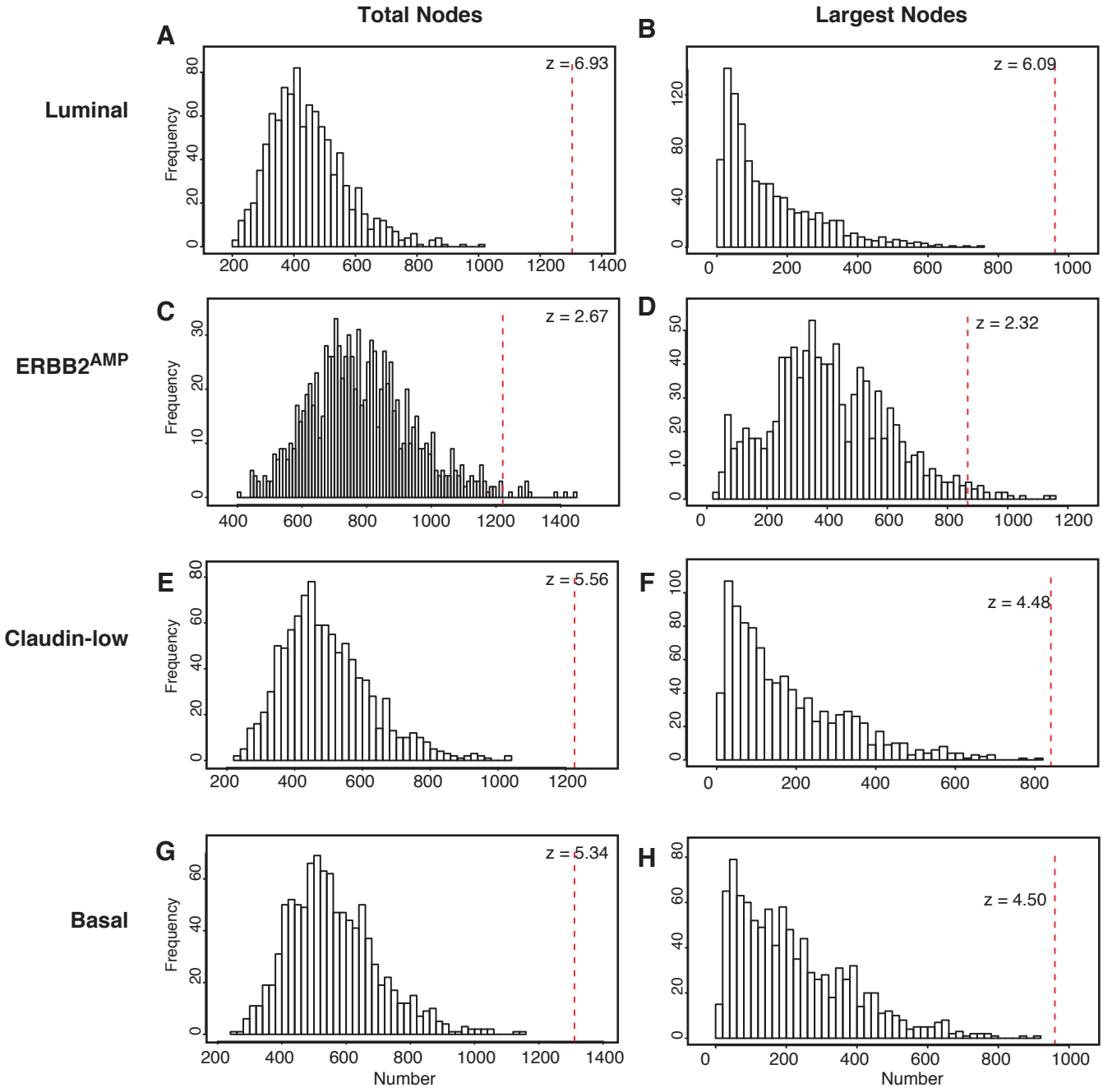
Total Nodes
Largest Nodes
A
B
C
D
E
F
G
H
Luminal
ERBB2AMP
Claudin-low
Basal
z = 6.93
z = 6.09
z = 2.67
z = 2.32
z = 5.56
z = 4.48
z = 5.34
z = 4.50
Frequency
Number

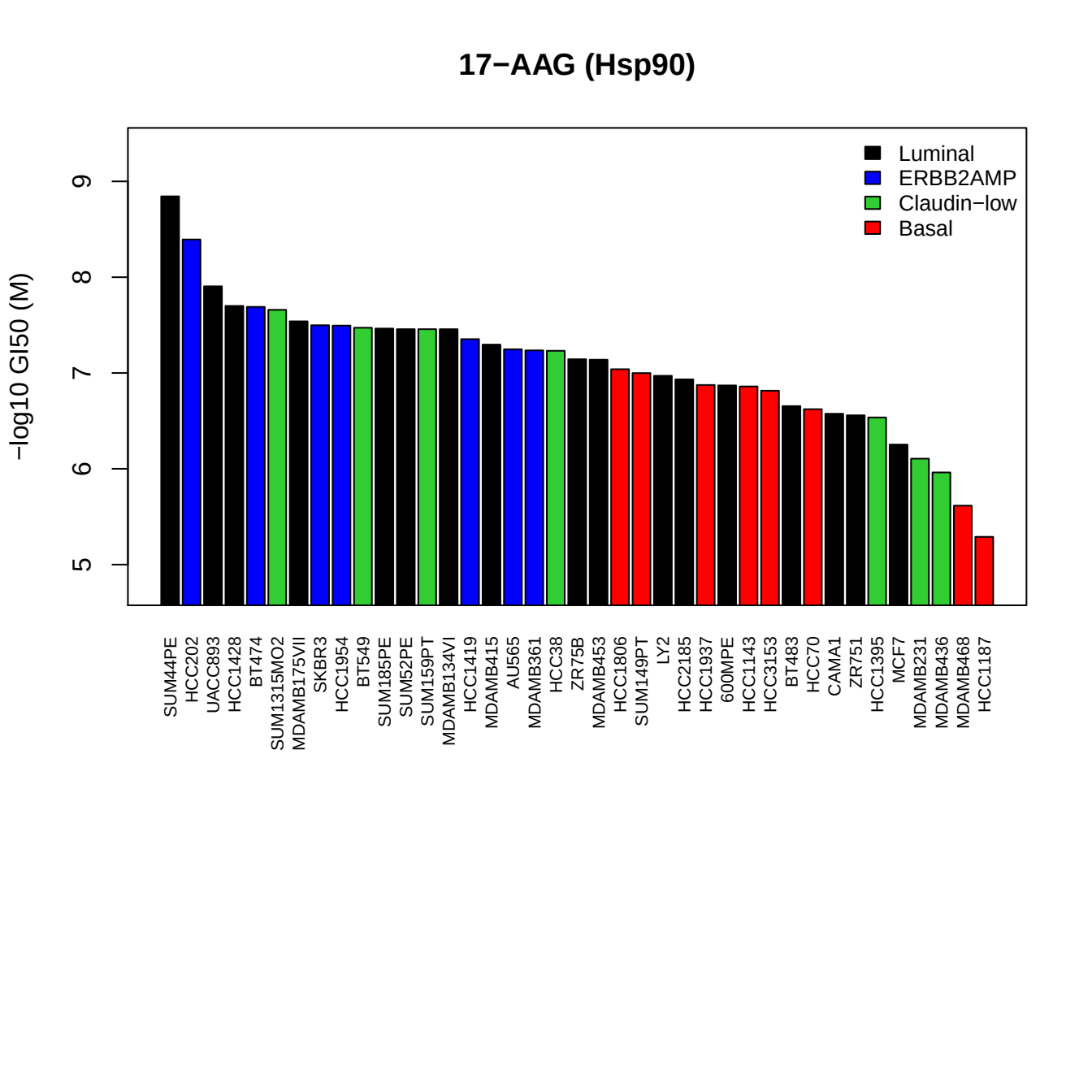
17−AAG (Hsp90)
−log10 GI50 (M)
5
6
7
8
9
Luminal
ERBB2AMP
Claudin−low
Basal
SUM44PE
HCC202
UACC893
HCC1428
BT474
SUM1315MO2
MDAMB175VII
SKBR3
HCC1954
BT549
SUM185PE
SUM52PE
SUM159PT
MDAMB134VI
HCC1419
MDAMB415
AU565
MDAMB361
HCC38
ZR75B
MDAMB453
HCC1806
SUM149PT
LY2
HCC2185
HCC1937
600MPE
HCC1143
HCC3153
BT483
HCC70
CAMA1
ZR751
HCC1395
MCF7
MDAMB231
MDAMB436
MDAMB468
HCC1187

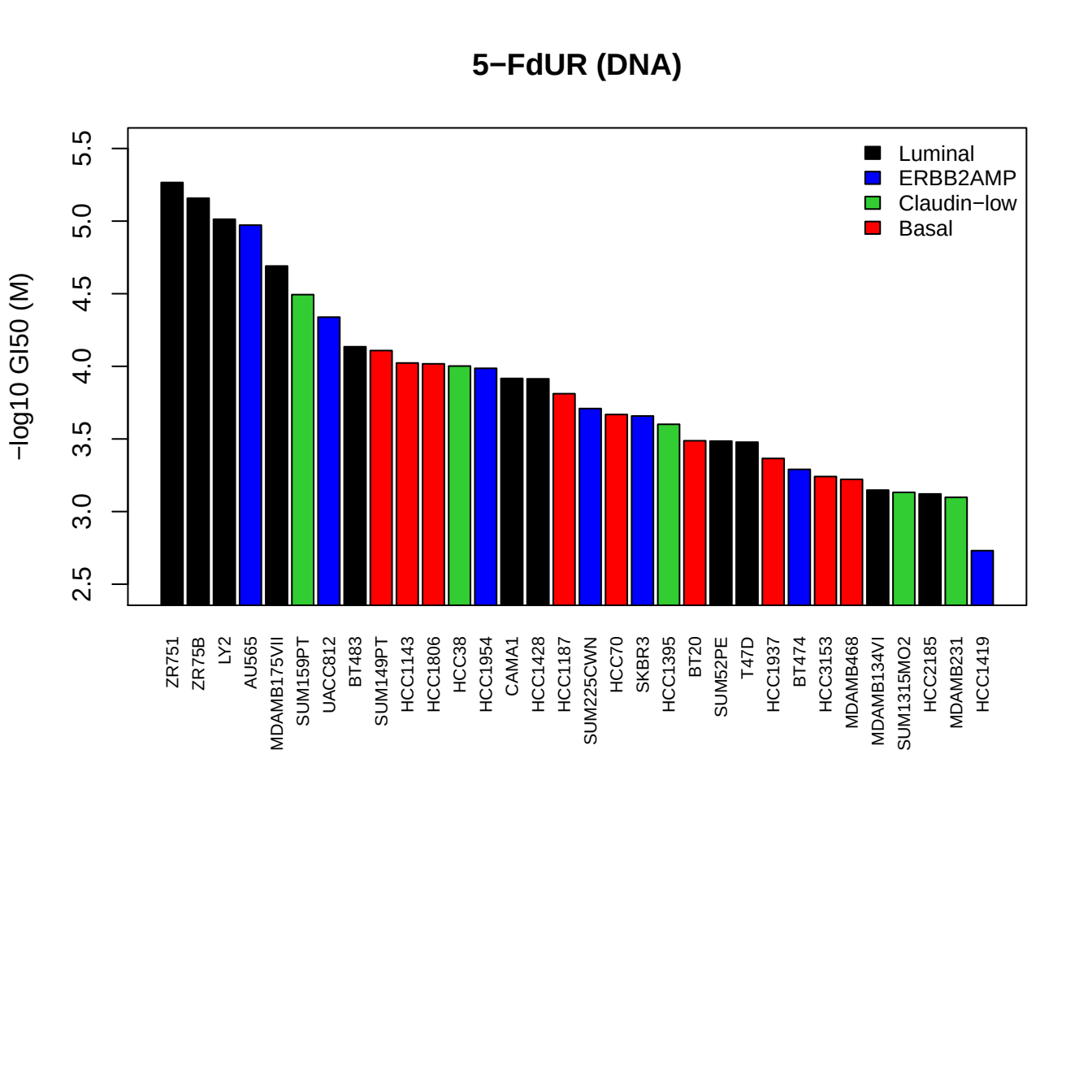
5−FdUR (DNA)
−log10 GI50 (M)
2.5
3.0
3.5
4.0
4.5
5.0
5.5
Luminal
ERBB2AMP
Claudin−low
Basal
ZR751
ZR75B
LY2
AU565
MDAMB175VII
SUM159PT
UACC812
BT483
SUM149PT
HCC1143
HCC1806
HCC38
HCC1954
CAMA1
HCC1428
HCC1187
SUM225CWN
HCC70
SKBR3
HCC1395
BT20
SUM52PE
T47D
HCC1937
BT474
HCC3153
MDAMB468
MDAMB134VI
SUM1315MO2
HCC2185
MDAMB231
HCC1419

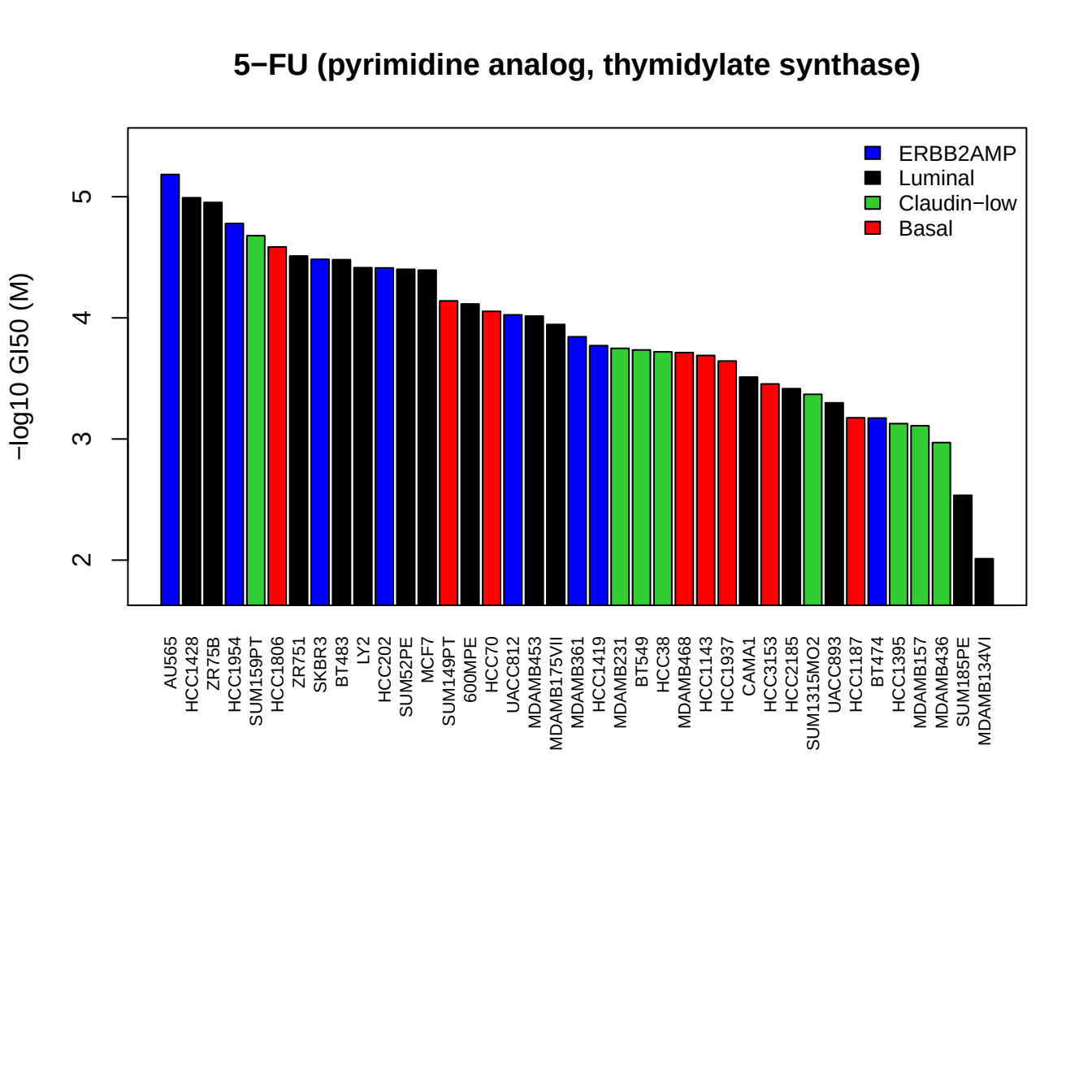
5−FU (pyrimidine analog, thymidylate synthase)
−log10 GI50 (M)
2
3
4
5
ERBB2AMP
Luminal
Claudin−low
Basal
AU565
HCC1428
ZR75B
HCC1954
SUM159PT
HCC1806
ZR751
SKBR3
BT483
LY2
HCC202
SUM52PE
MCF7
SUM149PT
600MPE
HCC70
UACC812
MDAMB453
MDAMB175VII
MDAMB361
HCC1419
MDAMB231
BT549
HCC38
MDAMB468
HCC1143
HCC1937
CAMA1
HCC3153
HCC2185
SUM1315MO2
UACC893
HCC1187
BT474
HCC1395
MDAMB157
MDAMB436
SUM185PE
MDAMB134VI

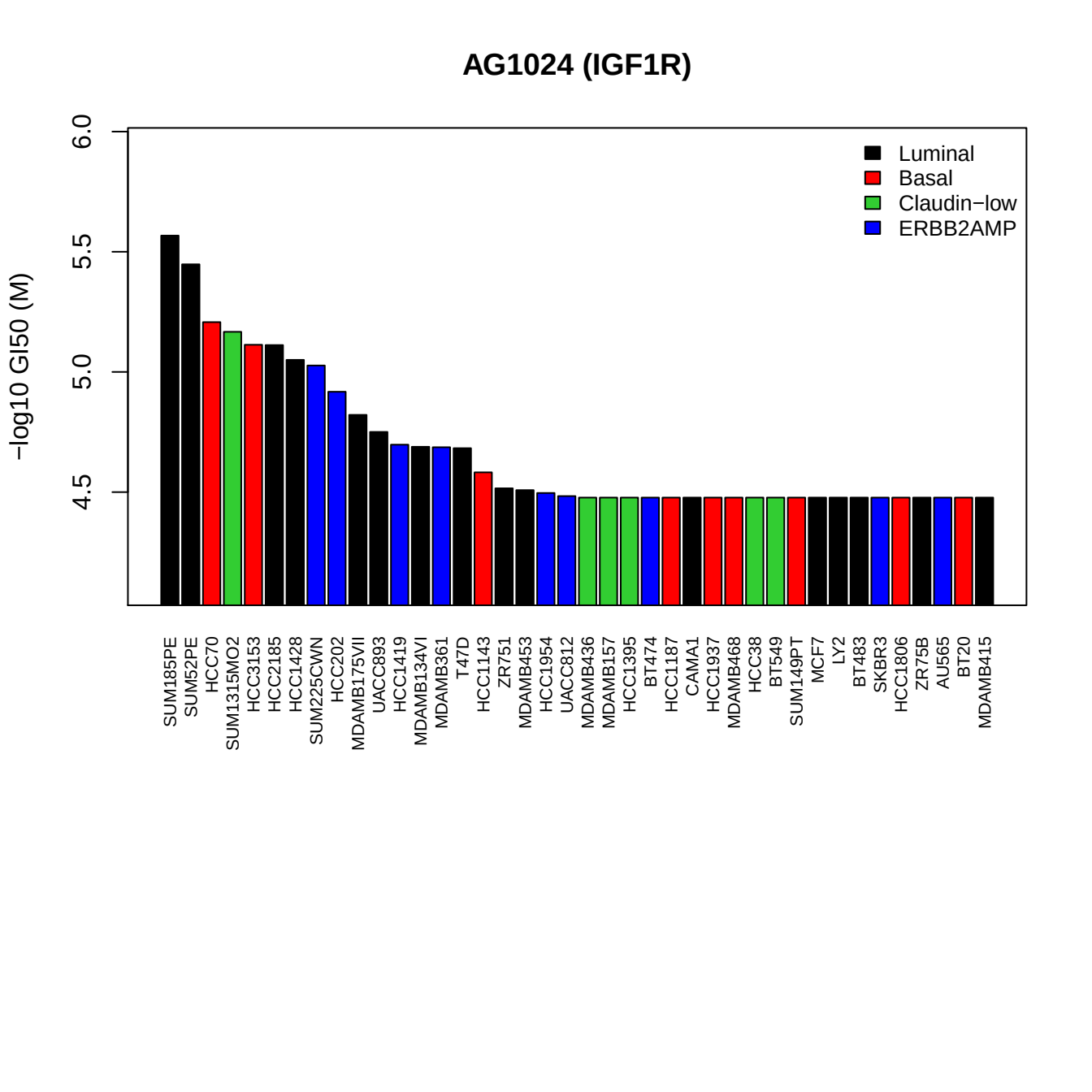
AG1024 (IGF1R)
−log10 GI50 (M)
6.0
5.5
5.0
4.5
Luminal
Basal
Claudin−low
ERBB2AMP
SUM185PE
SUM52PE
HCC70
SUM1315MO2
HCC3153
HCC2185
HCC1428
SUM225CWN
HCC202
MDAMB175VII
UACC893
HCC1419
MDAMB134VI
MDAMB361
T47D
HCC1143
ZR751
MDAMB453
HCC1954
UACC812
MDAMB436
MDAMB157
HCC1395
BT474
HCC1187
CAMA1
HCC1937
MDAMB468
HCC38
BT549
SUM149PT
MCF7
LY2
BT483
SKBR3
HCC1806
ZR75B
AU565
BT20
MDAMB415

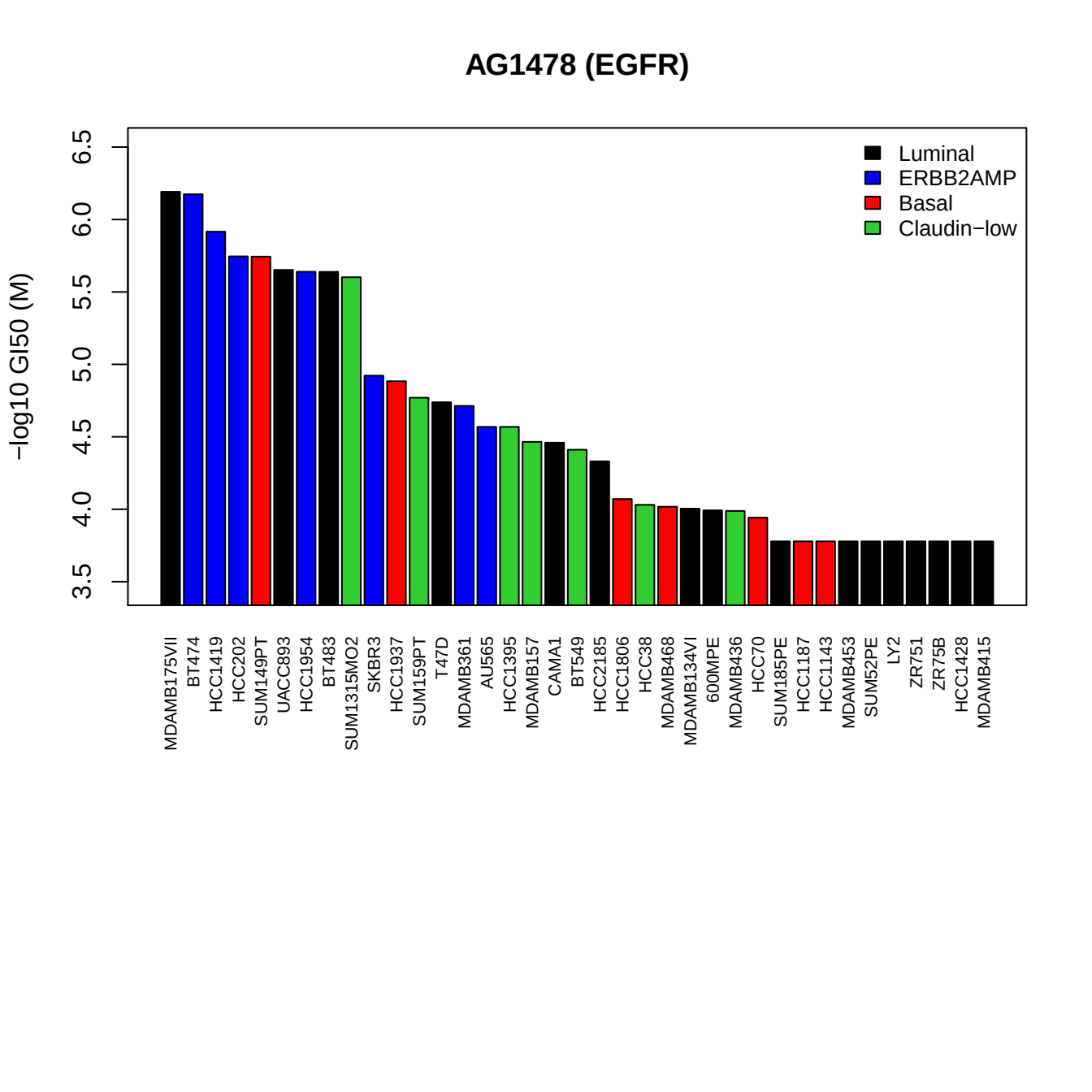
AG1478 (EGFR)
−log10 GI50 (M)
3.5
4.0
4.5
5.0
5.5
6.0
6.5
Luminal
ERBB2AMP
Basal
Claudin−low
MDAMB175VII
BT474
HCC1419
HCC202
SUM149PT
UACC893
HCC1954
BT483
SUM1315MO2
SKBR3
HCC1937
SUM159PT
T47D
MDAMB361
AU565
HCC1395
MDAMB157
CAMA1
BT549
HCC2185
HCC1806
HCC38
MDAMB468
MDAMB134VI
600MPE
MDAMB436
HCC70
SUM185PE
HCC1187
HCC1143
MDAMB453
SUM52PE
LY2
ZR751
ZR75B
HCC1428
MDAMB415

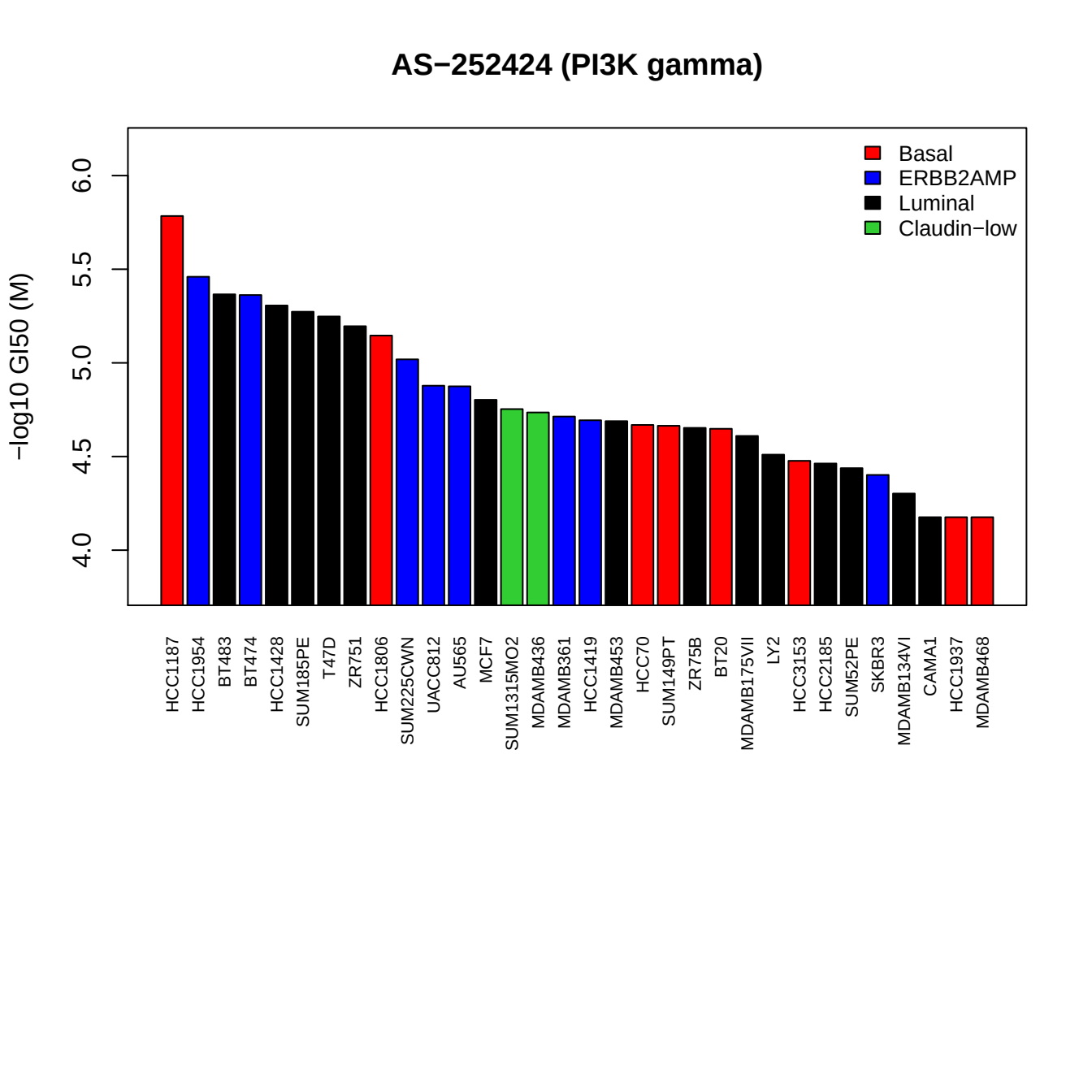
AS−252424 (PI3K gamma)
−log10 GI50 (M)
4.0
4.5
5.0
5.5
6.0
Basal
ERBB2AMP
Luminal
Claudin−low
HCC1187
HCC1954
BT483
BT474
HCC1428
SUM185PE
T47D
ZR751
HCC1806
SUM225CWN
UACC812
AU565
MCF7
SUM1315MO2
MDAMB436
MDAMB361
HCC1419
MDAMB453
HCC70
SUM149PT
ZR75B
BT20
MDAMB175VII
LY2
HCC3153
HCC2185
SUM52PE
SKBR3
MDAMB134VI
CAMA1
HCC1937
MDAMB468

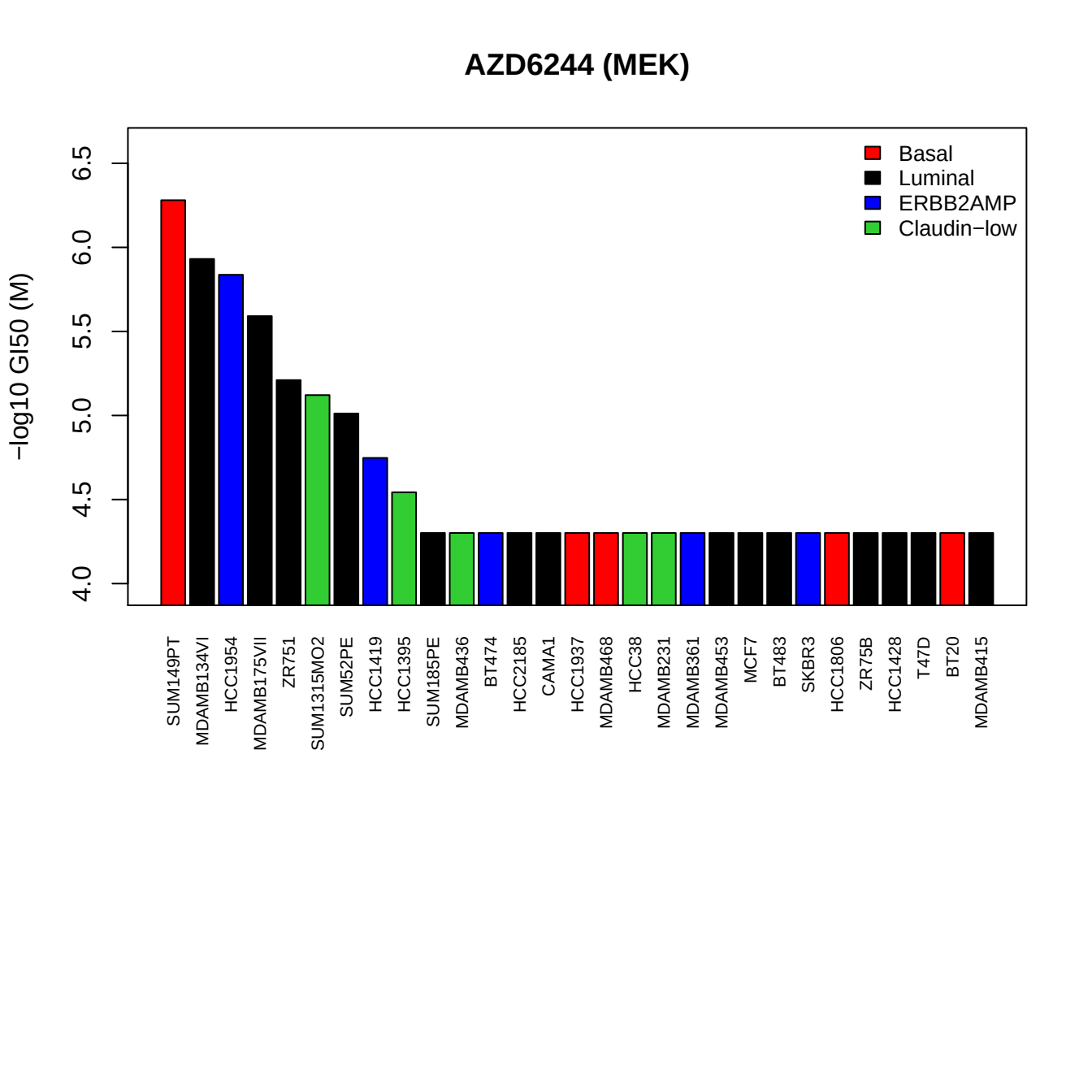
AZD6244 (MEK)
−log10 GI50 (M)
4.0
4.5
5.0
5.5
6.0
6.5
Basal
Luminal
ERBB2AMP
Claudin−low
SUM149PT
MDAMB134VI
HCC1954
MDAMB175VII
ZR751
SUM1315MO2
SUM52PE
HCC1419
HCC1395
SUM185PE
MDAMB436
BT474
HCC2185
CAMA1
HCC1937
MDAMB468
HCC38
MDAMB231
MDAMB361
MDAMB453
MCF7
BT483
SKBR3
HCC1806
ZR75B
HCC1428
T47D
BT20
MDAMB415

BEZ235 (PI3K)

−log10 GI50 (M)
4
5
6
7
8
Claudin−low
ERBB2AMP
Luminal
Basal
SUM159PT
HCC1954
MDAMB453
ZR75B
HCC70
SUM1315MO2
AU565
HCC2185
MDAMB415
SUM149PT
T47D
BT474
HCC38
SKBR3
MCF7
HCC3153
MDAMB361
MDAMB134VI
MDAMB175VII
BT20
BT483
SUM185PE
ZR751
UACC812
CAMA1
SUM52PE
HCC1428
HCC1187
MDAMB468

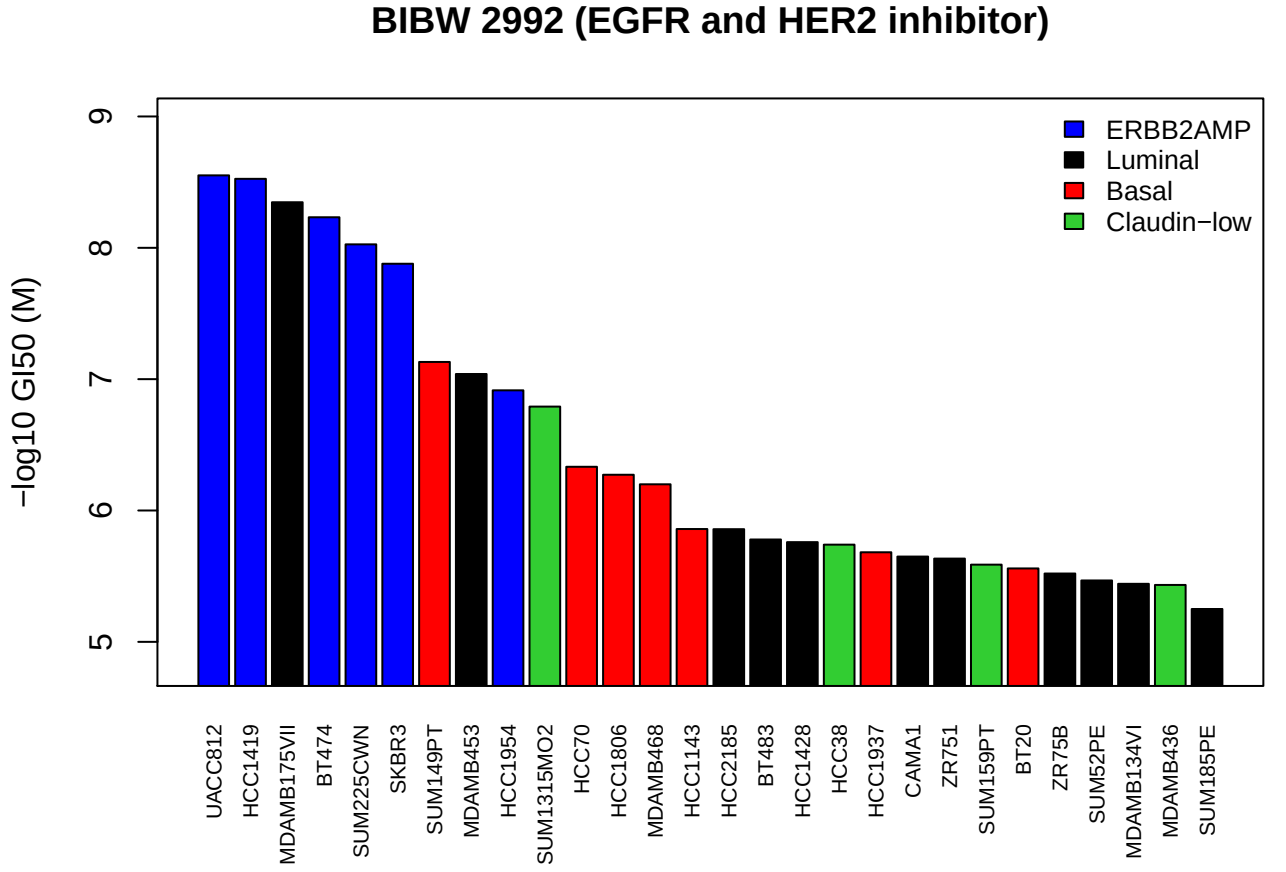
BIBW 2992 (EGFR and HER2 inhibitor)
−log10 GI50 (M)
5
6
7
8
9
ERBB2AMP
Luminal
Basal
Claudin−low
UACC812
HCC1419
MDAMB175VII
BT474
SUM225CWN
SKBR3
SUM149PT
MDAMB453
HCC1954
SUM1315MO2
HCC70
HCC1806
MDAMB468
HCC1143
HCC2185
BT483
HCC1428
HCC38
HCC1937
CAMA1
ZR751
SUM159PT
BT20
ZR75B
SUM52PE
MDAMB134VI
MDAMB436
SUM185PE

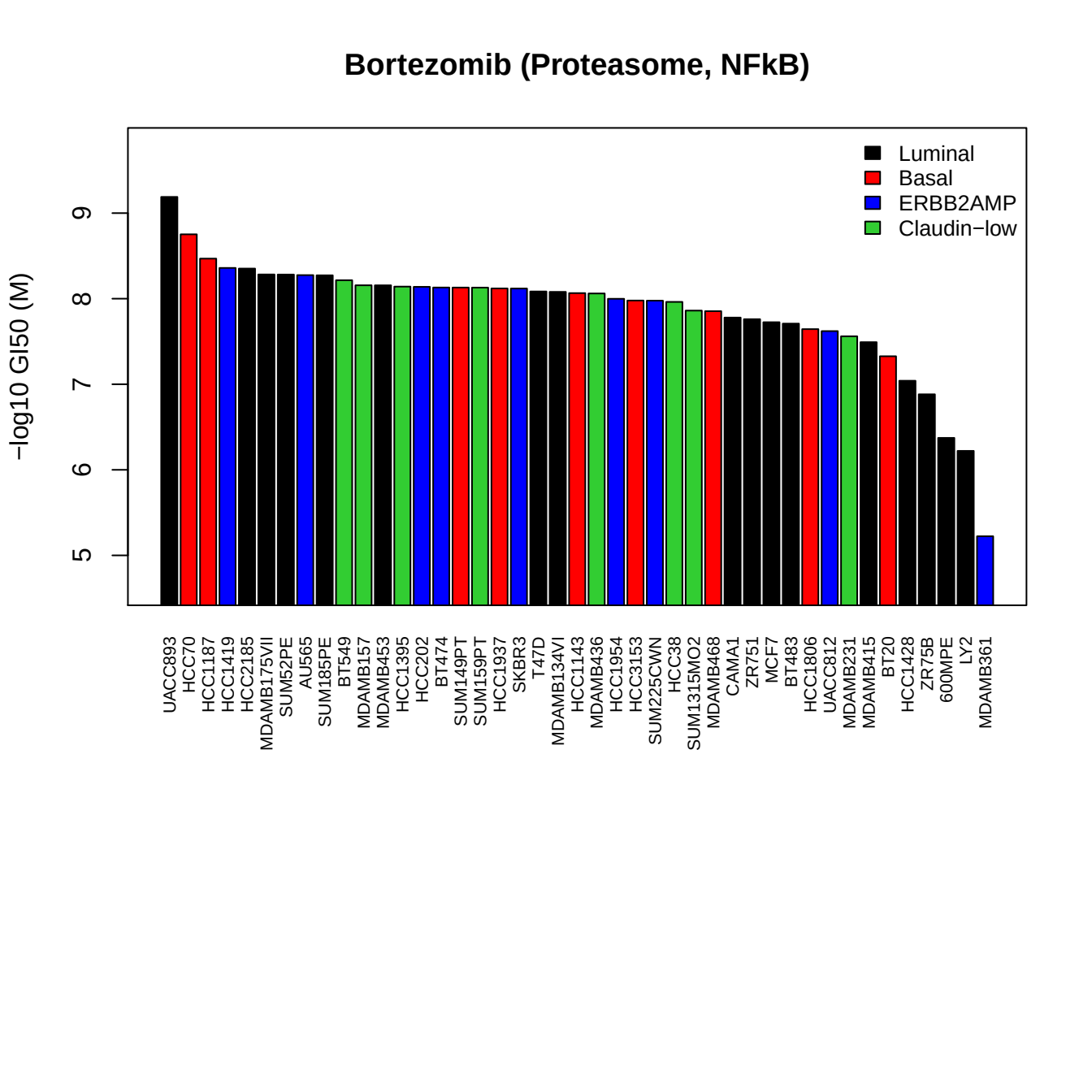
Bortezomib (Proteasome, NFkB)
−log10 GI50 (M)
5
6
7
8
9
Luminal
Basal
ERBB2AMP
Claudin−low
UACC893
HCC70
HCC1187
HCC1419
HCC2185
MDAMB175VII
SUM52PE
AU565
SUM185PE
BT549
MDAMB157
MDAMB453
HCC1395
HCC202
BT474
SUM149PT
SUM159PT
HCC1937
SKBR3
T47D
MDAMB134VI
HCC1143
MDAMB436
HCC1954
HCC3153
SUM225CWN
HCC38
SUM1315MO2
MDAMB468
CAMA1
ZR751
MCF7
BT483
HCC1806
UACC812
MDAMB231
MDAMB415
BT20
HCC1428
ZR75B
600MPE
LY2
MDAMB361

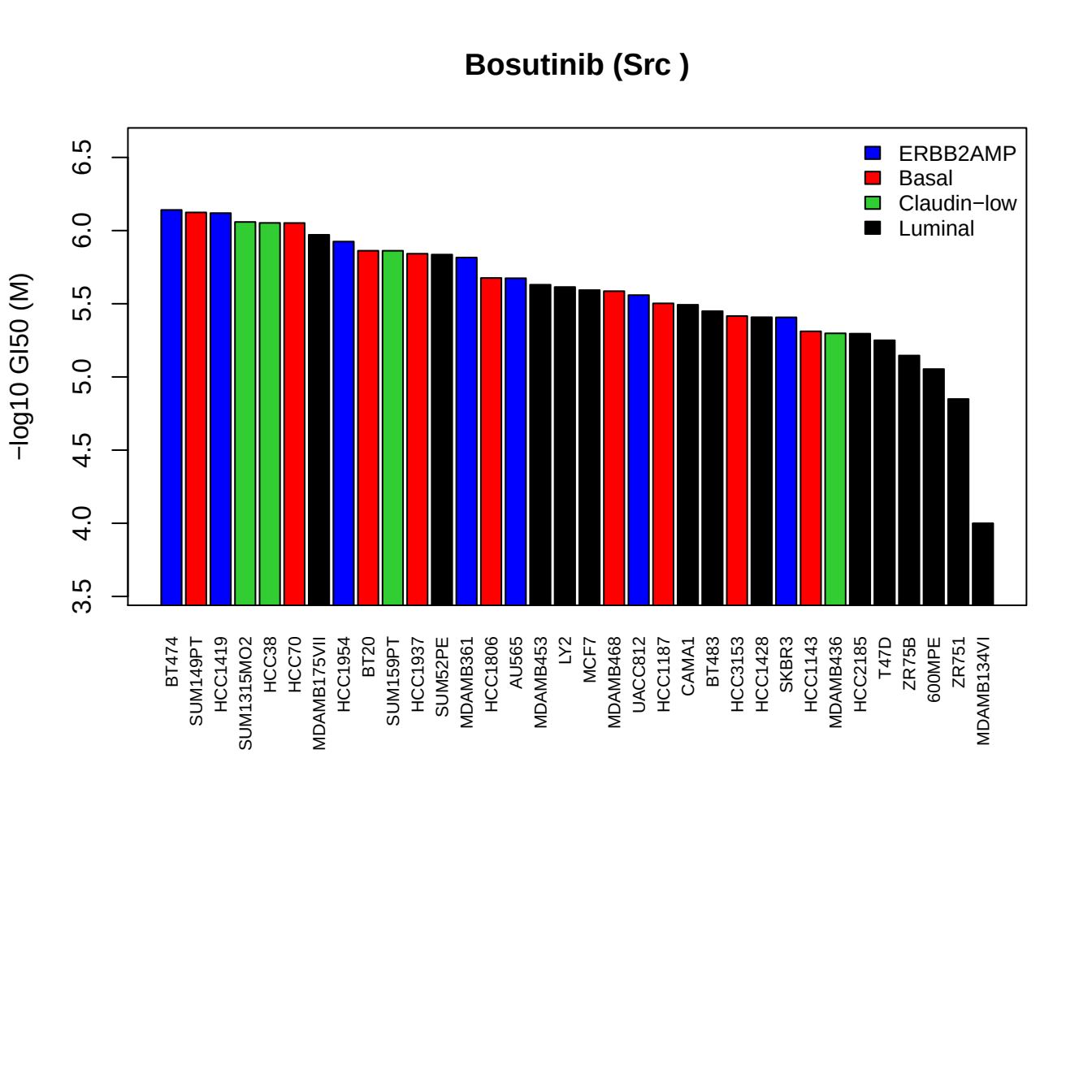
Bosutinib (Src)
−log10 GI50 (M)
3.5
4.0
4.5
5.0
5.5
6.0
6.5
ERBB2AMP
Basal
Claudin−low
Luminal
BT474
SUM149PT
HCC1419
SUM1315MO2
HCC38
HCC70
MDAMB175VII
HCC1954
BT20
SUM159PT
HCC1937
SUM52PE
MDAMB361
HCC1806
AU565
MDAMB453
LY2
MCF7
MDAMB468
UACC812
HCC1187
CAMA1
BT483
HCC3153
HCC1428
SKBR3
HCC1143
MDAMB436
HCC2185
T47D
ZR75B
600MPE
ZR751
MDAMB134VI

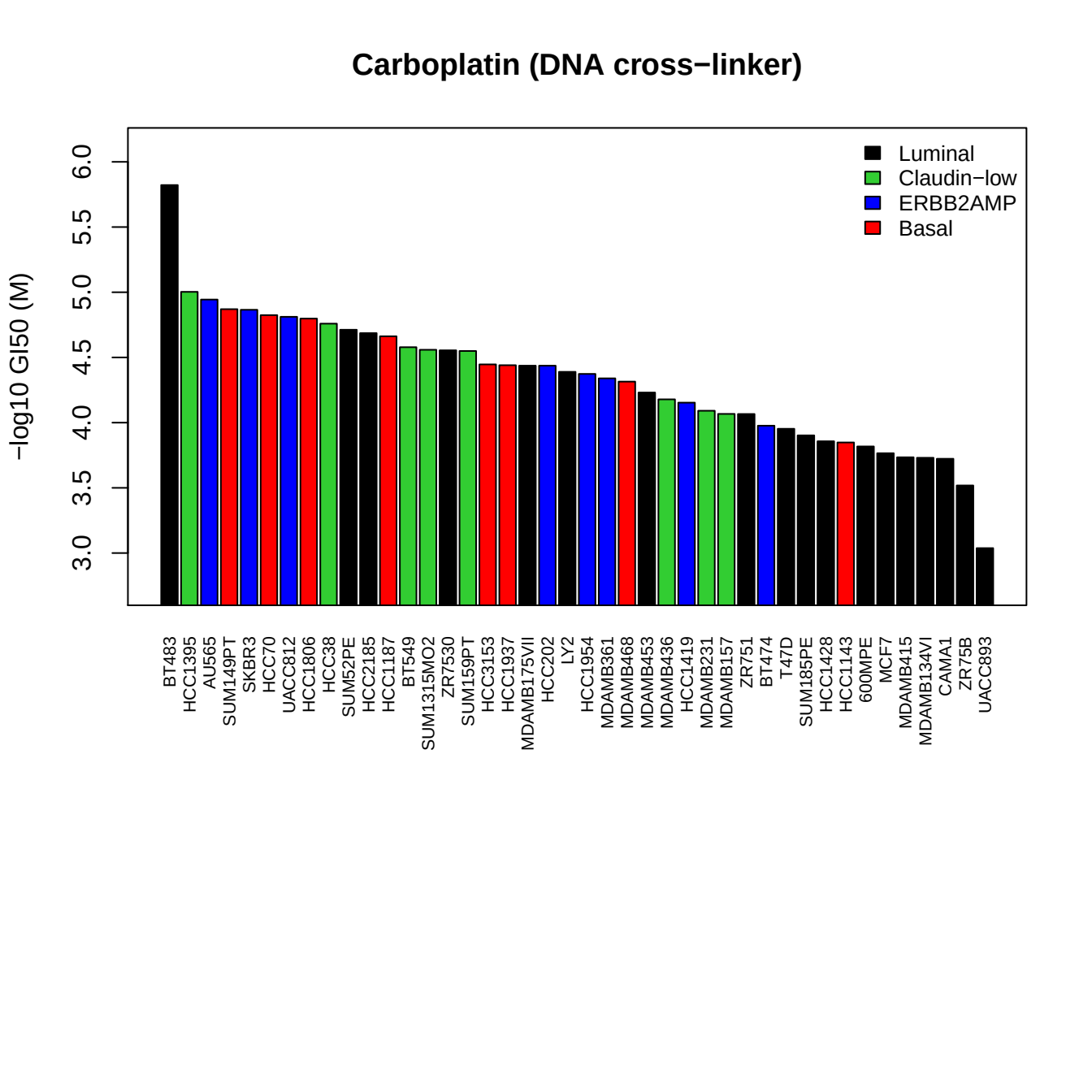
Carboplatin (DNA cross−linker)
−log10 GI50 (M)
3.0
3.5
4.0
4.5
5.0
5.5
6.0
Luminal
Claudin−low
ERBB2AMP
Basal
BT483
HCC1395
AU565
SUM149PT
SKBR3
HCC70
UACC812
HCC1806
HCC38
SUM52PE
HCC2185
HCC1187
BT549
SUM1315MO2
ZR7530
SUM159PT
HCC3153
HCC1937
MDAMB175VII
HCC202
LY2
HCC1954
MDAMB361
MDAMB468
MDAMB453
MDAMB436
HCC1419
MDAMB231
MDAMB157
ZR751
BT474
T47D
SUM185PE
HCC1428
HCC1143
600MPE
MCF7
MDAMB415
MDAMB134VI
CAMA1
ZR75B
UACC893

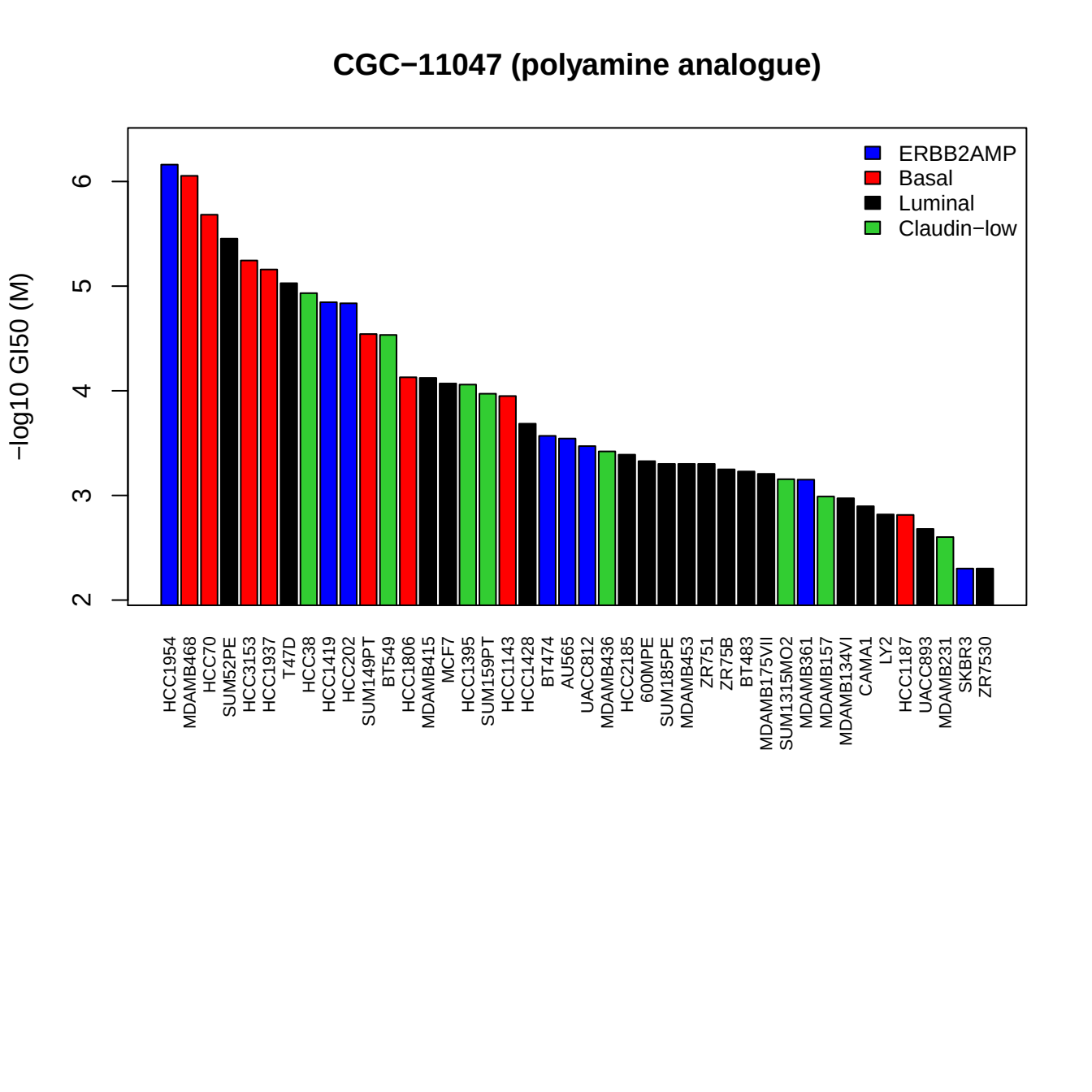
CGC−11047 (polyamine analogue)
−log10 GI50 (M)
2
3
4
5
6
ERBB2AMP
Basal
Luminal
Claudin−low
HCC1954
MDAMB468
HCC70
SUM52PE
HCC3153
HCC1937
T47D
HCC38
HCC1419
HCC202
SUM149PT
BT549
HCC1806
MDAMB415
MCF7
HCC1395
SUM159PT
HCC1143
HCC1428
BT474
AU565
UACC812
MDAMB436
HCC2185
600MPE
SUM185PE
MDAMB453
ZR751
ZR75B
BT483
MDAMB175VII
SUM1315MO2
MDAMB361
MDAMB157
MDAMB134VI
CAMA1
LY2
HCC1187
UACC893
MDAMB231
SKBR3
ZR7530

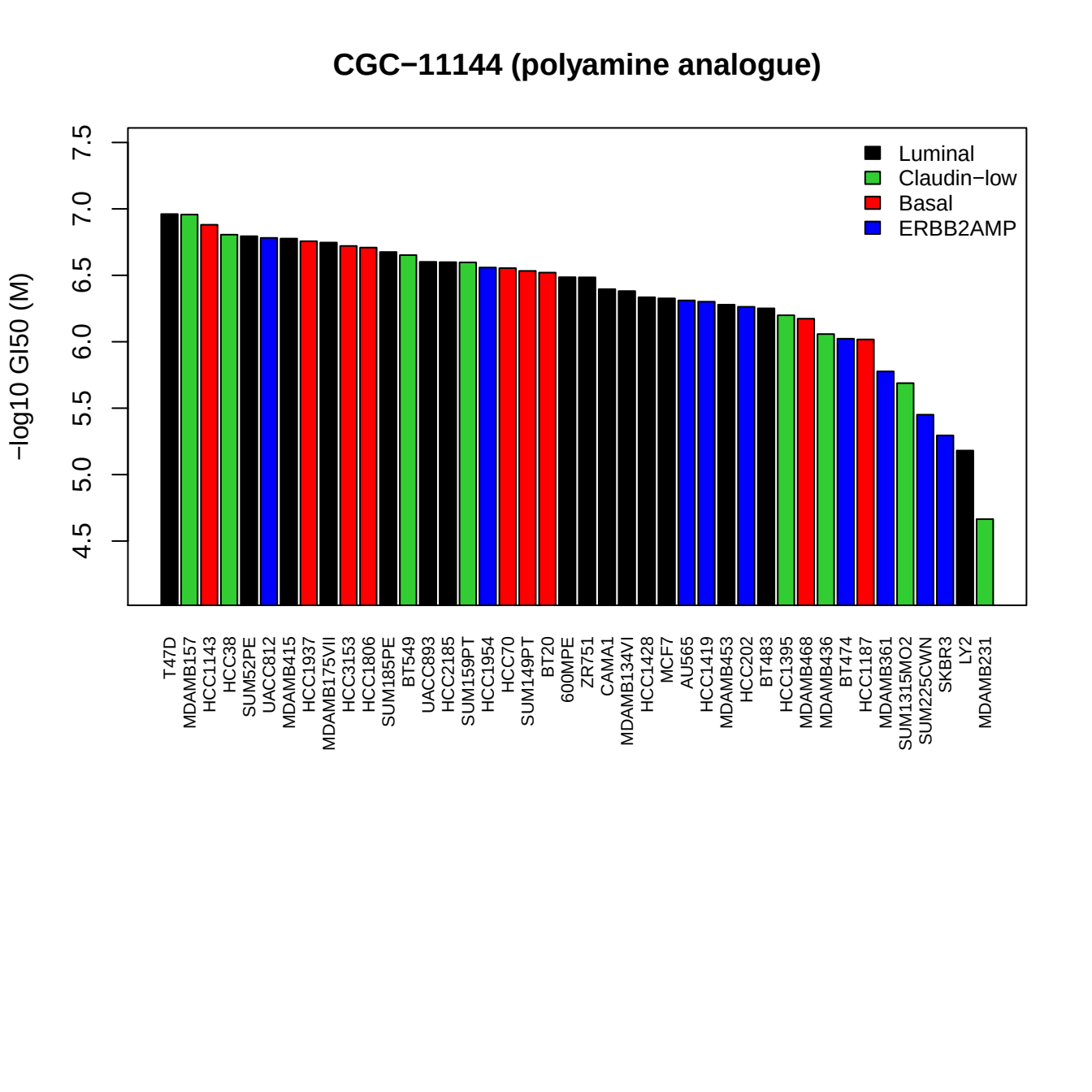
CGC−11144 (polyamine analogue)
−log10 GI50 (M)
4.5
5.0
5.5
6.0
6.5
7.0
7.5
Luminal
Claudin−low
Basal
ERBB2AMP
T47D
MDAMB157
HCC1143
HCC38
SUM52PE
UACC812
MDAMB415
HCC1937
MDAMB175VII
HCC3153
HCC1806
SUM185PE
BT549
UACC893
HCC2185
SUM159PT
HCC1954
HCC70
SUM149PT
BT20
600MPE
ZR751
CAMA1
MDAMB134VI
HCC1428
MCF7
AU565
HCC1419
MDAMB453
HCC202
BT483
HCC1395
MDAMB468
MDAMB436
BT474
HCC1187
MDAMB361
SUM1315MO2
SUM225CWN
SKBR3
LY2
MDAMB231

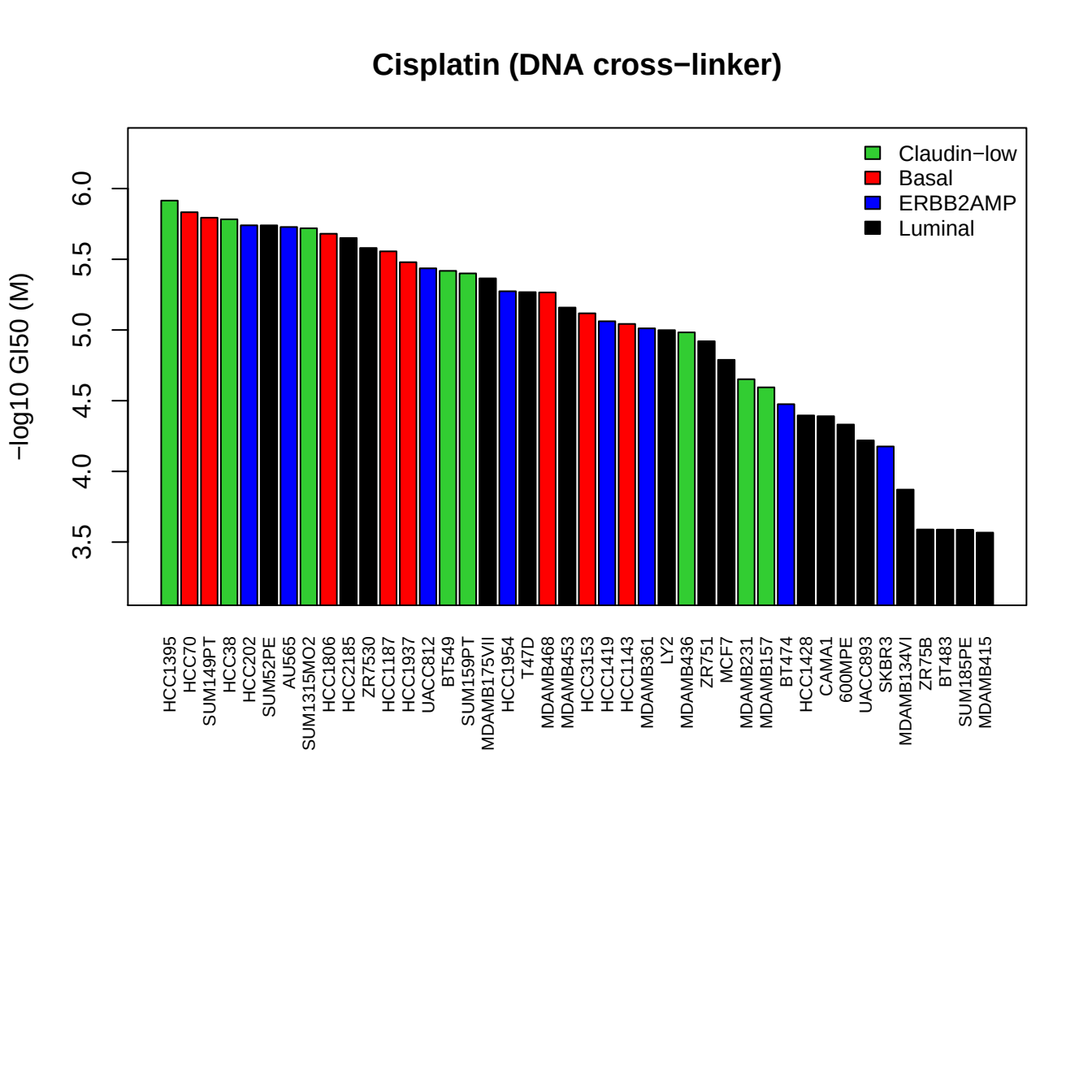
Cisplatin (DNA cross−linker)
−log10 GI50 (M)
3.5
4.0
4.5
5.0
5.5
6.0
Claudin−low
Basal
ERBB2AMP
Luminal
HCC1395
HCC70
SUM149PT
HCC38
HCC202
SUM52PE
AU565
SUM1315MO2
HCC1806
HCC2185
ZR7530
HCC1187
HCC1937
UACC812
BT549
SUM159PT
MDAMB175VII
HCC1954
T47D
MDAMB468
MDAMB453
HCC3153
HCC1419
HCC1143
MDAMB361
LY2
MDAMB436
ZR751
MCF7
MDAMB231
MDAMB157
BT474
HCC1428
CAMA1
600MPE
UACC893
SKBR3
MDAMB134VI
ZR75B
BT483
SUM185PE
MDAMB415

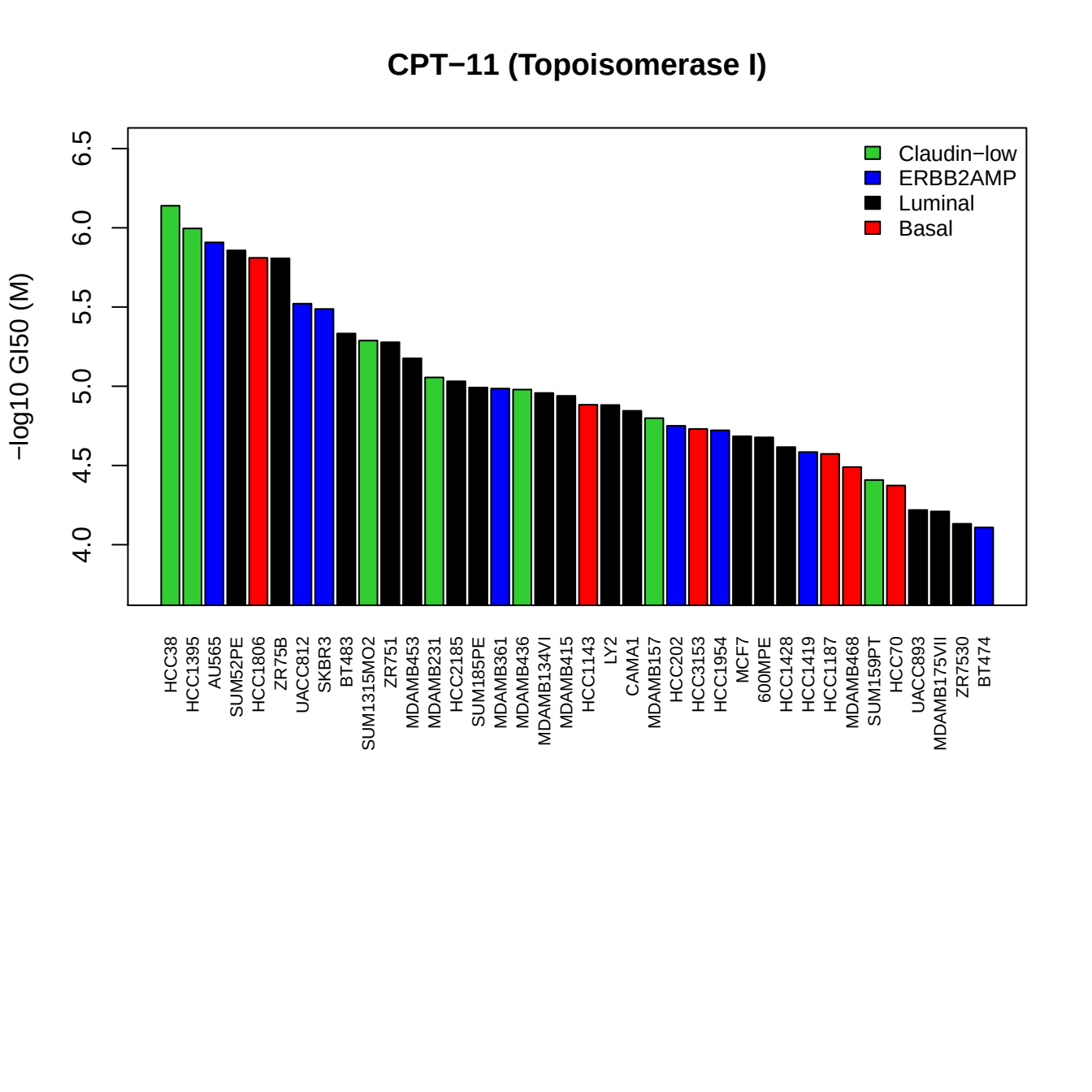
CPT−11 (Topoisomerase I)
−log10 GI50 (M)
4.0
4.5
5.0
5.5
6.0
6.5
Claudin−low
ERBB2AMP
Luminal
Basal
HCC38
HCC1395
AU565
SUM52PE
HCC1806
ZR75B
UACC812
SKBR3
BT483
SUM1315MO2
ZR751
MDAMB453
MDAMB231
HCC2185
SUM185PE
MDAMB361
MDAMB436
MDAMB134VI
MDAMB415
HCC1143
LY2
CAMA1
MDAMB157
HCC202
HCC3153
HCC1954
MCF7
600MPE
HCC1428
HCC1419
HCC1187
MDAMB468
SUM159PT
HCC70
UACC893
MDAMB175VII
ZR7530
BT474

Docetaxel (Microtubule)

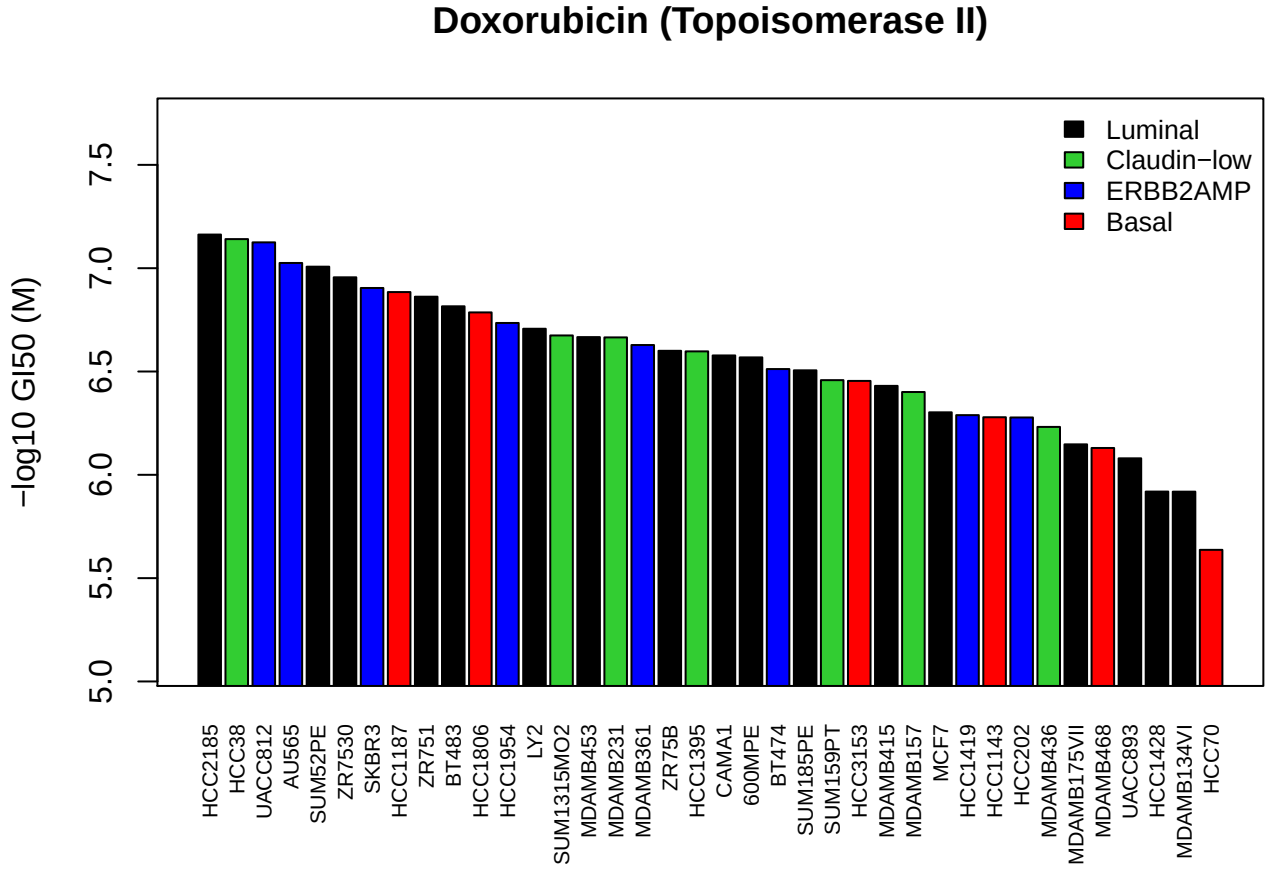
Doxorubicin (Topoisomerase II)
−log10 GI50 (M)
5.0
5.5
6.0
6.5
7.0
7.5
Luminal
Claudin−low
ERBB2AMP
Basal
HCC2185
HCC38
UACC812
AU565
SUM52PE
ZR7530
SKBR3
HCC1187
ZR751
BT483
HCC1806
HCC1954
LY2
SUM1315MO2
MDAMB453
MDAMB231
MDAMB361
ZR75B
HCC1395
CAMA1
600MPE
BT474
SUM185PE
SUM159PT
HCC3153
MDAMB415
MDAMB157
MCF7
HCC1419
HCC1143
HCC202
MDAMB436
MDAMB175VII
MDAMB468
UACC893
HCC1428
MDAMB134VI
HCC70

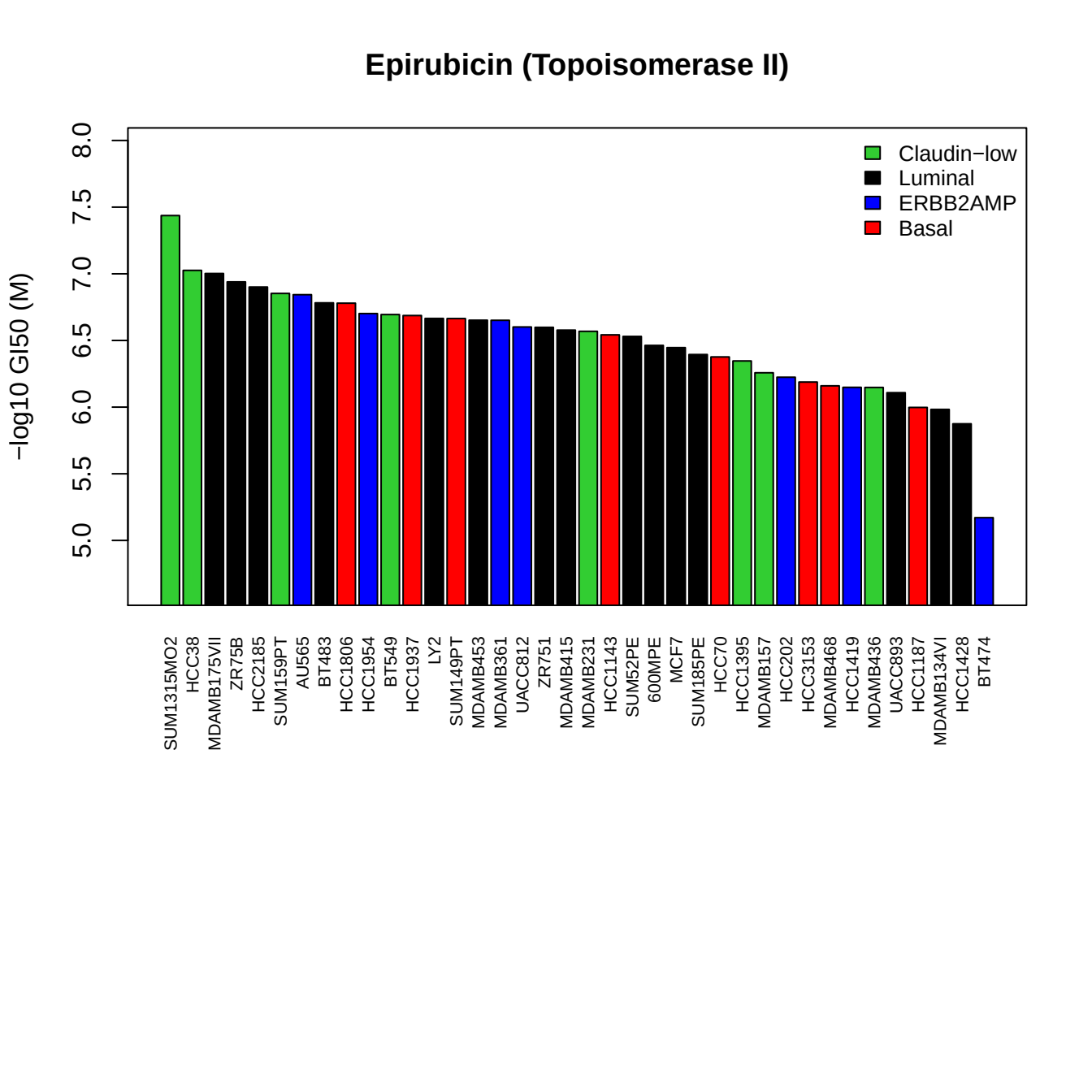
Epirubicin (Topoisomerase II)
−log10 GI50 (M)
5.0
5.5
6.0
6.5
7.0
7.5
8.0
Claudin−low
Luminal
ERBB2AMP
Basal
SUM1315MO2
HCC38
MDAMB175VII
ZR75B
HCC2185
SUM159PT
AU565
BT483
HCC1806
HCC1954
BT549
HCC1937
LY2
SUM149PT
MDAMB453
MDAMB361
UACC812
ZR751
MDAMB415
MDAMB231
HCC1143
SUM52PE
600MPE
MCF7
SUM185PE
HCC70
HCC1395
MDAMB157
HCC202
HCC3153
MDAMB468
HCC1419
MDAMB436
UACC893
HCC1187
MDAMB134VI
HCC1428
BT474

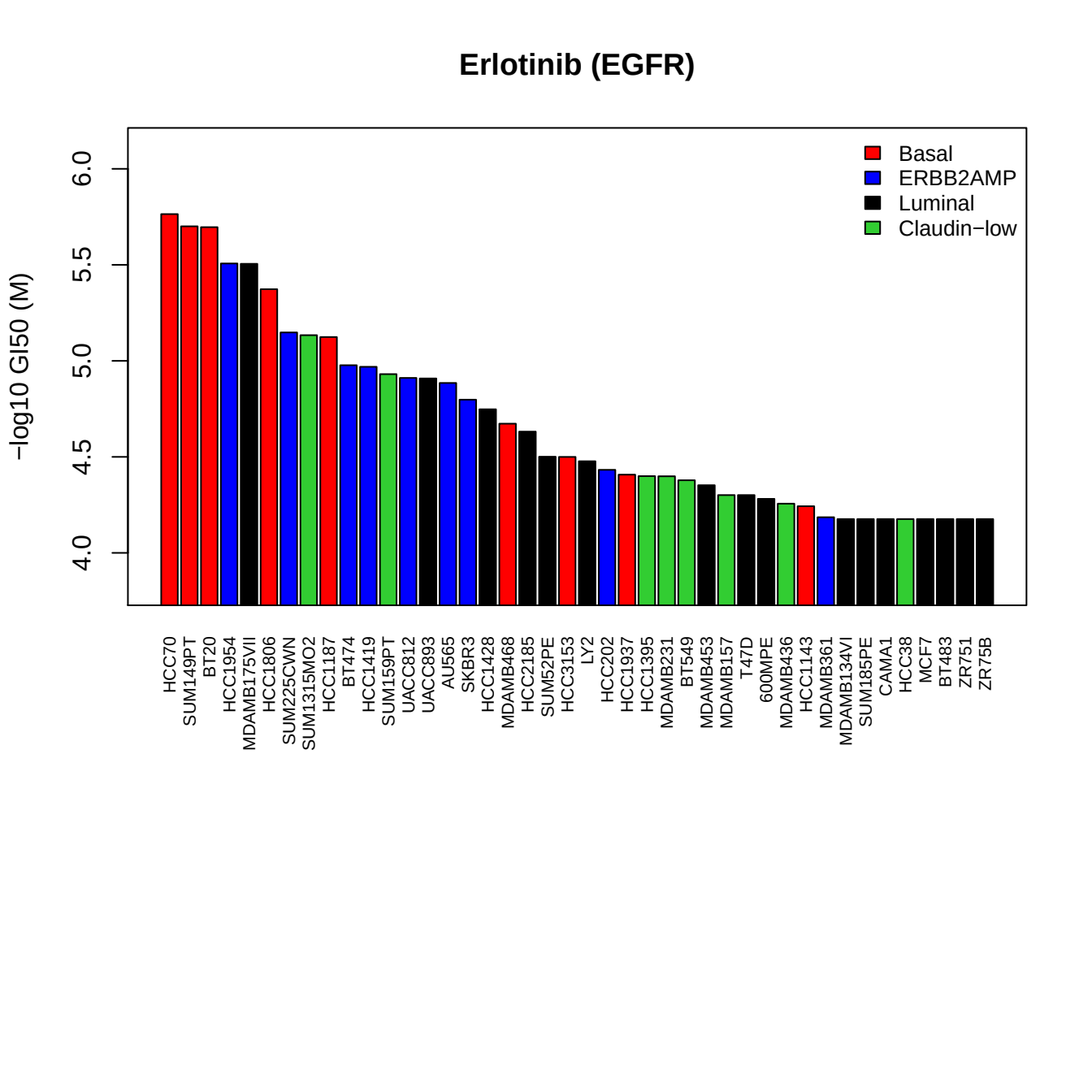
Erlotinib (EGFR)
−log10 GI50 (M)
4.0
4.5
5.0
5.5
6.0
Basal
ERBB2AMP
Luminal
Claudin−low
HCC70
SUM149PT
BT20
HCC1954
MDAMB175VII
HCC1806
SUM225CWN
SUM1315MO2
HCC1187
BT474
HCC1419
SUM159PT
UACC812
UACC893
AU565
SKBR3
HCC1428
MDAMB468
HCC2185
SUM52PE
HCC3153
LY2
HCC202
HCC1937
HCC1395
MDAMB231
BT549
MDAMB453
MDAMB157
T47D
600MPE
MDAMB436
HCC1143
MDAMB361
MDAMB134VI
SUM185PE
CAMA1
HCC38
MCF7
BT483
ZR751
ZR75B

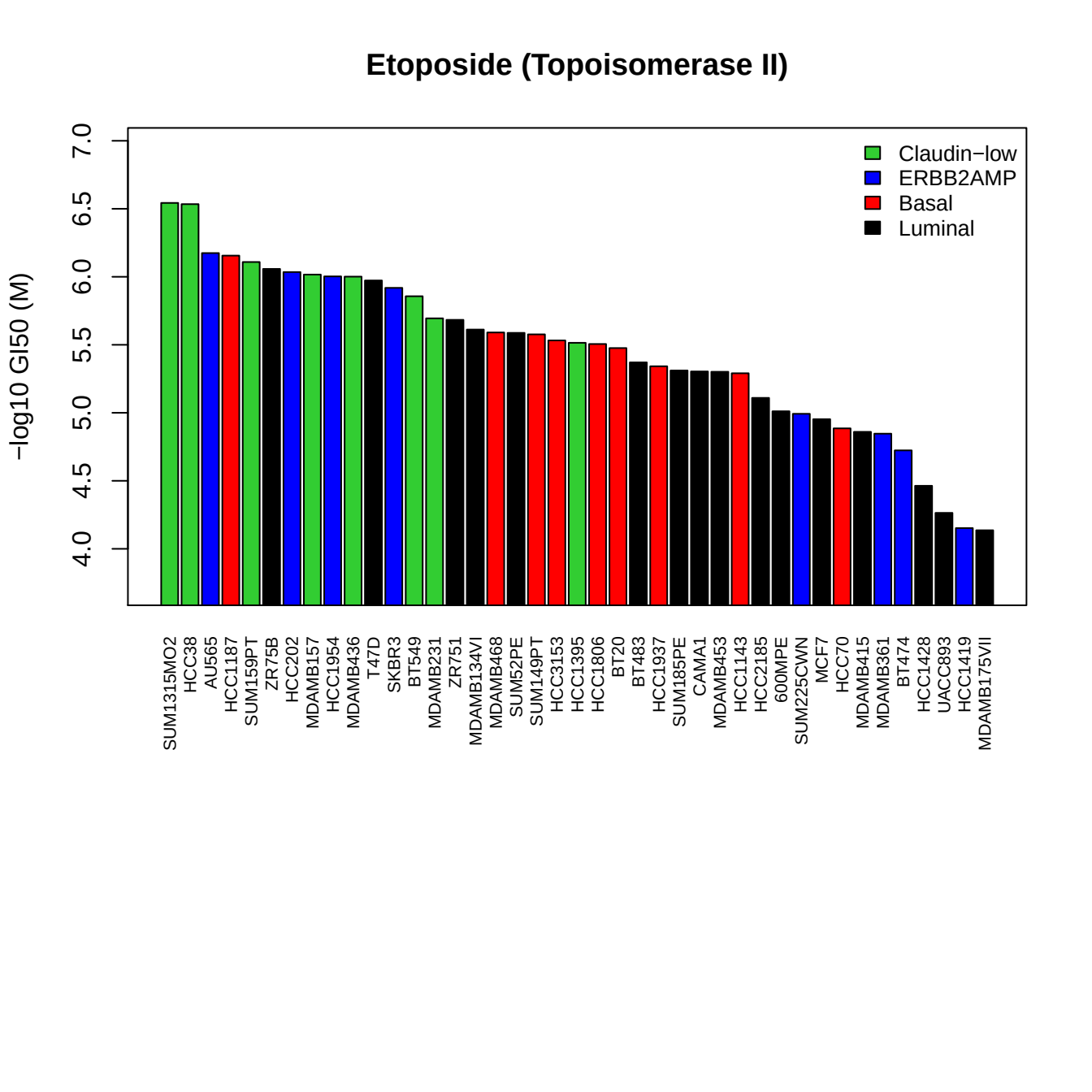
Etoposide (Topoisomerase II)
−log10 GI50 (M)
4.0
4.5
5.0
5.5
6.0
6.5
7.0
Claudin−low
ERBB2AMP
Basal
Luminal
SUM1315MO2
HCC38
AU565
HCC1187
SUM159PT
ZR75B
HCC202
MDAMB157
HCC1954
MDAMB436
T47D
SKBR3
BT549
MDAMB231
ZR751
MDAMB134VI
MDAMB468
SUM52PE
SUM149PT
HCC3153
HCC1395
HCC1806
BT20
BT483
HCC1937
SUM185PE
CAMA1
MDAMB453
HCC1143
HCC2185
600MPE
SUM225CWN
MCF7
HCC70
MDAMB415
MDAMB361
BT474
HCC1428
UACC893
HCC1419
MDAMB175VII

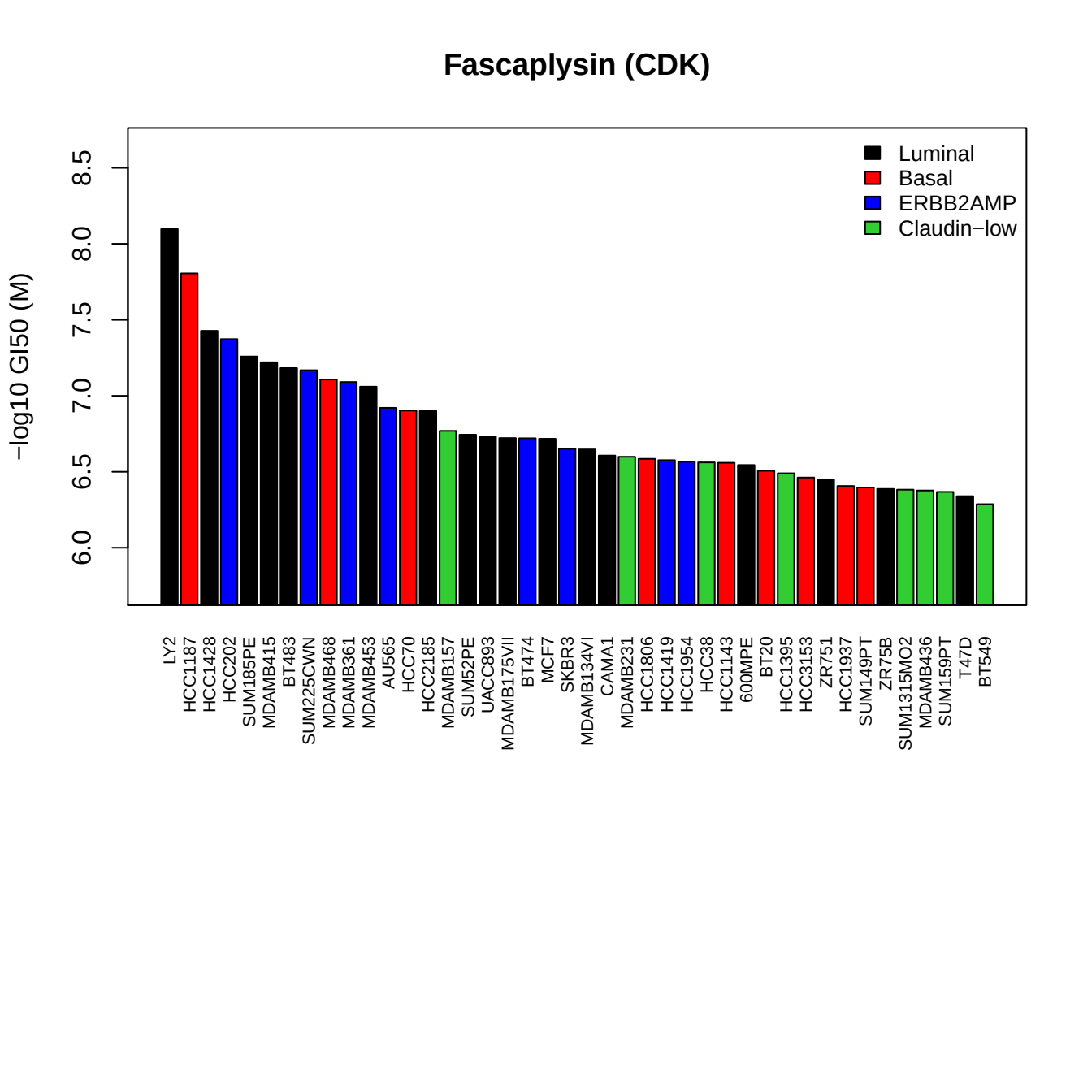
Fascaplysin (CDK)
−log10 GI50 (M)
6.0
6.5
7.0
7.5
8.0
8.5
Luminal
Basal
ERBB2AMP
Claudin−low
LY2
HCC1187
HCC1428
HCC202
SUM185PE
MDAMB415
BT483
SUM225CWN
MDAMB468
MDAMB361
MDAMB453
AU565
HCC70
HCC2185
MDAMB157
SUM52PE
UACC893
MDAMB175VII
BT474
MCF7
SKBR3
MDAMB134VI
CAMA1
MDAMB231
HCC1806
HCC1419
HCC1954
HCC38
HCC1143
600MPE
BT20
HCC1395
HCC3153
ZR751
HCC1937
SUM149PT
ZR75B
SUM1315MO2
MDAMB436
SUM159PT
T47D
BT549

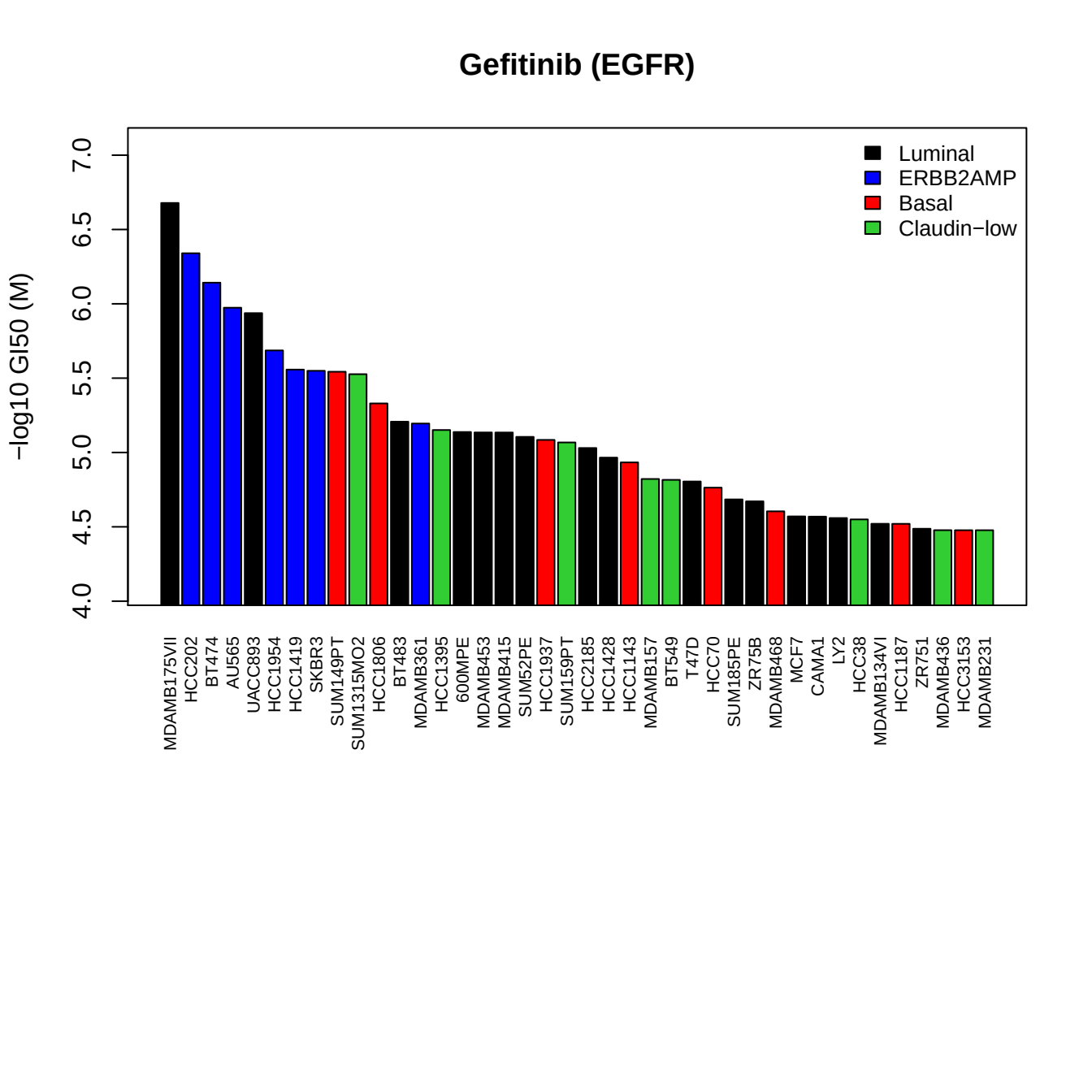
Gefitinib (EGFR)
−log10 GI50 (M)
4.0
4.5
5.0
5.5
6.0
6.5
7.0
Luminal
ERBB2AMP
Basal
Claudin−low
MDAMB175VII
HCC202
BT474
AU565
UACC893
HCC1954
HCC1419
SKBR3
SUM149PT
SUM1315MO2
HCC1806
BT483
MDAMB361
HCC1395
600MPE
MDAMB453
MDAMB415
SUM52PE
HCC1937
SUM159PT
HCC2185
HCC1428
HCC1143
MDAMB157
BT549
T47D
HCC70
SUM185PE
ZR75B
MDAMB468
MCF7
CAMA1
LY2
HCC38
MDAMB134VI
HCC1187
ZR751
MDAMB436
HCC3153
MDAMB231

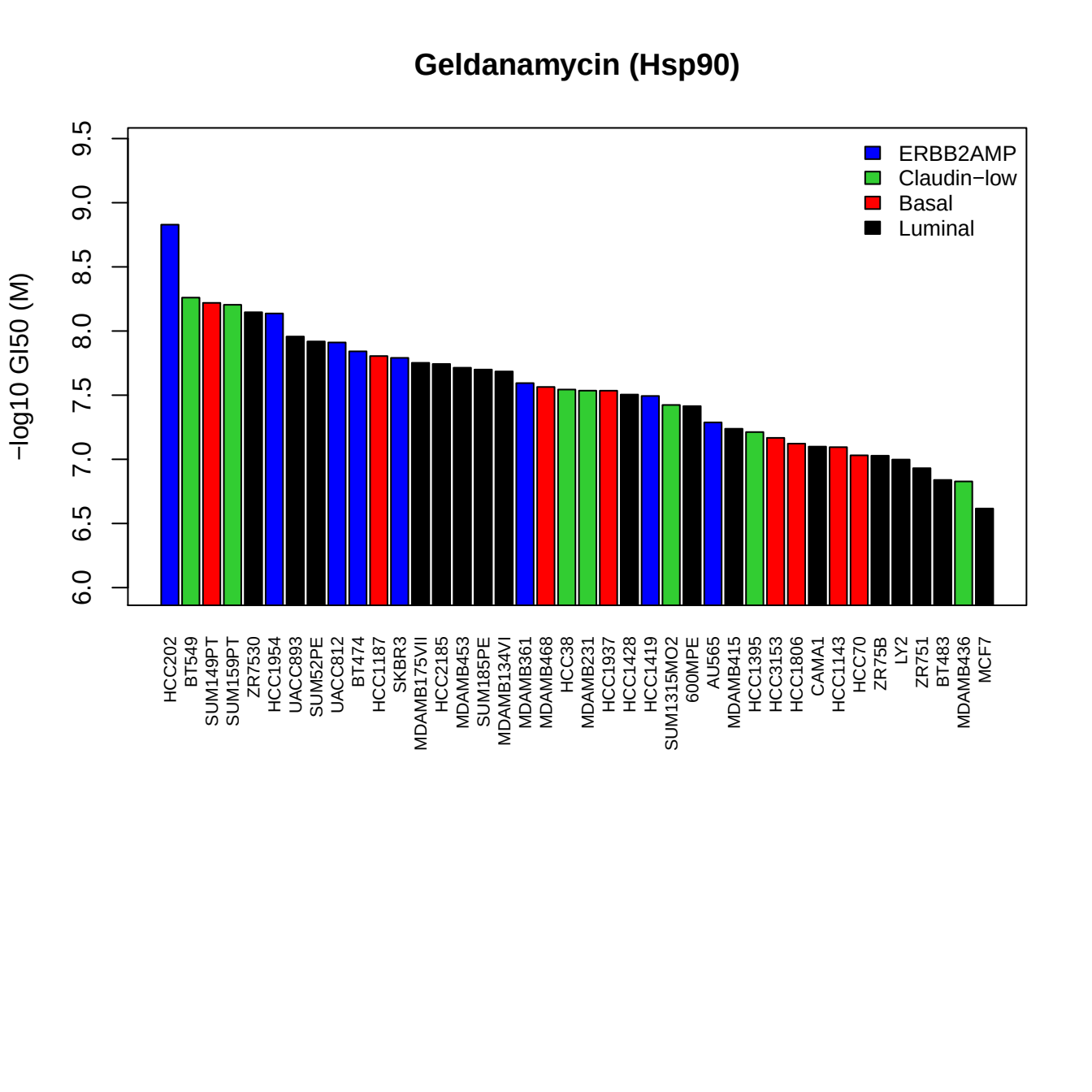
Geldanamycin (Hsp90)
−log10 GI50 (M)
6.0
6.5
7.0
7.5
8.0
8.5
9.0
9.5
ERBB2AMP
Claudin−low
Basal
Luminal
HCC202
BT549
SUM149PT
SUM159PT
ZR7530
HCC1954
UACC893
SUM52PE
UACC812
BT474
HCC1187
SKBR3
MDAMB175VII
HCC2185
MDAMB453
SUM185PE
MDAMB134VI
MDAMB361
MDAMB468
HCC38
MDAMB231
HCC1937
HCC1428
HCC1419
SUM1315MO2
600MPE
AU565
MDAMB415
HCC1395
HCC3153
HCC1806
CAMA1
HCC1143
HCC70
ZR75B
LY2
ZR751
BT483
MDAMB436
MCF7

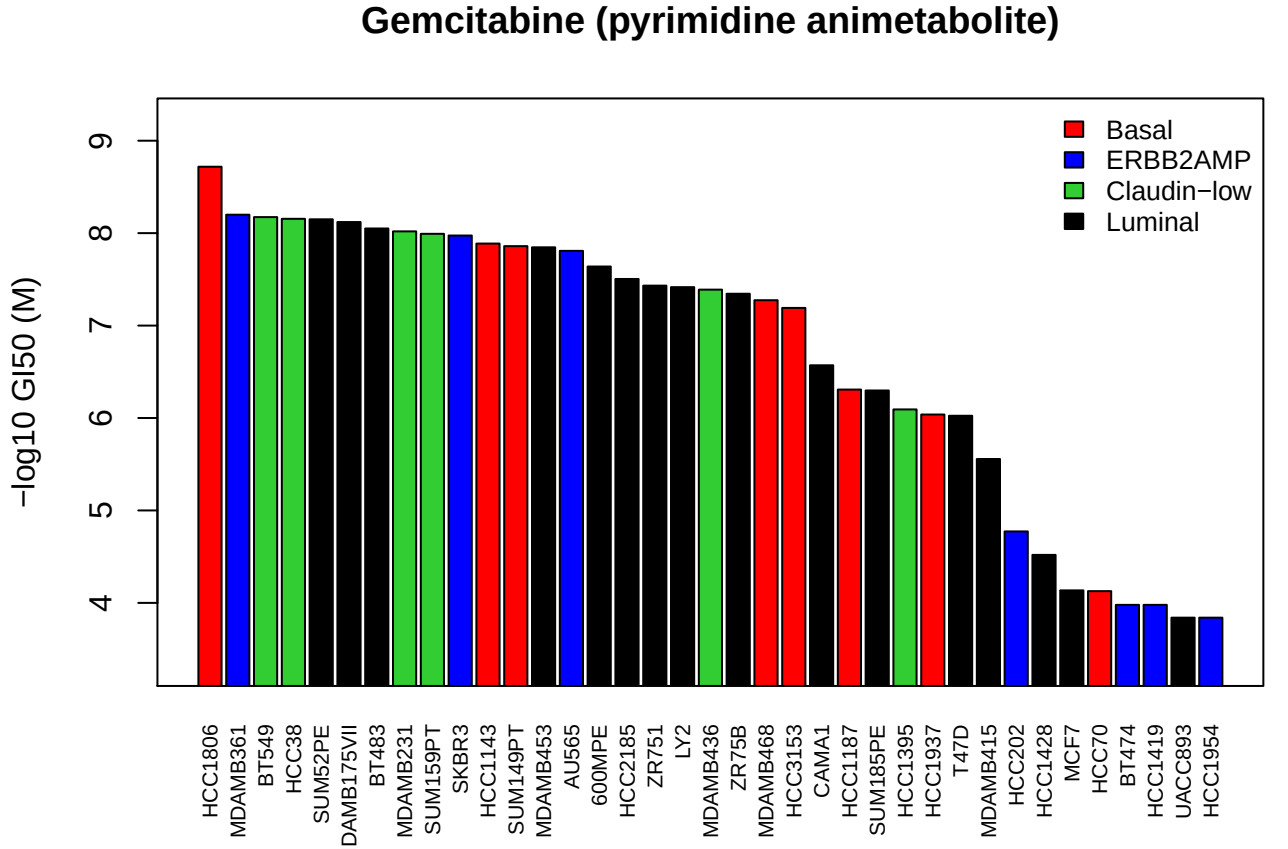
Gemcitabine (pyrimidine animetabolite)
−log10 GI50 (M)
4
5
6
7
8
9
Basal
ERBB2AMP
Claudin−low
Luminal
HCC1806
MDAMB361
BT549
HCC38
SUM52PE
MDAMB175VII
BT483
MDAMB231
SUM159PT
SKBR3
HCC1143
SUM149PT
MDAMB453
AU565
600MPE
HCC2185
ZR751
LY2
MDAMB436
ZR75B
MDAMB468
HCC3153
CAMA1
HCC1187
SUM185PE
HCC1395
HCC1937
T47D
MDAMB415
HCC202
HCC1428
MCF7
HCC70
BT474
HCC1419
UACC893
HCC1954

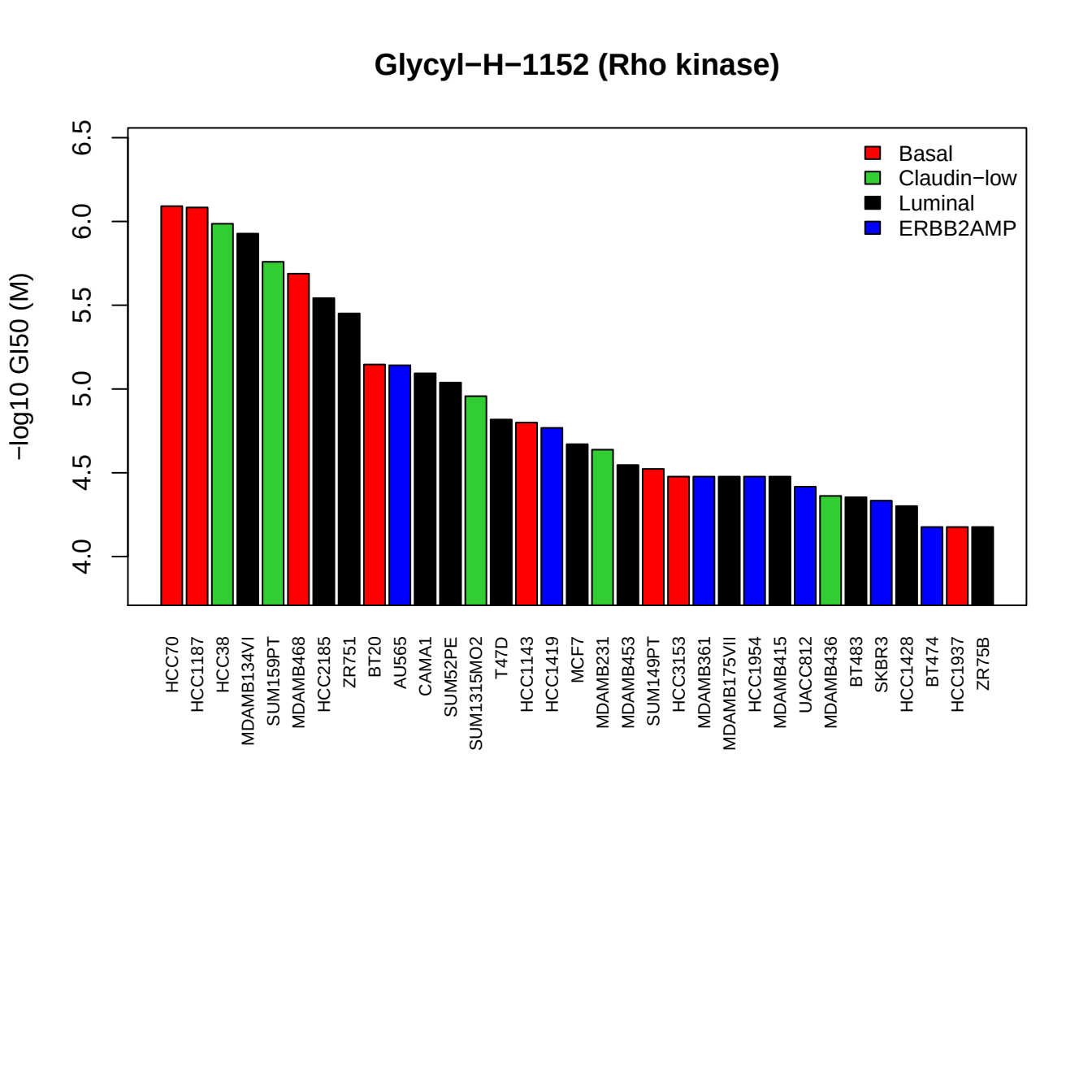
Glycyl−H−1152 (Rho kinase)
−log10 GI50 (M)
4.0
4.5
5.0
5.5
6.0
6.5
Basal
Claudin−low
Luminal
ERBB2AMP
HCC70
HCC1187
HCC38
MDAMB134VI
SUM159PT
MDAMB468
HCC2185
ZR751
BT20
AU565
CAMA1
SUM52PE
SUM1315MO2
T47D
HCC1143
HCC1419
MCF7
MDAMB231
MDAMB453
SUM149PT
HCC3153
MDAMB361
MDAMB175VII
HCC1954
MDAMB415
UACC812
MDAMB436
BT483
SKBR3
HCC1428
BT474
HCC1937
ZR75B

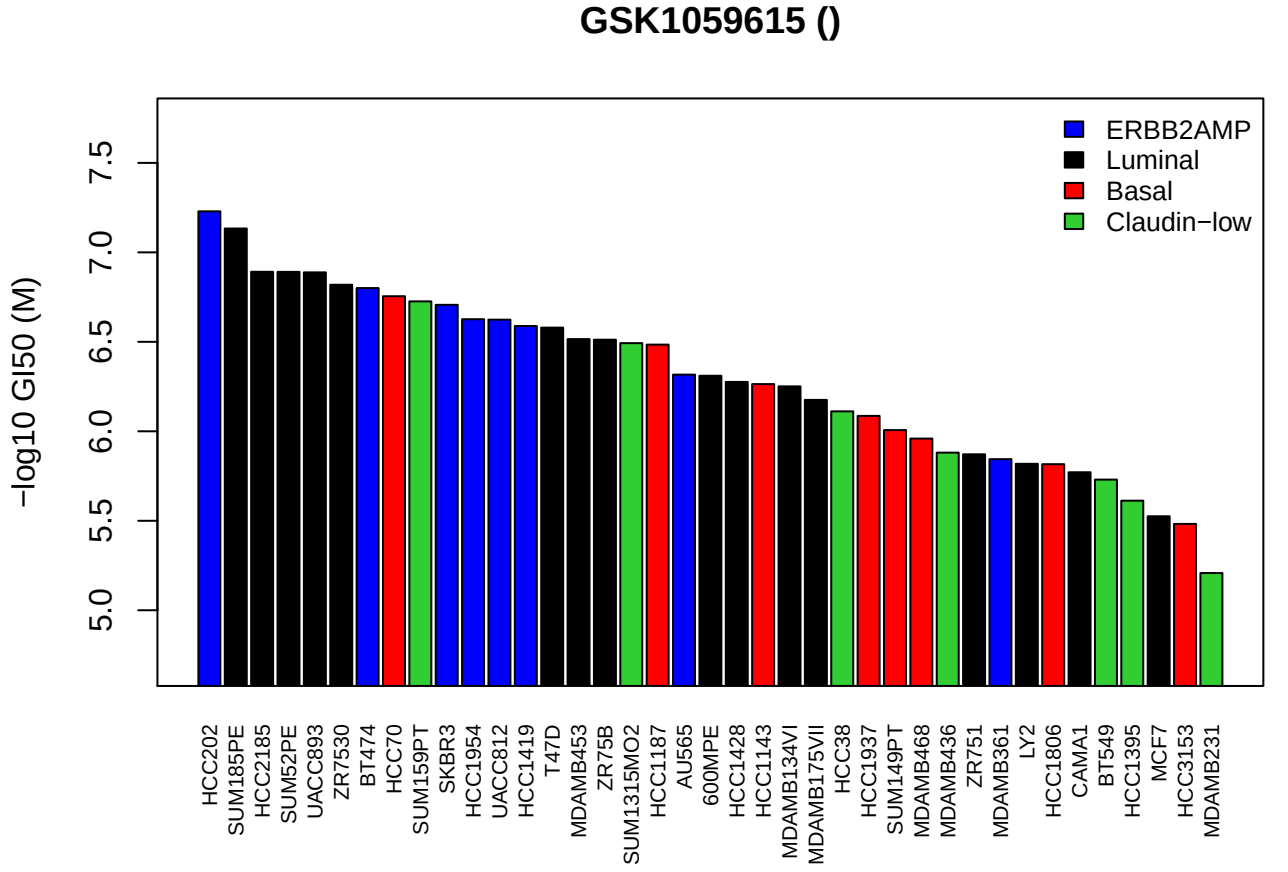
GSK1059615 ()
−log10 GI50 (M)
5.0
5.5
6.0
6.5
7.0
7.5
ERBB2AMP
Luminal
Basal
Claudin−low
HCC202
SUM185PE
HCC2185
SUM52PE
UACC893
ZR7530
BT474
HCC70
SUM159PT
SKBR3
HCC1954
UACC812
HCC1419
T47D
MDAMB453
ZR75B
SUM1315MO2
HCC1187
AU565
600MPE
HCC1428
HCC1143
MDAMB134VI
MDAMB175VII
HCC38
HCC1937
SUM149PT
MDAMB468
MDAMB436
ZR751
MDAMB361
LY2
HCC1806
CAMA1
BT549
HCC1395
MCF7
HCC3153
MDAMB231

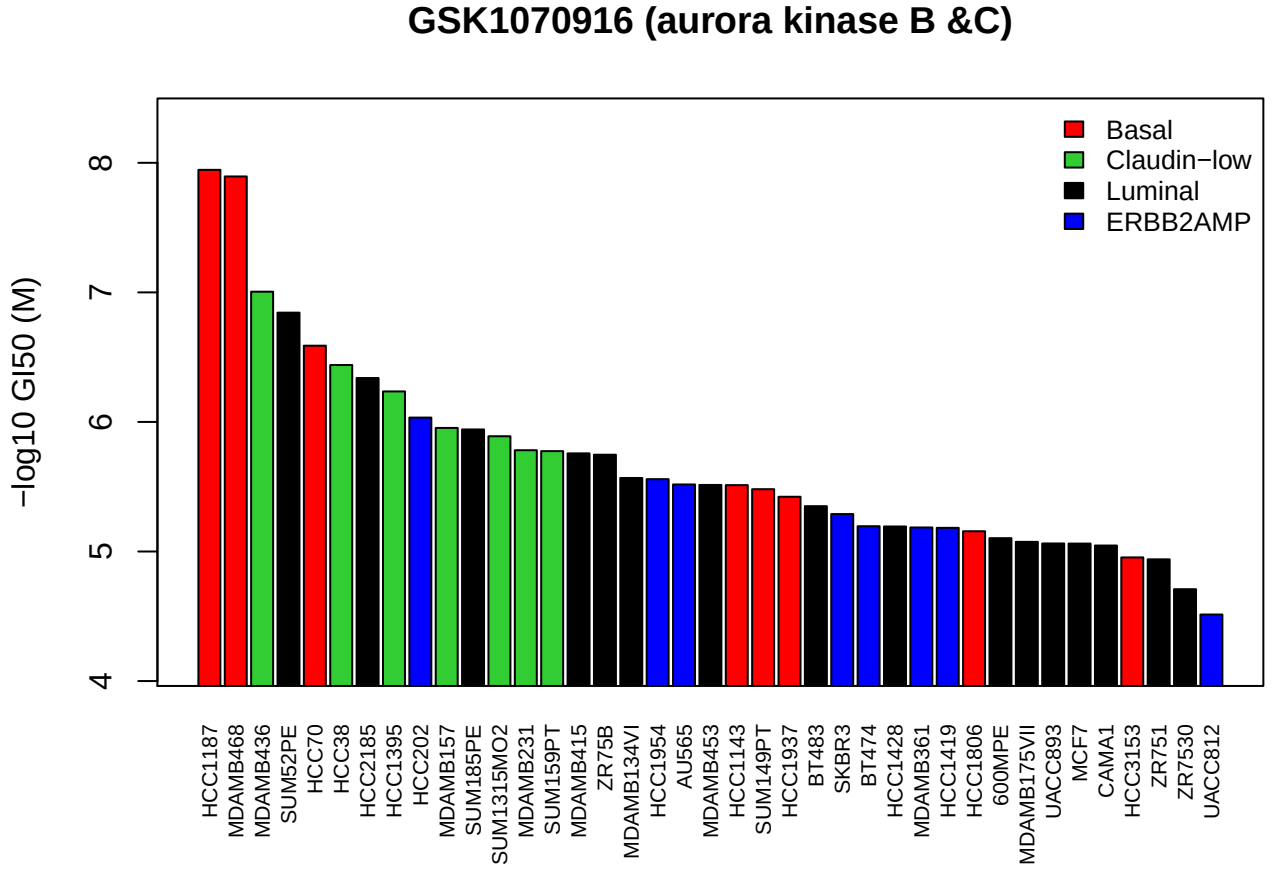
GSK1070916 (aurora kinase B &C)
−log10 GI50 (M)
4
5
6
7
8
Basal
Claudin−low
Luminal
ERBB2AMP
HCC1187
MDAMB468
MDAMB436
SUM52PE
HCC70
HCC38
HCC2185
HCC1395
HCC202
MDAMB157
SUM185PE
SUM1315MO2
MDAMB231
SUM159PT
MDAMB415
ZR75B
MDAMB134VI
HCC1954
AU565
MDAMB453
HCC1143
SUM149PT
HCC1937
BT483
SKBR3
BT474
HCC1428
MDAMB361
HCC1419
HCC1806
600MPE
MDAMB175VII
UACC893
MCF7
CAMA1
HCC3153
ZR751
ZR7530
UACC812

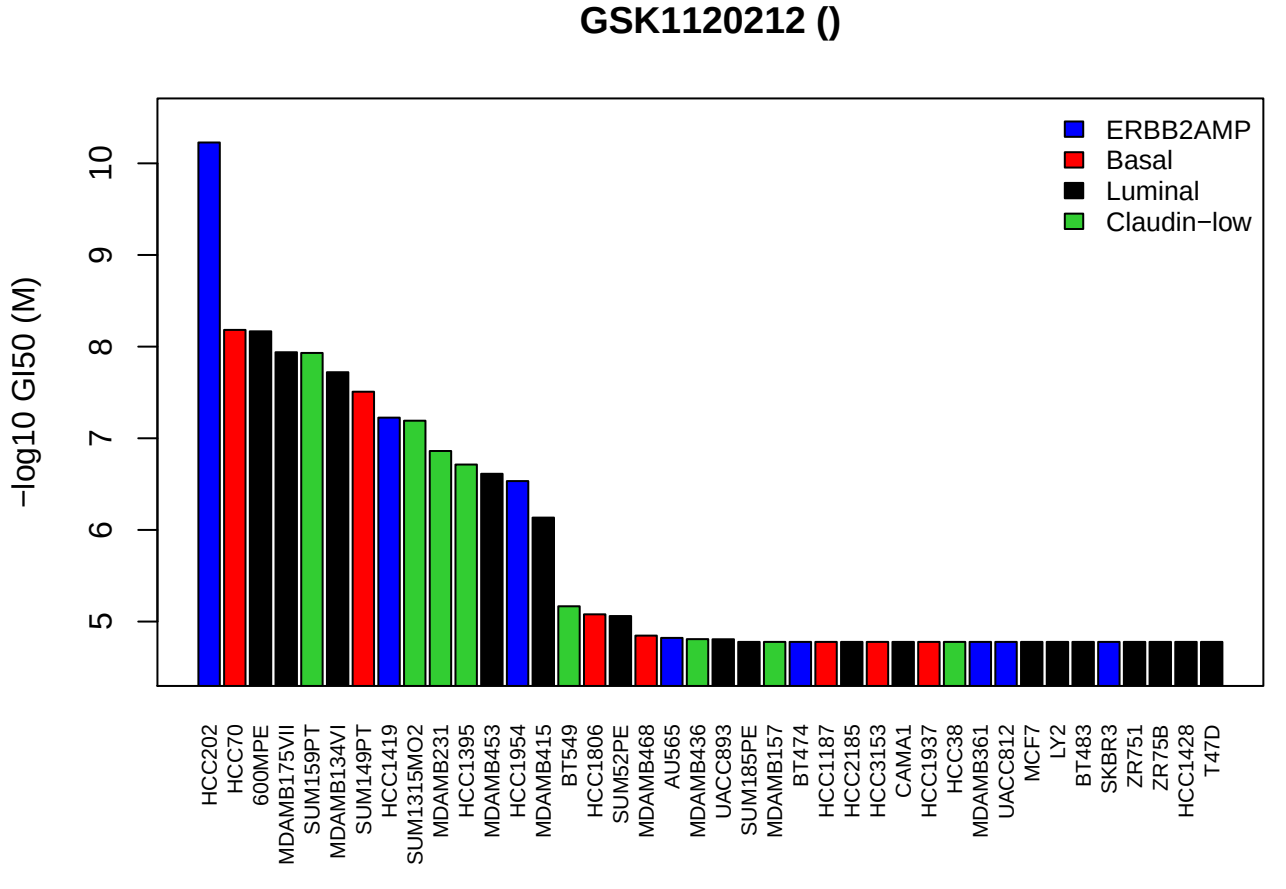
GSK1120212 ()
−log10 GI50 (M)
5
6
7
8
9
10
ERBB2AMP
Basal
Luminal
Claudin−low
HCC202
HCC70
600MPE
MDAMB175VII
SUM159PT
MDAMB134VI
SUM149PT
HCC1419
SUM1315MO2
MDAMB231
HCC1395
MDAMB453
HCC1954
MDAMB415
BT549
HCC1806
SUM52PE
MDAMB468
AU565
MDAMB436
UACC893
SUM185PE
MDAMB157
BT474
HCC1187
HCC2185
HCC3153
CAMA1
HCC1937
HCC38
MDAMB361
UACC812
MCF7
LY2
BT483
SKBR3
ZR751
ZR75B
HCC1428
T47D

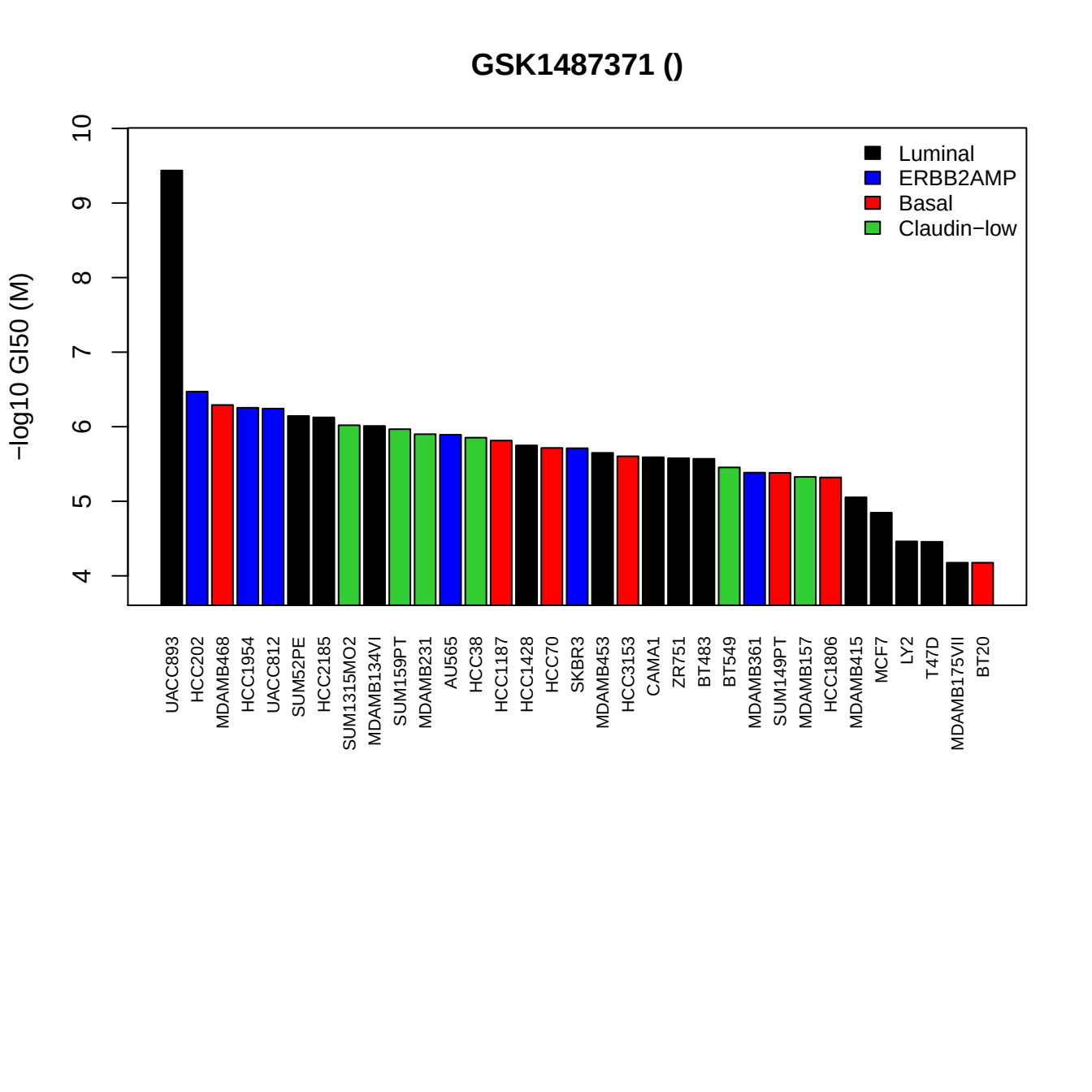
GSK1487371 ()
−log10 GI50 (M)
4
5
6
7
8
9
10
Luminal
ERBB2AMP
Basal
Claudin−low
UACC893
HCC202
MDAMB468
HCC1954
UACC812
SUM52PE
HCC2185
SUM1315MO2
MDAMB134VI
SUM159PT
MDAMB231
AU565
HCC38
HCC1187
HCC1428
HCC70
SKBR3
MDAMB453
HCC3153
CAMA1
ZR751
BT483
BT549
MDAMB361
SUM149PT
MDAMB157
HCC1806
MDAMB415
MCF7
LY2
T47D
MDAMB175VII
BT20

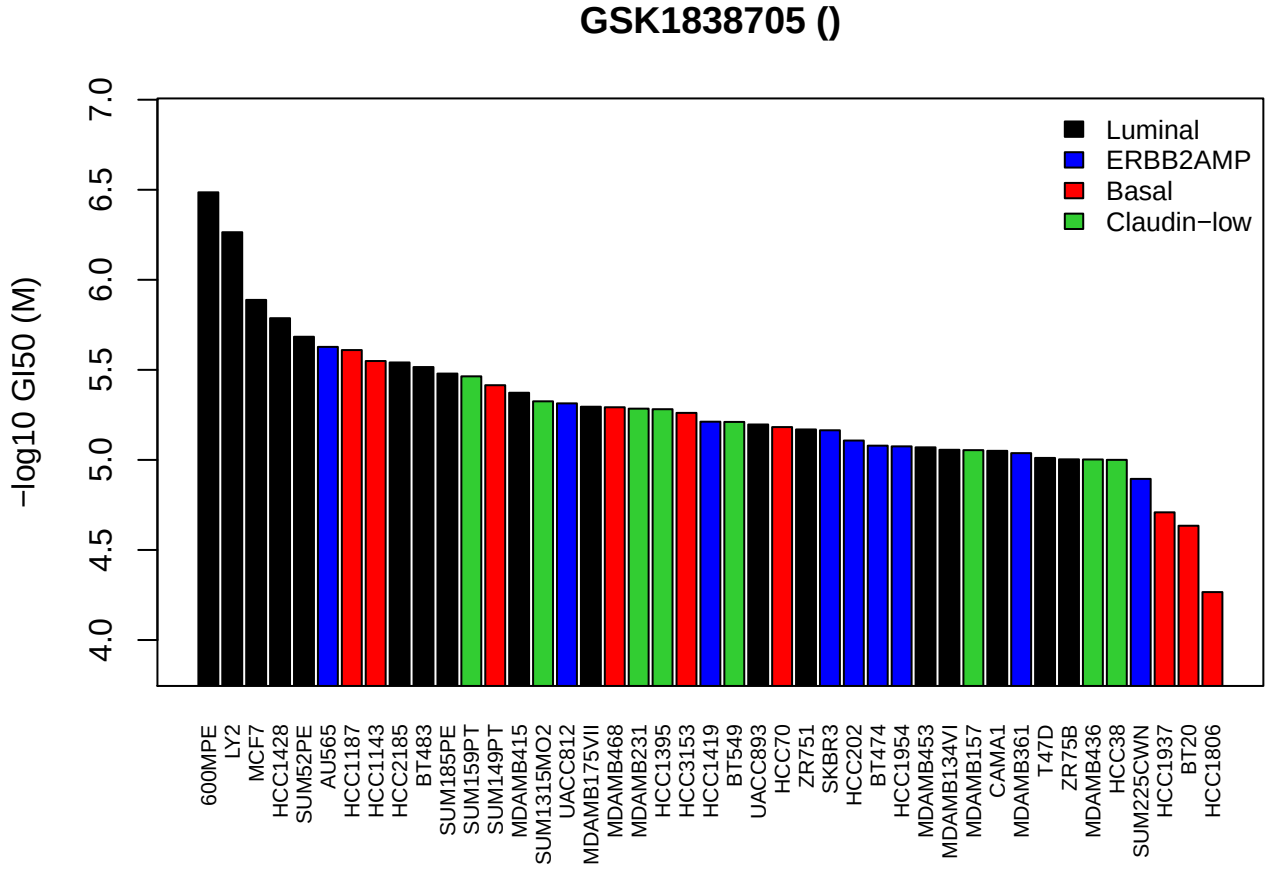
GSK1838705 ()
−log10 GI50 (M)
4.0
4.5
5.0
5.5
6.0
6.5
7.0
Luminal
ERBB2AMP
Basal
Claudin−low
600MPE
LY2
MCF7
HCC1428
SUM52PE
AU565
HCC1187
HCC1143
HCC2185
BT483
SUM185PE
SUM159PT
SUM149PT
MDAMB415
SUM1315MO2
UACC812
MDAMB175VII
MDAMB468
MDAMB231
HCC1395
HCC3153
HCC1419
BT549
UACC893
HCC70
ZR751
SKBR3
HCC202
BT474
HCC1954
MDAMB453
MDAMB134VI
MDAMB157
CAMA1
MDAMB361
T47D
ZR75B
MDAMB436
HCC38
SUM225CWN
HCC1937
BT20
HCC1806

GSK2119563 ()

−log10 GI50 (M)
4
5
6
7
8
ERBB2AMP
Luminal
Claudin−low
Basal
HCC202
SUM52PE
BT483
HCC1419
T47D
UACC812
BT474
SKBR3
UACC893
SUM159PT
MDAMB453
LY2
MDAMB134VI
AU565
SUM1315MO2
600MPE
HCC1187
HCC70
HCC38
MCF7
HCC1428
HCC1954
BT20
MDAMB175VII
MDAMB468
HCC1806
SUM149PT
ZR75B
MDAMB361
ZR751
HCC1937
MDAMB436
HCC1143
BT549
HCC1395
MDAMB231
CAMA1
MDAMB157
HCC3153

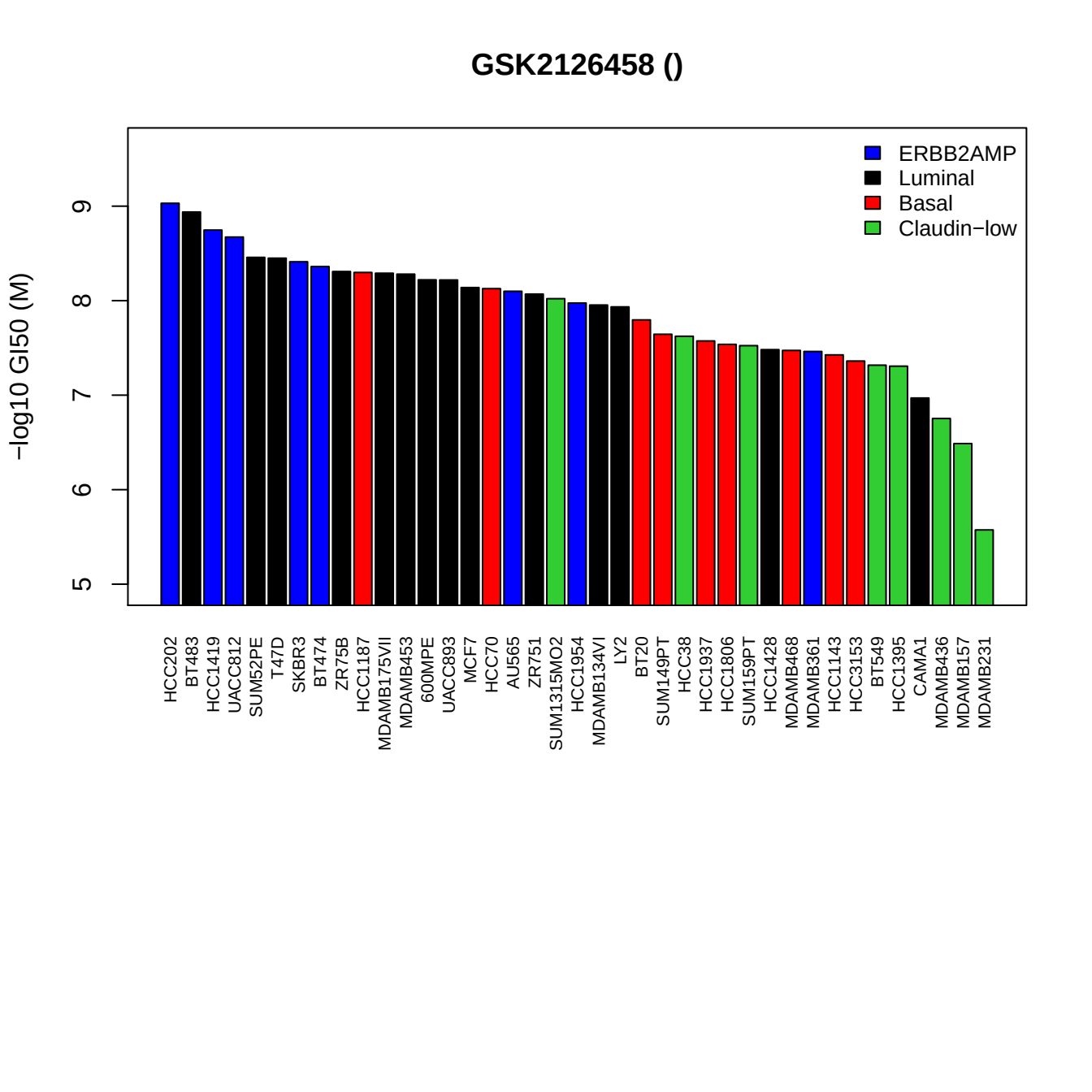
GSK2126458 ()
−log10 GI50 (M)
5
6
7
8
9
ERBB2AMP
Luminal
Basal
Claudin−low
HCC202
BT483
HCC1419
UACC812
SUM52PE
T47D
SKBR3
BT474
ZR75B
HCC1187
MDAMB175VII
MDAMB453
600MPE
UACC893
MCF7
HCC70
AU565
ZR751
SUM1315MO2
HCC1954
MDAMB134VI
LY2
BT20
SUM149PT
HCC38
HCC1937
HCC1806
SUM159PT
HCC1428
MDAMB468
MDAMB361
HCC1143
HCC3153
BT549
HCC1395
CAMA1
MDAMB436
MDAMB157
MDAMB231

GSK461364 ()

−log10 GI50 (M)
4
5
6
7
8
9
Claudin−low
ERBB2AMP
Basal
Luminal
MDAMB157
MDAMB361
MDAMB468
AU565
HCC1395
HCC2185
SUM52PE
HCC1954
UACC893
MDAMB453
HCC1806
MDAMB436
MDAMB134VI
MCF7
SKBR3
SUM149PT
MDAMB231
HCC1937
SUM1315MO2
HCC3153
SUM159PT
HCC1187
HCC38
HCC1143
MDAMB415
ZR75B
HCC70
SUM185PE
BT483
HCC1428
MDAMB175VII
ZR7530
CAMA1
600MPE
HCC1419
BT474
UACC812
ZR751
HCC202

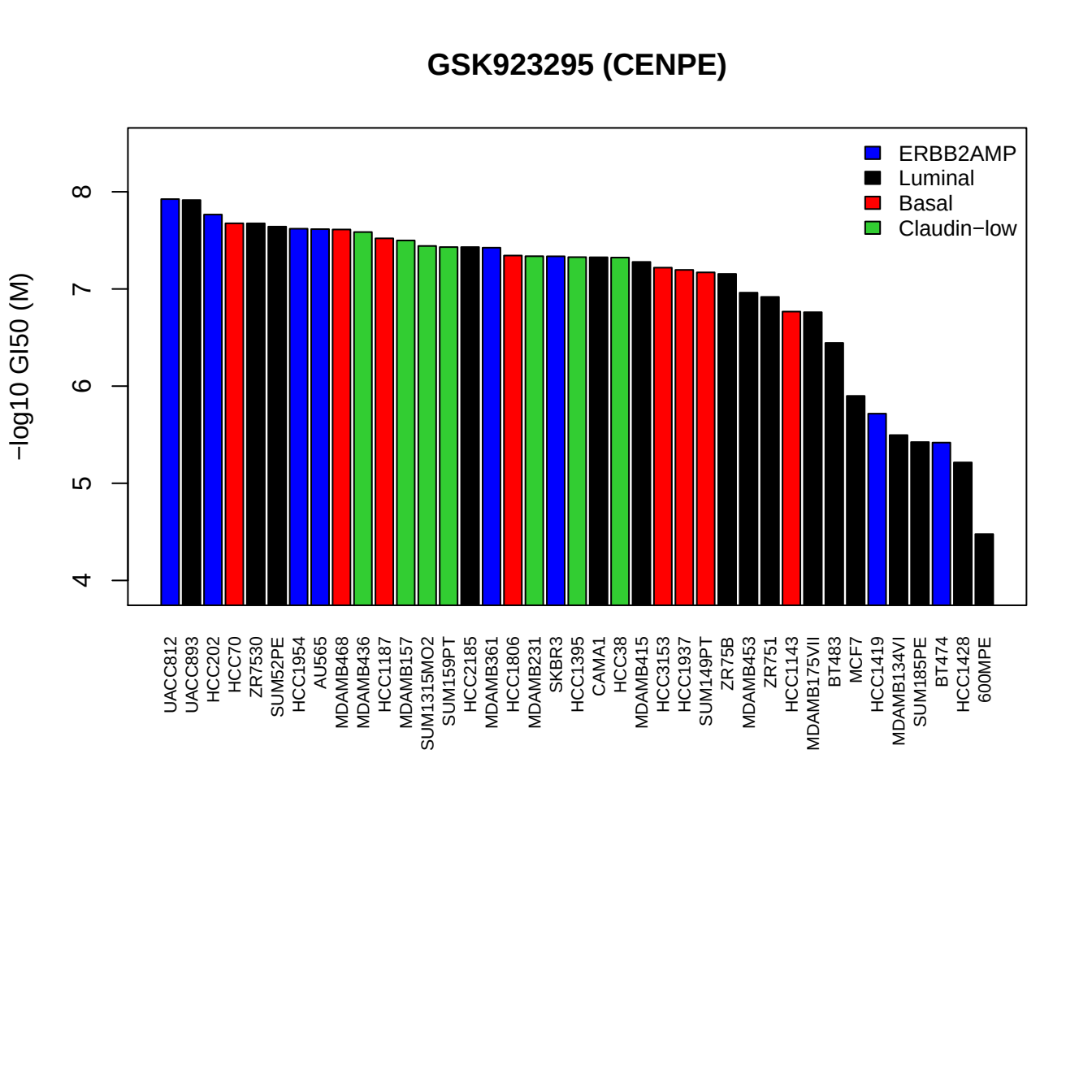
GSK923295 (CENPE)
−log10 GI50 (M)
4
5
6
7
8
ERBB2AMP
Luminal
Basal
Claudin−low
UACC812
UACC893
HCC202
HCC70
ZR7530
SUM52PE
HCC1954
AU565
MDAMB468
MDAMB436
HCC1187
MDAMB157
SUM1315MO2
SUM159PT
HCC2185
MDAMB361
HCC1806
MDAMB231
SKBR3
HCC1395
CAMA1
HCC38
MDAMB415
HCC3153
HCC1937
SUM149PT
ZR75B
MDAMB453
ZR751
HCC1143
MDAMB175VII
BT483
MCF7
HCC1419
MDAMB134VI
SUM185PE
BT474
HCC1428
600MPE

Ibandronate sodium salt (farnesyl diphosphate synthase)

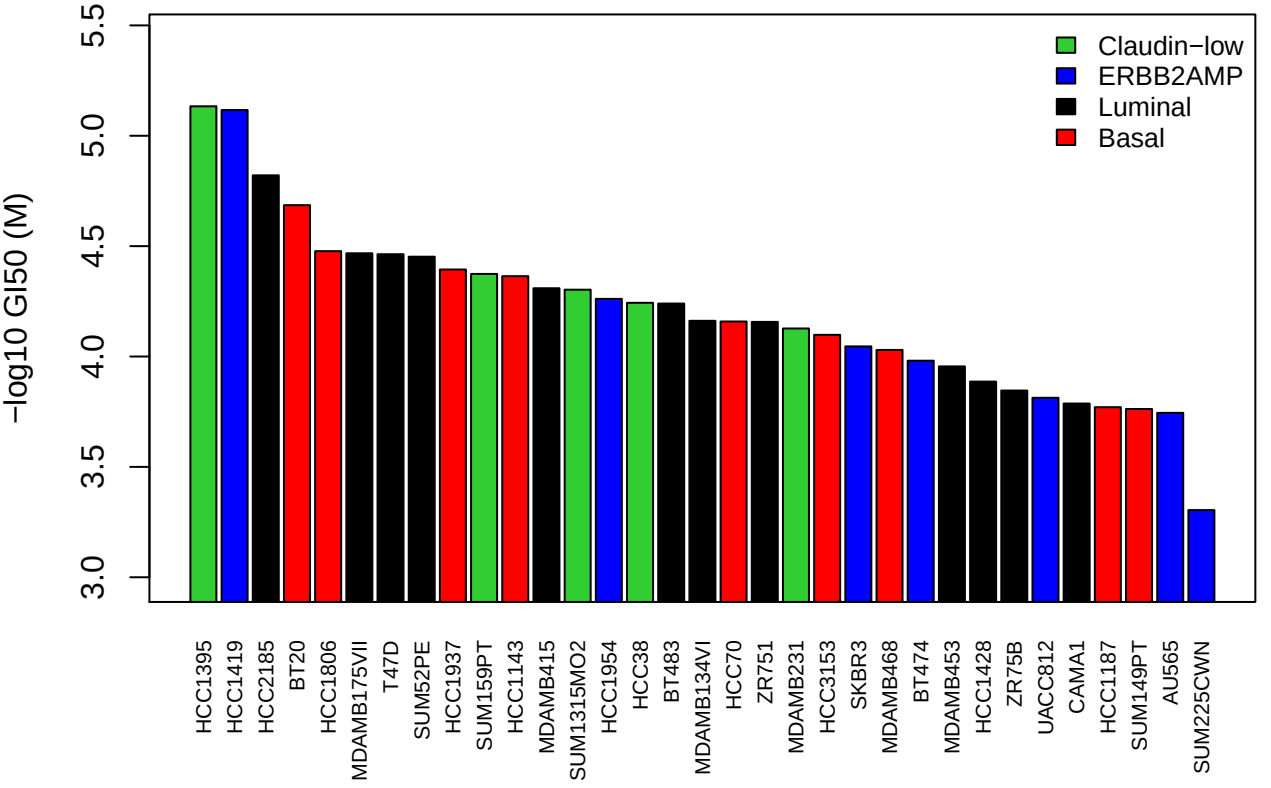

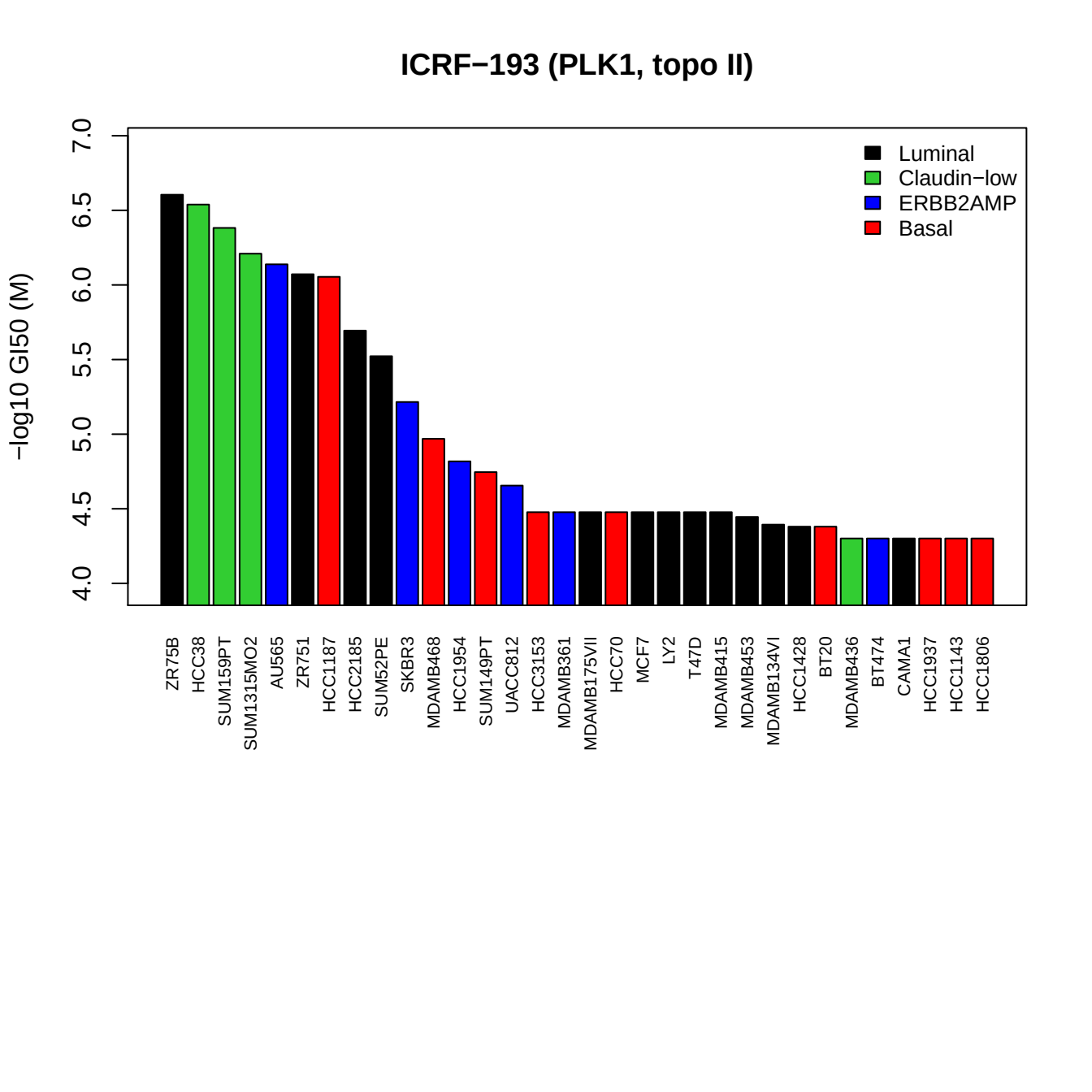
ICRF−193 (PLK1, topo II)
−log10 GI50 (M)
4.0
4.5
5.0
5.5
6.0
6.5
7.0
Luminal
Claudin−low
ERBB2AMP
Basal
ZR75B
HCC38
SUM159PT
SUM1315MO2
AU565
ZR751
HCC1187
HCC2185
SUM52PE
SKBR3
MDAMB468
HCC1954
SUM149PT
UACC812
HCC3153
MDAMB361
MDAMB175VII
HCC70
MCF7
LY2
T47D
MDAMB415
MDAMB453
MDAMB134VI
HCC1428
BT20
MDAMB436
BT474
CAMA1
HCC1937
HCC1143
HCC1806

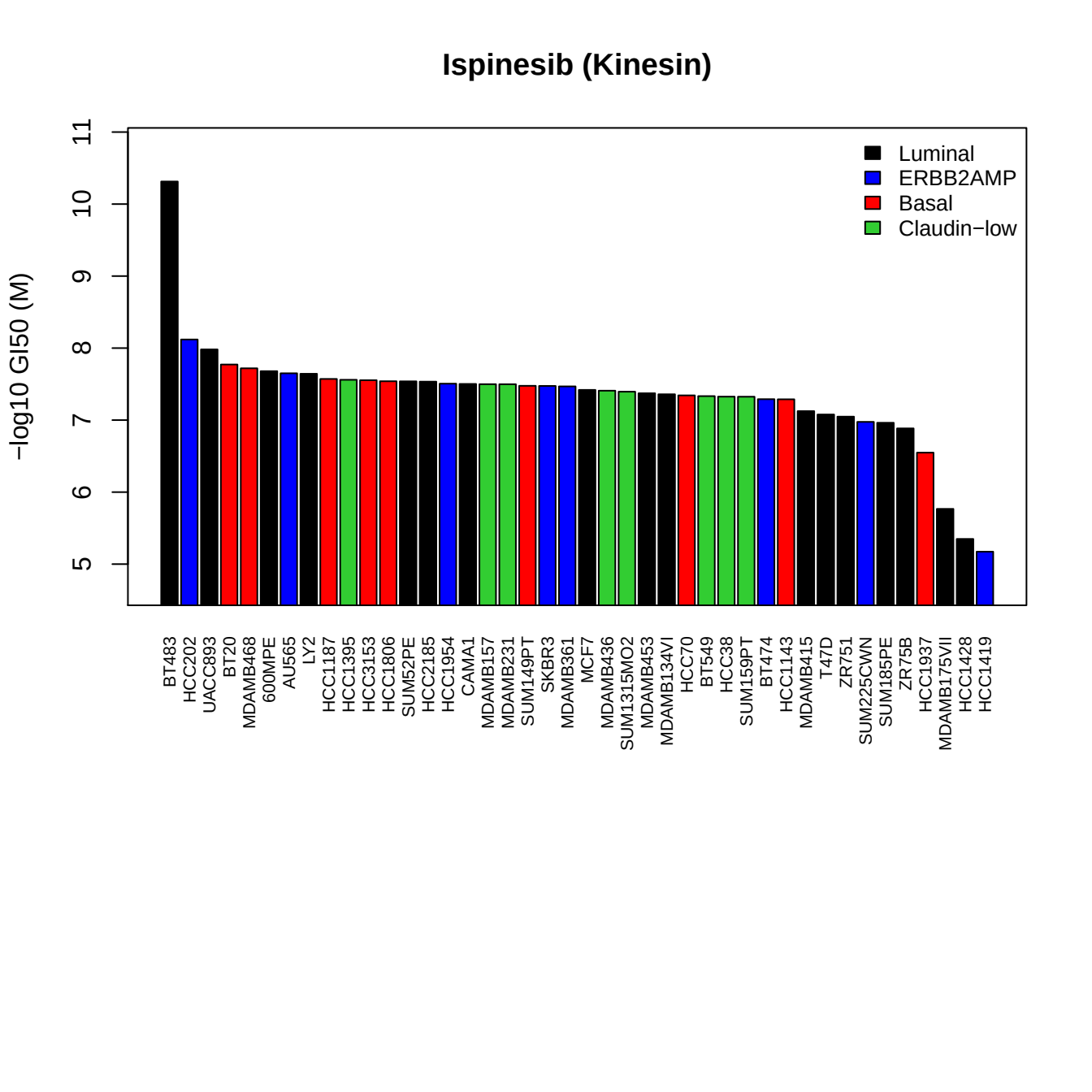
Ispinesib (Kinesin)
−log10 GI50 (M)
5
6
7
8
9
10
11
Luminal
ERBB2AMP
Basal
Claudin−low
BT483
HCC202
UACC893
BT20
MDAMB468
600MPE
AU565
LY2
HCC1187
HCC1395
HCC3153
HCC1806
SUM52PE
HCC2185
HCC1954
CAMA1
MDAMB157
MDAMB231
SUM149PT
SKBR3
MDAMB361
MCF7
MDAMB436
SUM1315MO2
MDAMB453
MDAMB134VI
HCC70
BT549
HCC38
SUM159PT
BT474
HCC1143
MDAMB415
T47D
ZR751
SUM225CWN
SUM185PE
ZR75B
HCC1937
MDAMB175VII
HCC1428
HCC1419

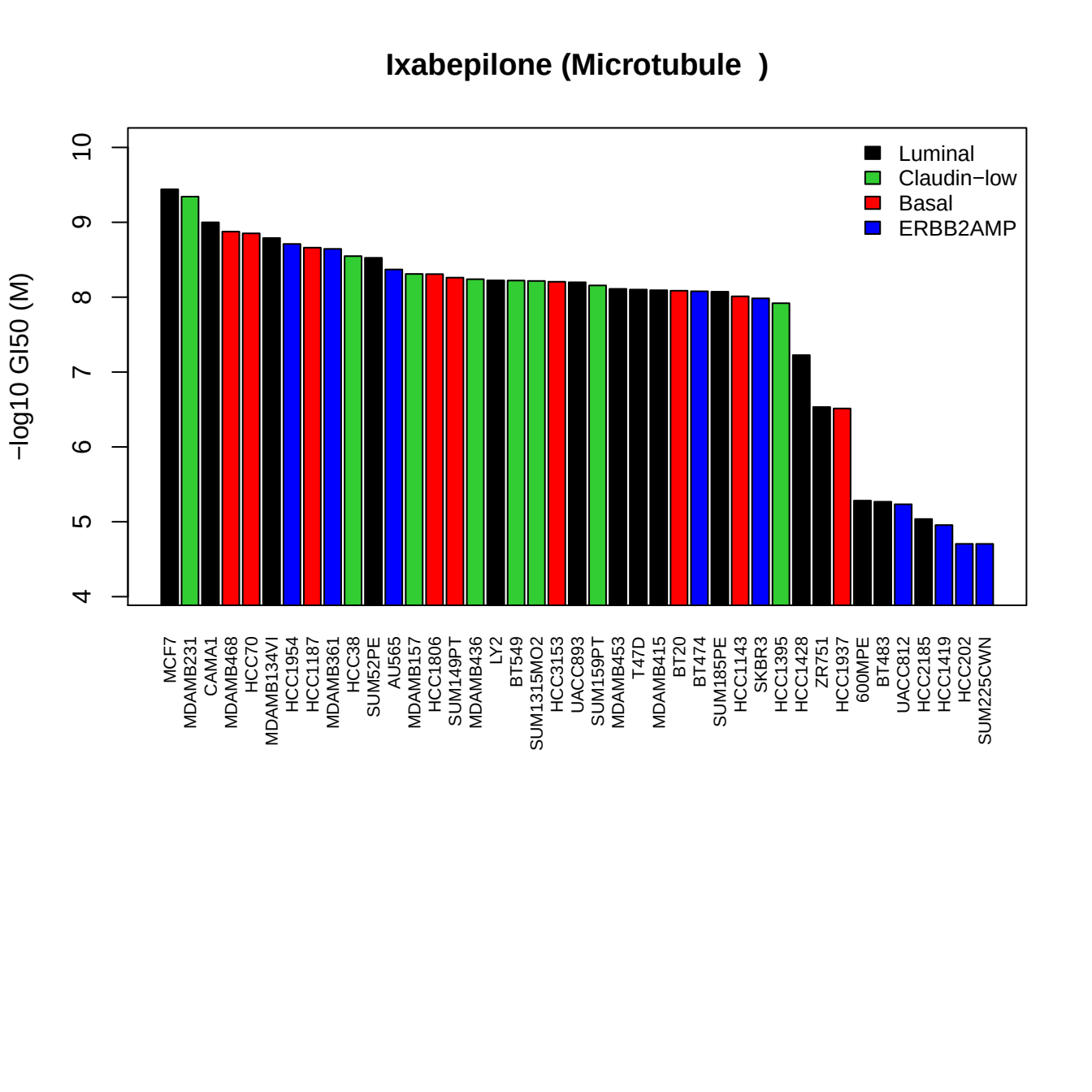
Ixabepilone (Microtubule)
−log10 GI50 (M)
4
5
6
7
8
9
10
Luminal
Claudin−low
Basal
ERBB2AMP
MCF7
MDAMB231
CAMA1
MDAMB468
HCC70
MDAMB134VI
HCC1954
HCC1187
MDAMB361
HCC38
SUM52PE
AU565
MDAMB157
HCC1806
SUM149PT
MDAMB436
LY2
BT549
SUM1315MO2
HCC3153
UACC893
SUM159PT
MDAMB453
T47D
MDAMB415
BT20
BT474
SUM185PE
HCC1143
SKBR3
HCC1395
HCC1428
ZR751
HCC1937
600MPE
BT483
UACC812
HCC2185
HCC1419
HCC202
SUM225CWN

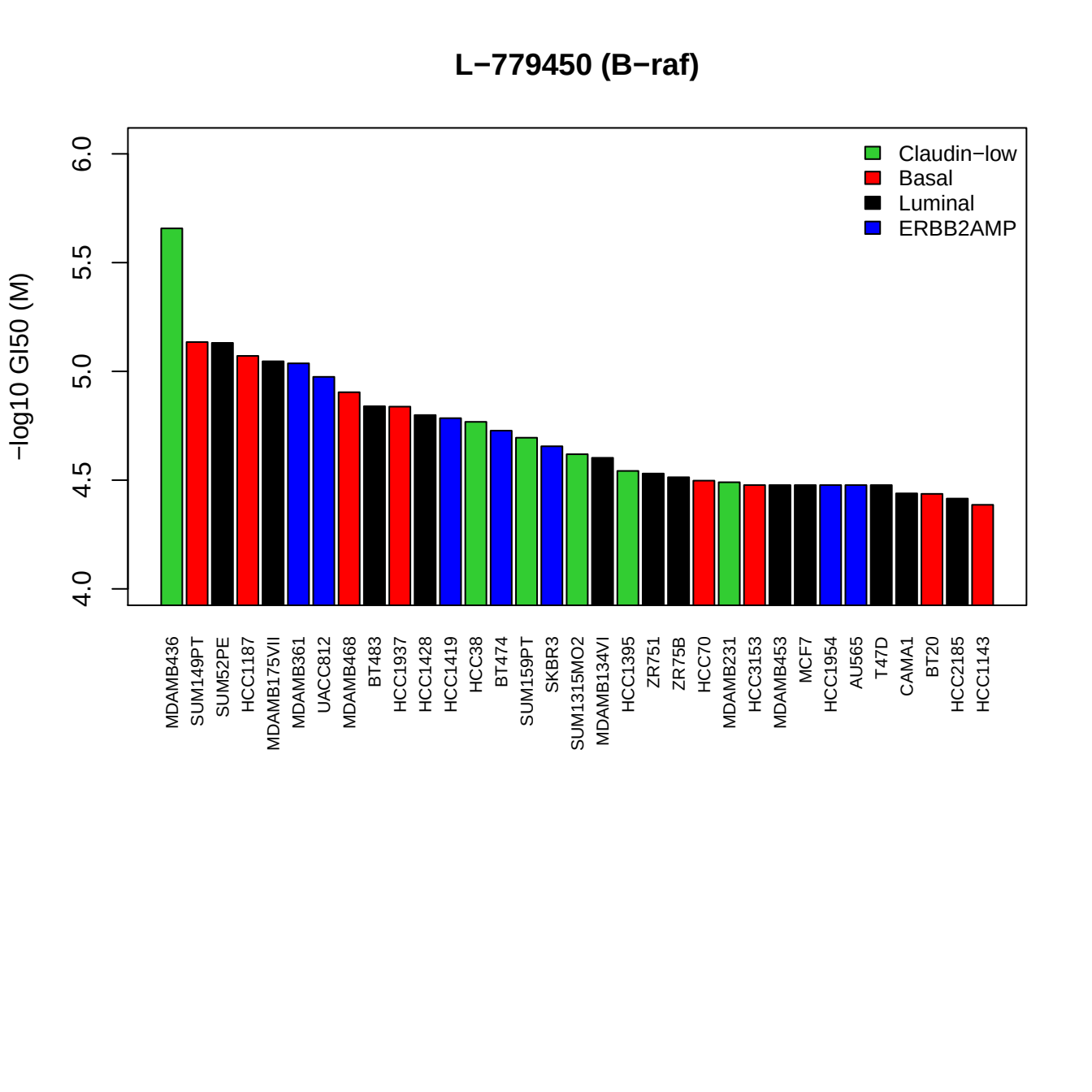
L−779450 (B−raf)
−log10 GI50 (M)
4.0
4.5
5.0
5.5
6.0
Claudin−low
Basal
Luminal
ERBB2AMP
MDAMB436
SUM149PT
SUM52PE
HCC1187
MDAMB175VII
MDAMB361
UACC812
MDAMB468
BT483
HCC1937
HCC1428
HCC1419
HCC38
BT474
SUM159PT
SKBR3
SUM1315MO2
MDAMB134VI
HCC1395
ZR751
ZR75B
HCC70
MDAMB231
HCC3153
MDAMB453
MCF7
HCC1954
AU565
T47D
CAMA1
BT20
HCC2185
HCC1143

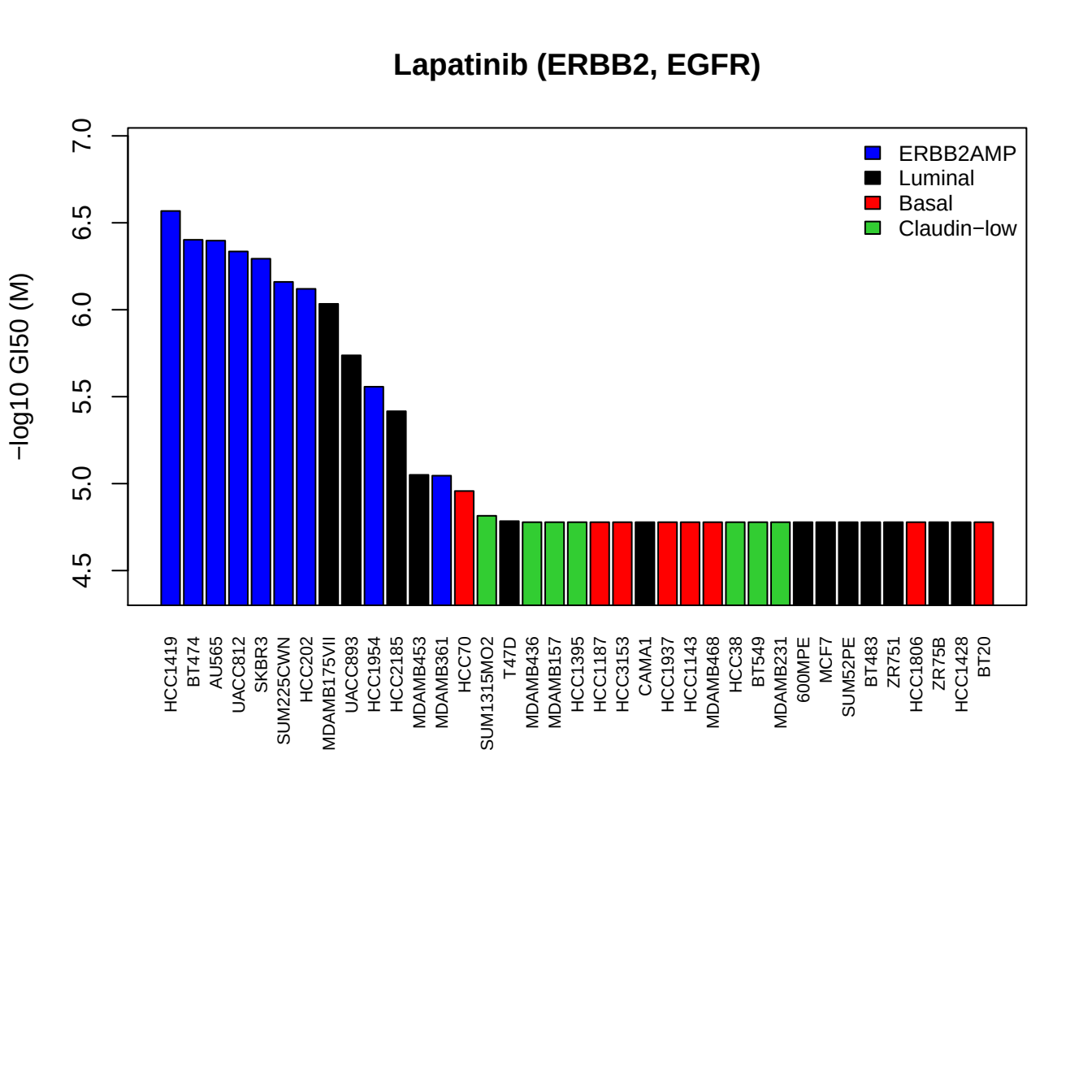
Lapatinib (ERBB2, EGFR)
−log10 GI50 (M)
4.5
5.0
5.5
6.0
6.5
7.0
ERBB2AMP
Luminal
Basal
Claudin−low
HCC1419
BT474
AU565
UACC812
SKBR3
SUM225CWN
HCC202
MDAMB175VII
UACC893
HCC1954
HCC2185
MDAMB453
MDAMB361
HCC70
SUM1315MO2
T47D
MDAMB436
MDAMB157
HCC1395
HCC1187
HCC3153
CAMA1
HCC1937
HCC1143
MDAMB468
HCC38
BT549
MDAMB231
600MPE
MCF7
SUM52PE
BT483
ZR751
HCC1806
ZR75B
HCC1428
BT20

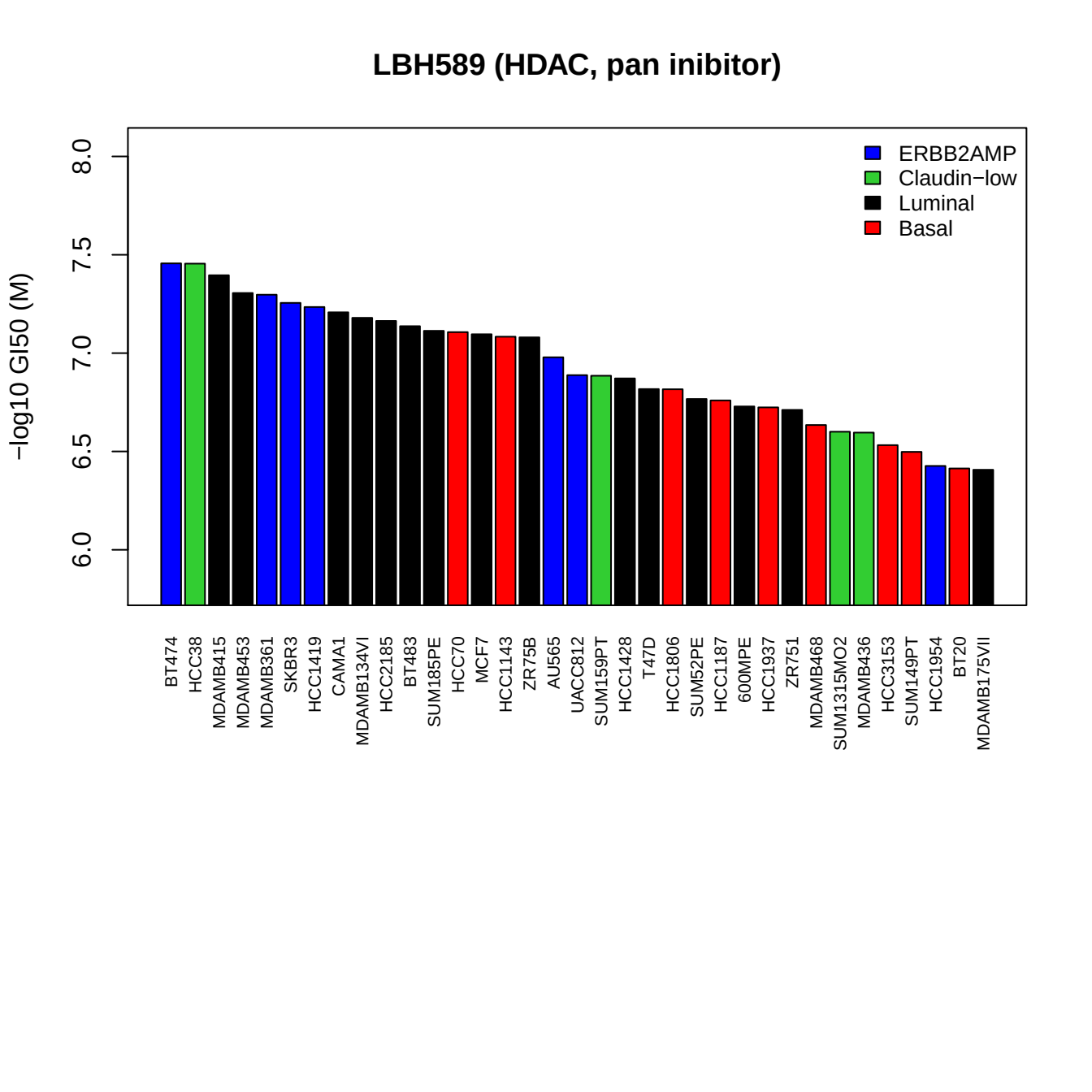
LBH589 (HDAC, pan inibitor)
−log10 GI50 (M)
6.0
6.5
7.0
7.5
8.0
ERBB2AMP
Claudin−low
Luminal
Basal
BT474
HCC38
MDAMB415
MDAMB453
MDAMB361
SKBR3
HCC1419
CAMA1
MDAMB134VI
HCC2185
BT483
SUM185PE
HCC70
MCF7
HCC1143
ZR75B
AU565
UACC812
SUM159PT
HCC1428
T47D
HCC1806
SUM52PE
HCC1187
600MPE
HCC1937
ZR751
MDAMB468
SUM1315MO2
MDAMB436
HCC3153
SUM149PT
HCC1954
BT20
MDAMB175VII

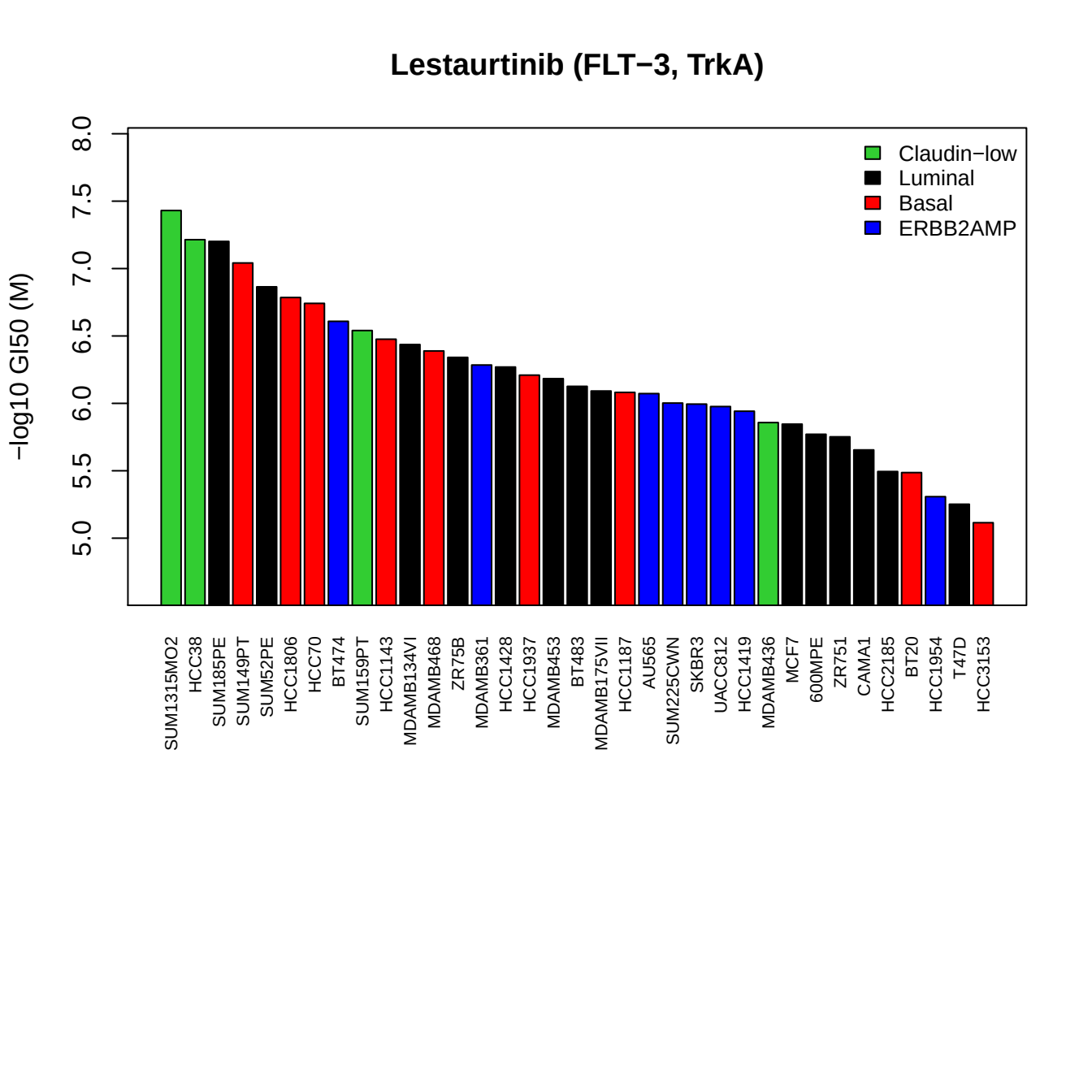
Lestaurtinib (FLT−3, TrkA)
−log10 GI50 (M)
5.0
5.5
6.0
6.5
7.0
7.5
8.0
Claudin−low
Luminal
Basal
ERBB2AMP
SUM1315MO2
HCC38
SUM185PE
SUM149PT
SUM52PE
HCC1806
HCC70
BT474
SUM159PT
HCC1143
MDAMB134VI
MDAMB468
ZR75B
MDAMB361
HCC1428
HCC1937
MDAMB453
BT483
MDAMB175VII
HCC1187
AU565
SUM225CWN
SKBR3
UACC812
HCC1419
MDAMB436
MCF7
600MPE
ZR751
CAMA1
HCC2185
BT20
HCC1954
T47D
HCC3153

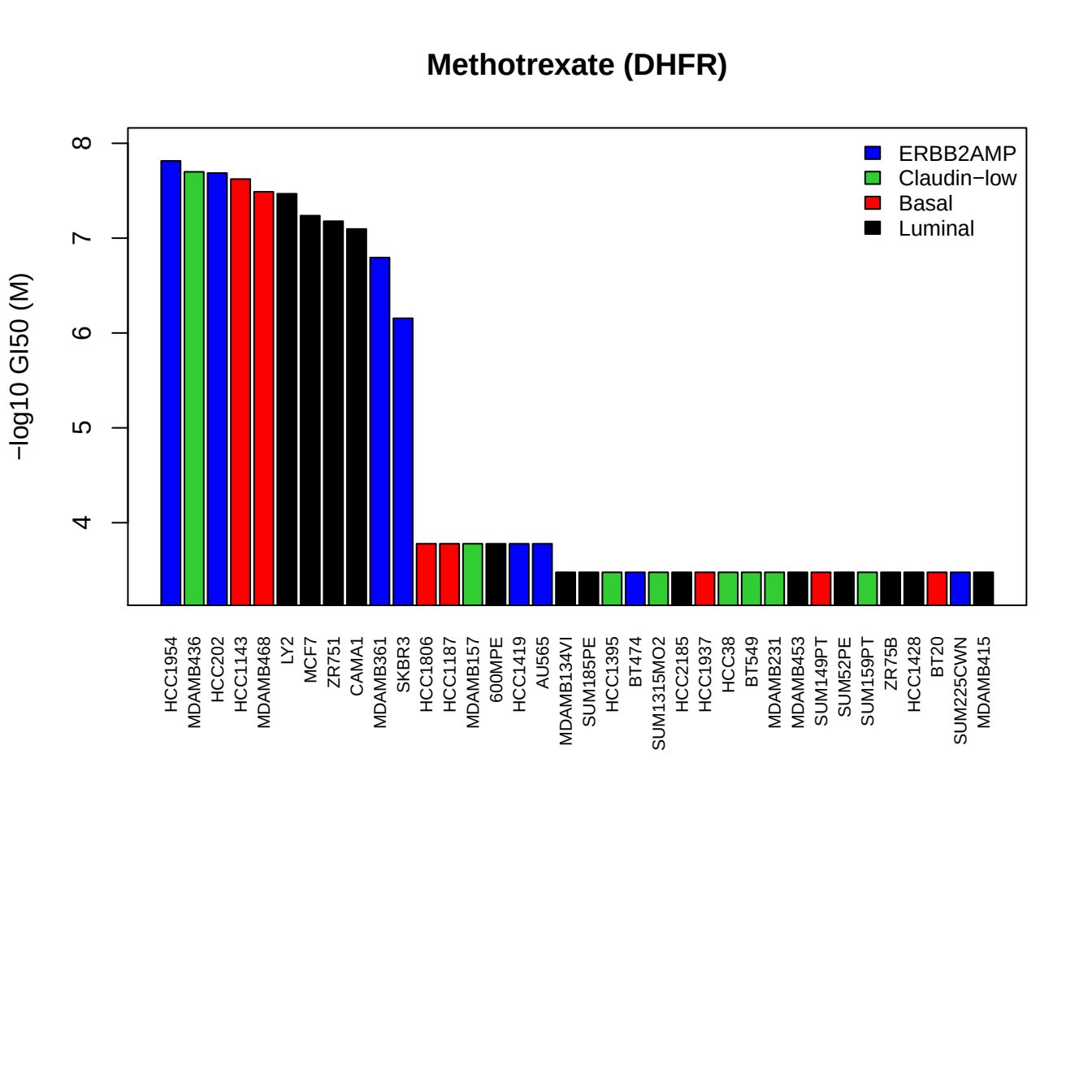
Methotrexate (DHFR)
−log10 GI50 (M)
4
5
6
7
8
ERBB2AMP
Claudin−low
Basal
Luminal
HCC1954
MDAMB436
HCC202
HCC1143
MDAMB468
LY2
MCF7
ZR751
CAMA1
MDAMB361
SKBR3
HCC1806
HCC1187
MDAMB157
600MPE
HCC1419
AU565
MDAMB134VI
SUM185PE
HCC1395
BT474
SUM1315MO2
HCC2185
HCC1937
HCC38
BT549
MDAMB231
MDAMB453
SUM149PT
SUM52PE
SUM159PT
ZR75B
HCC1428
BT20
SUM225CWN
MDAMB415

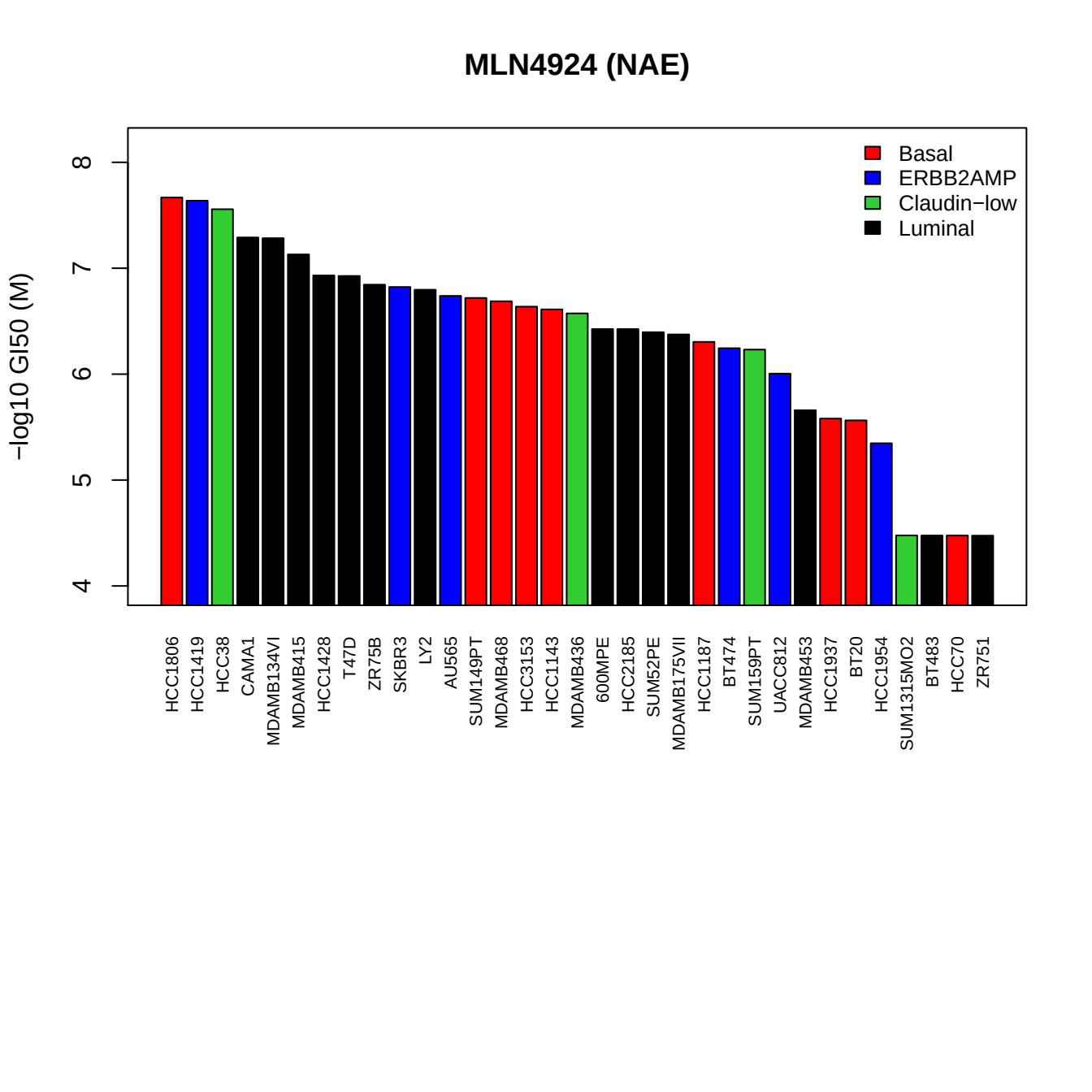
MLN4924 (NAE)
−log10 GI50 (M)
4
5
6
7
8
Basal
ERBB2AMP
Claudin−low
Luminal
HCC1806
HCC1419
HCC38
CAMA1
MDAMB134VI
MDAMB415
HCC1428
T47D
ZR75B
SKBR3
LY2
AU565
SUM149PT
MDAMB468
HCC3153
HCC1143
MDAMB436
600MPE
HCC2185
SUM52PE
MDAMB175VII
HCC1187
BT474
SUM159PT
UACC812
MDAMB453
HCC1937
BT20
HCC1954
SUM1315MO2
BT483
HCC70
ZR751

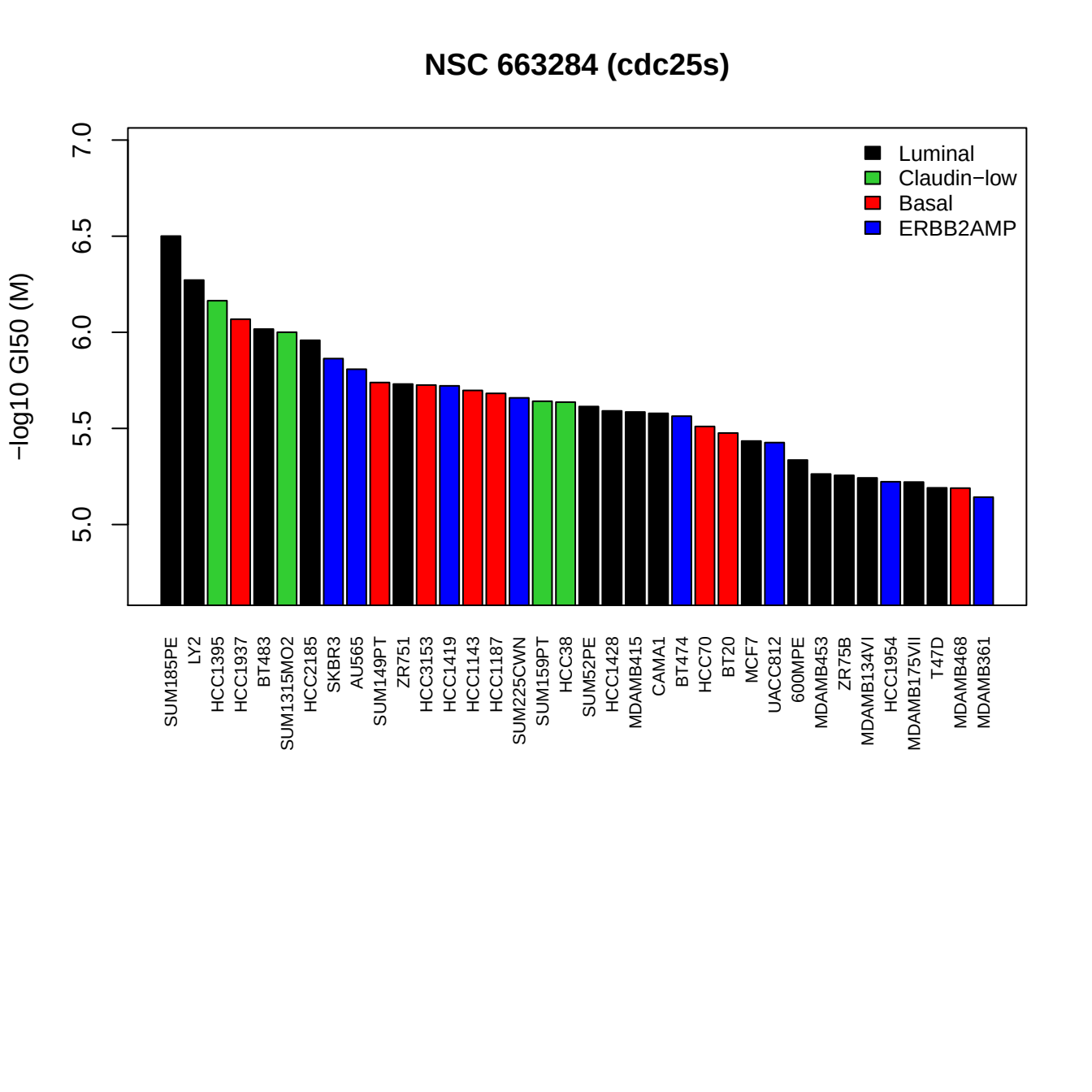
NSC 663284 (cdc25s)
−log10 GI50 (M)
5.0
5.5
6.0
6.5
7.0
Luminal
Claudin−low
Basal
ERBB2AMP
SUM185PE
LY2
HCC1395
HCC1937
BT483
SUM1315MO2
HCC2185
SKBR3
AU565
SUM149PT
ZR751
HCC3153
HCC1419
HCC1143
HCC1187
SUM225CWN
SUM159PT
HCC38
SUM52PE
HCC1428
MDAMB415
CAMA1
BT474
HCC70
BT20
MCF7
UACC812
600MPE
MDAMB453
ZR75B
MDAMB134VI
HCC1954
MDAMB175VII
T47D
MDAMB468
MDAMB361

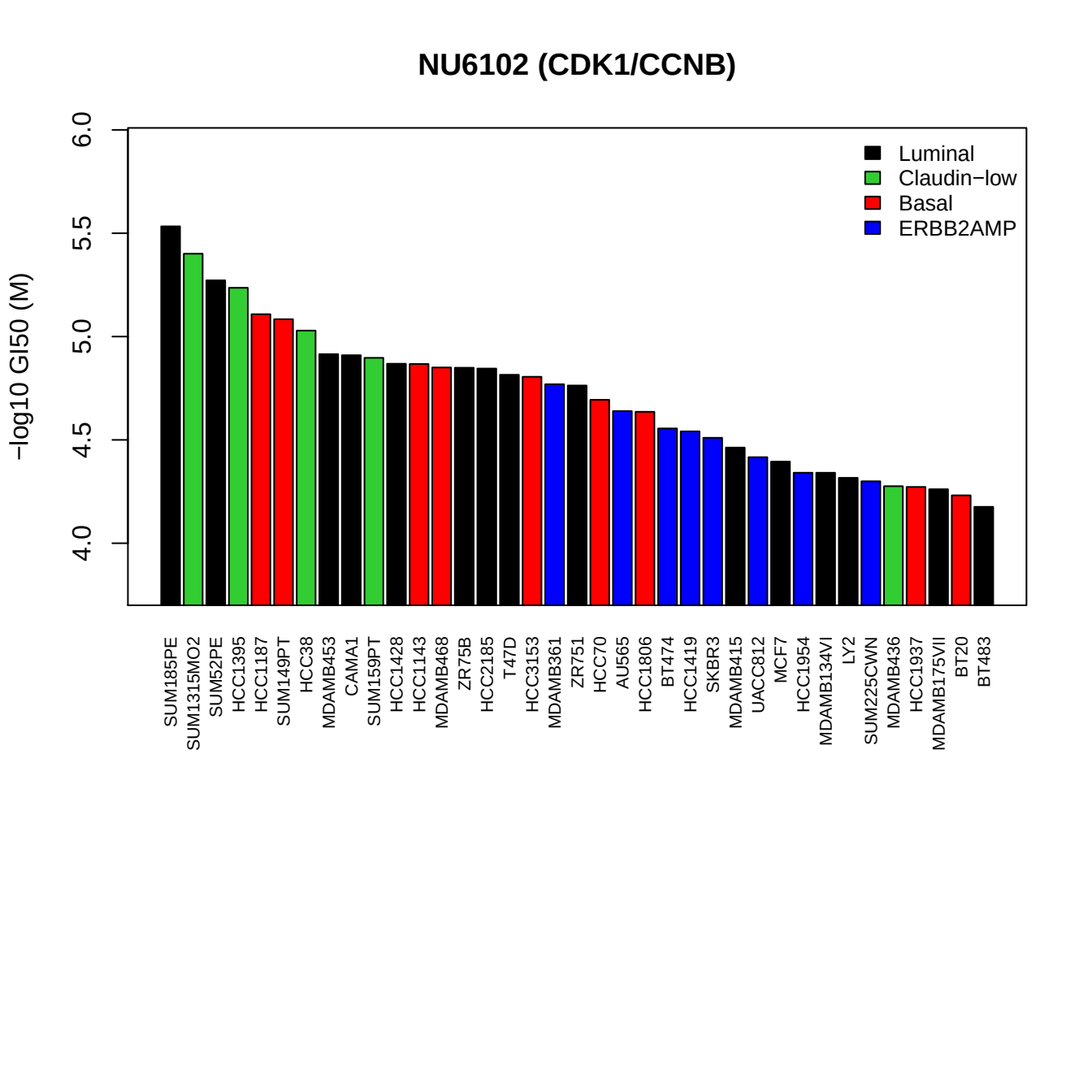
NU6102 (CDK1/CCNB)
−log10 GI50 (M)
4.0
4.5
5.0
5.5
6.0
Luminal
Claudin−low
Basal
ERBB2AMP
SUM185PE
SUM1315MO2
SUM52PE
HCC1395
HCC1187
SUM149PT
HCC38
MDAMB453
CAMA1
SUM159PT
HCC1428
HCC1143
MDAMB468
ZR75B
HCC2185
T47D
HCC3153
MDAMB361
ZR751
HCC70
AU565
HCC1806
BT474
HCC1419
SKBR3
MDAMB415
UACC812
MCF7
HCC1954
MDAMB134VI
LY2
SUM225CWN
MDAMB436
HCC1937
MDAMB175VII
BT20
BT483

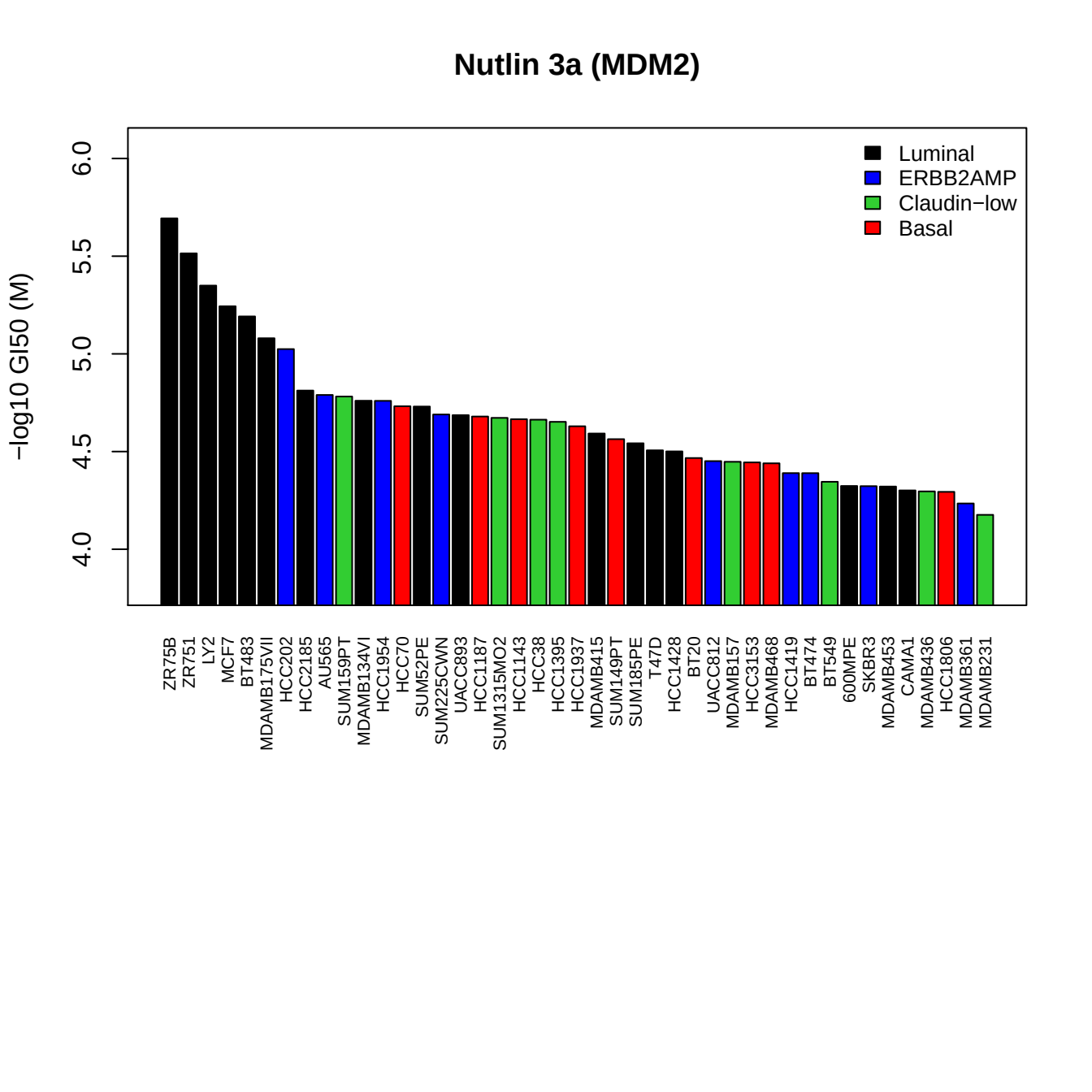
Nutlin 3a (MDM2)
−log10 GI50 (M)
4.0
4.5
5.0
5.5
6.0
Luminal
ERBB2AMP
Claudin−low
Basal
ZR75B
ZR751
LY2
MCF7
BT483
MDAMB175VII
HCC202
HCC2185
AU565
SUM159PT
MDAMB134VI
HCC1954
HCC70
SUM52PE
SUM225CWN
UACC893
HCC1187
SUM1315MO2
HCC1143
HCC38
HCC1395
HCC1937
MDAMB415
SUM149PT
SUM185PE
T47D
HCC1428
BT20
UACC812
MDAMB157
HCC3153
MDAMB468
HCC1419
BT474
BT549
600MPE
SKBR3
MDAMB453
CAMA1
MDAMB436
HCC1806
MDAMB361
MDAMB231

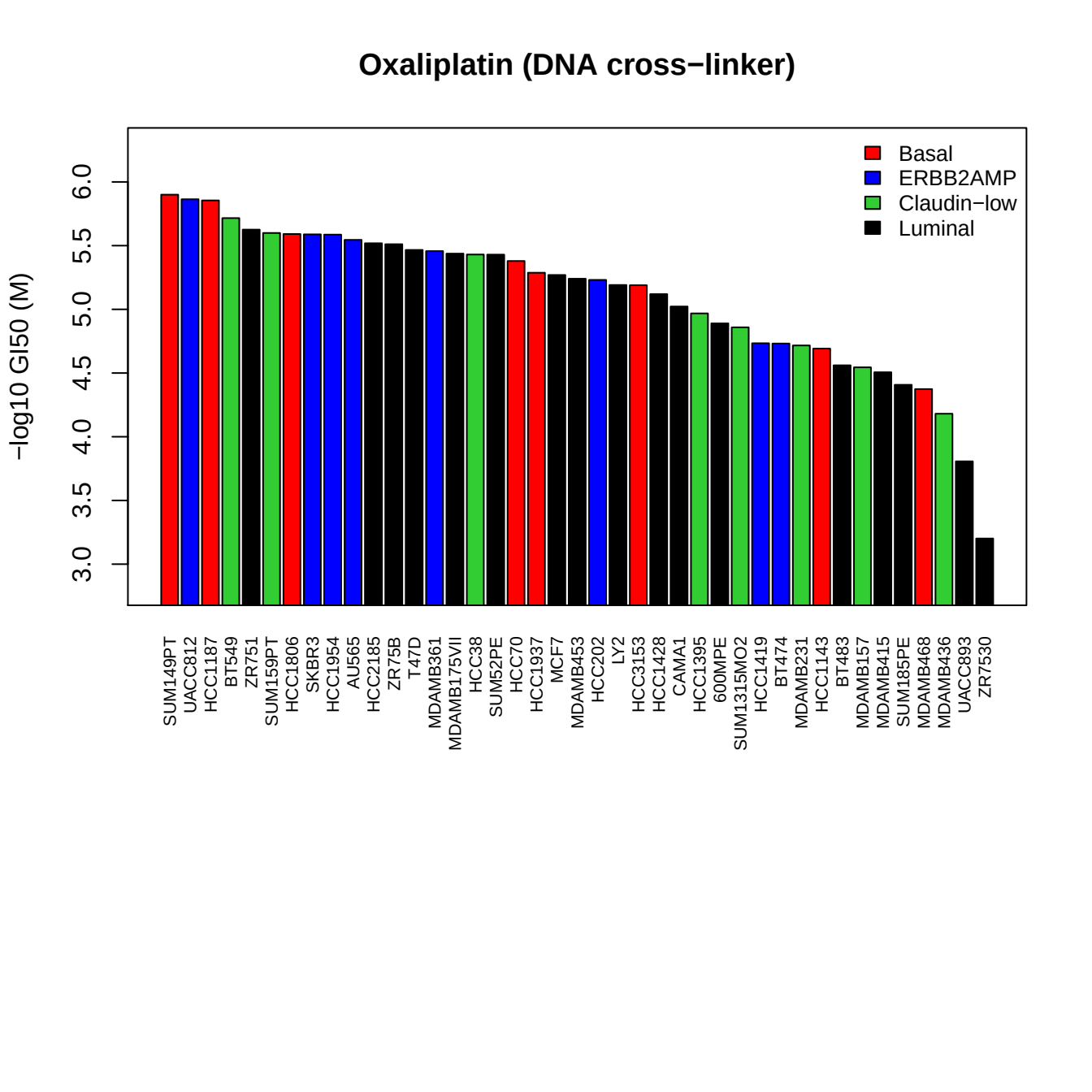
Oxaliplatin (DNA cross−linker)
−log10 GI50 (M)
3.0
3.5
4.0
4.5
5.0
5.5
6.0
Basal
ERBB2AMP
Claudin−low
Luminal
SUM149PT
UACC812
HCC1187
BT549
ZR751
SUM159PT
HCC1806
SKBR3
HCC1954
AU565
HCC2185
ZR75B
T47D
MDAMB361
MDAMB175VII
HCC38
SUM52PE
HCC70
HCC1937
MCF7
MDAMB453
HCC202
LY2
HCC3153
HCC1428
CAMA1
HCC1395
600MPE
SUM1315MO2
HCC1419
BT474
MDAMB231
HCC1143
BT483
MDAMB157
MDAMB415
SUM185PE
MDAMB468
MDAMB436
UACC893
ZR7530

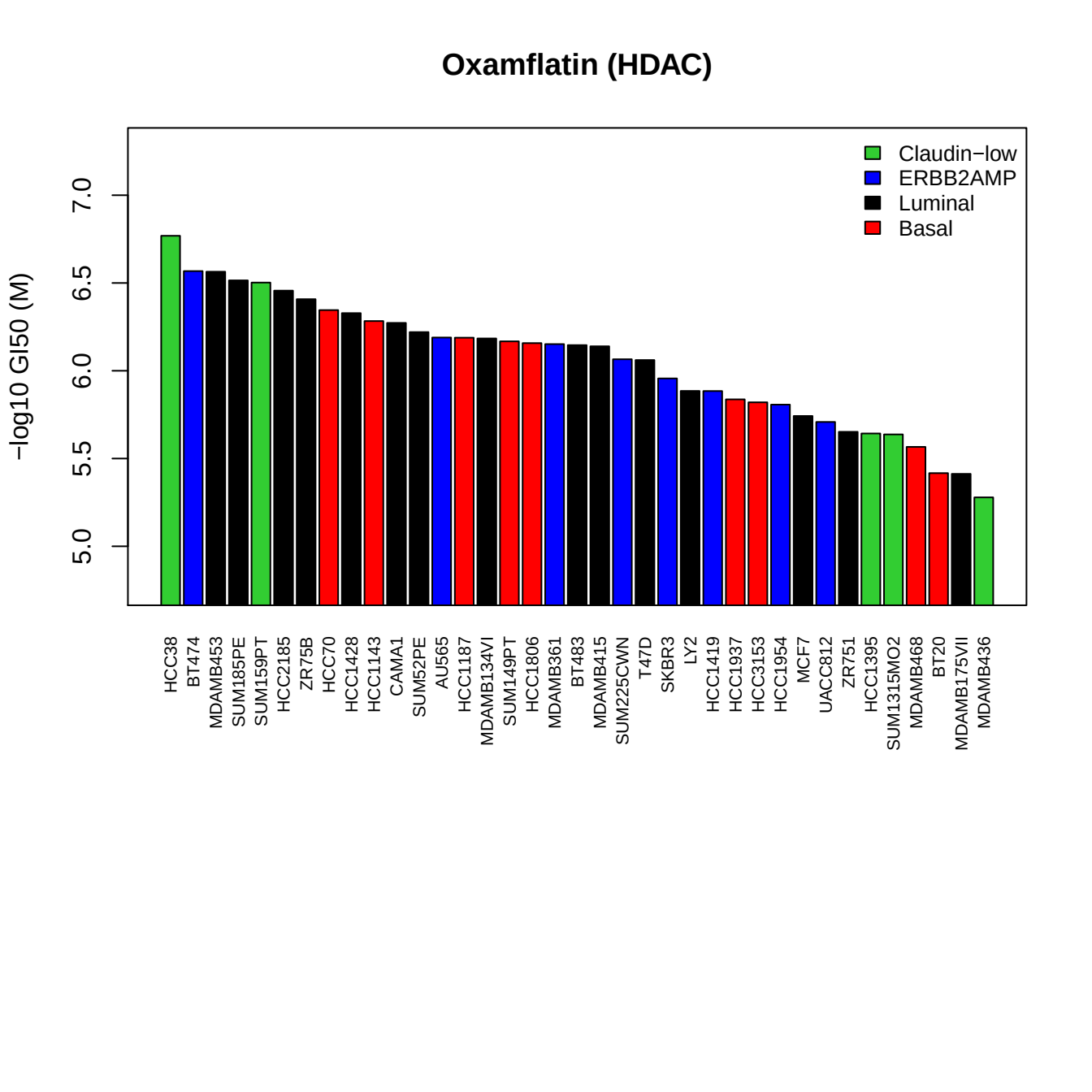
Oxamflatin (HDAC)
−log10 GI50 (M)
5.0
5.5
6.0
6.5
7.0
Claudin−low
ERBB2AMP
Luminal
Basal
HCC38
BT474
MDAMB453
SUM185PE
SUM159PT
HCC2185
ZR75B
HCC70
HCC1428
HCC1143
CAMA1
SUM52PE
AU565
HCC1187
MDAMB134VI
SUM149PT
HCC1806
MDAMB361
BT483
MDAMB415
SUM225CWN
T47D
SKBR3
LY2
HCC1419
HCC1937
HCC3153
HCC1954
MCF7
UACC812
ZR751
HCC1395
SUM1315MO2
MDAMB468
BT20
MDAMB175VII
MDAMB436

Paclitaxel (Microtubule)

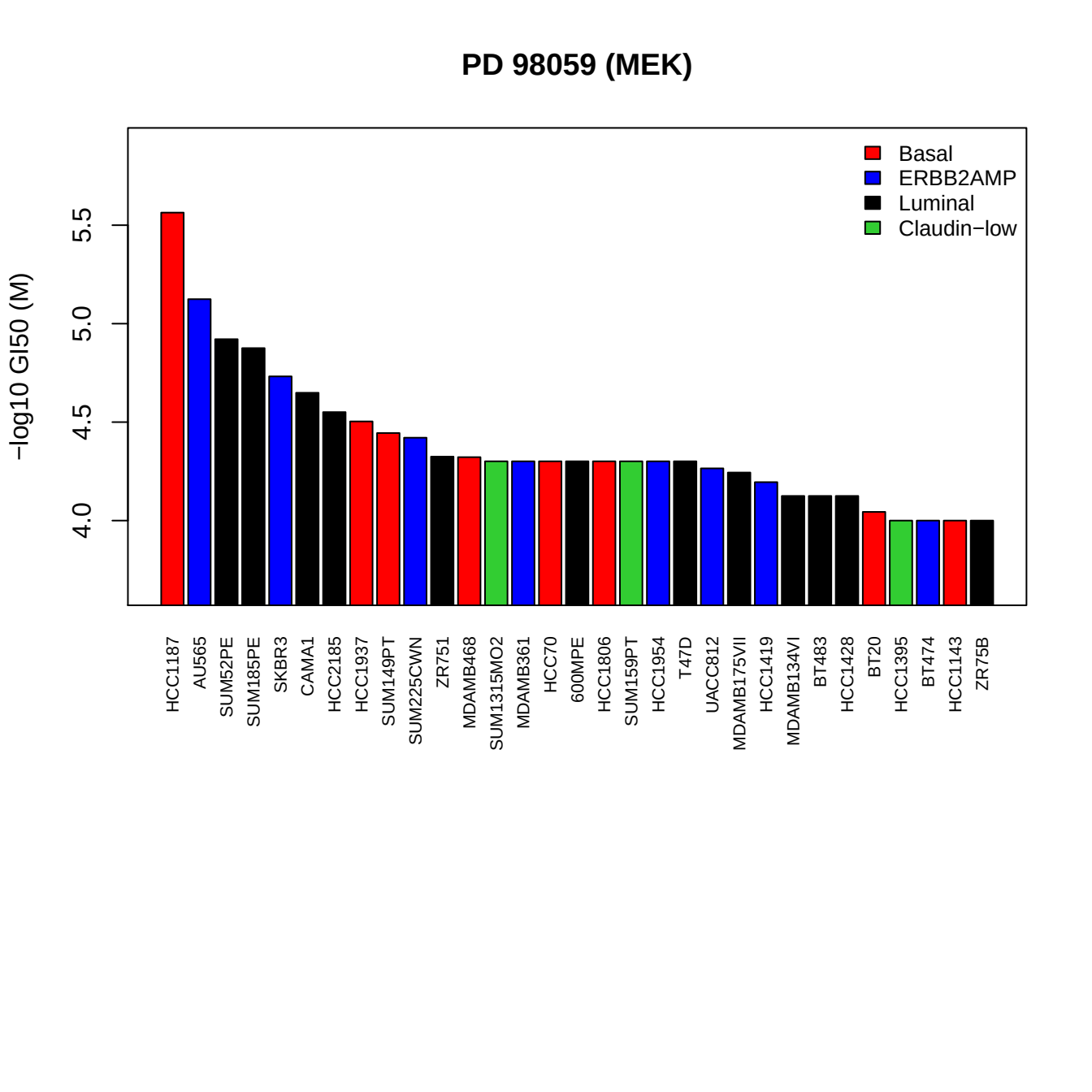
PD 98059 (MEK)
−log10 GI50 (M)
4.0
4.5
5.0
5.5
Basal
ERBB2AMP
Luminal
Claudin−low
HCC1187
AU565
SUM52PE
SUM185PE
SKBR3
CAMA1
HCC2185
HCC1937
SUM149PT
SUM225CWN
ZR751
MDAMB468
SUM1315MO2
MDAMB361
HCC70
600MPE
HCC1806
SUM159PT
HCC1954
T47D
UACC812
MDAMB175VII
HCC1419
MDAMB134VI
BT483
HCC1428
BT20
HCC1395
BT474
HCC1143
ZR75B

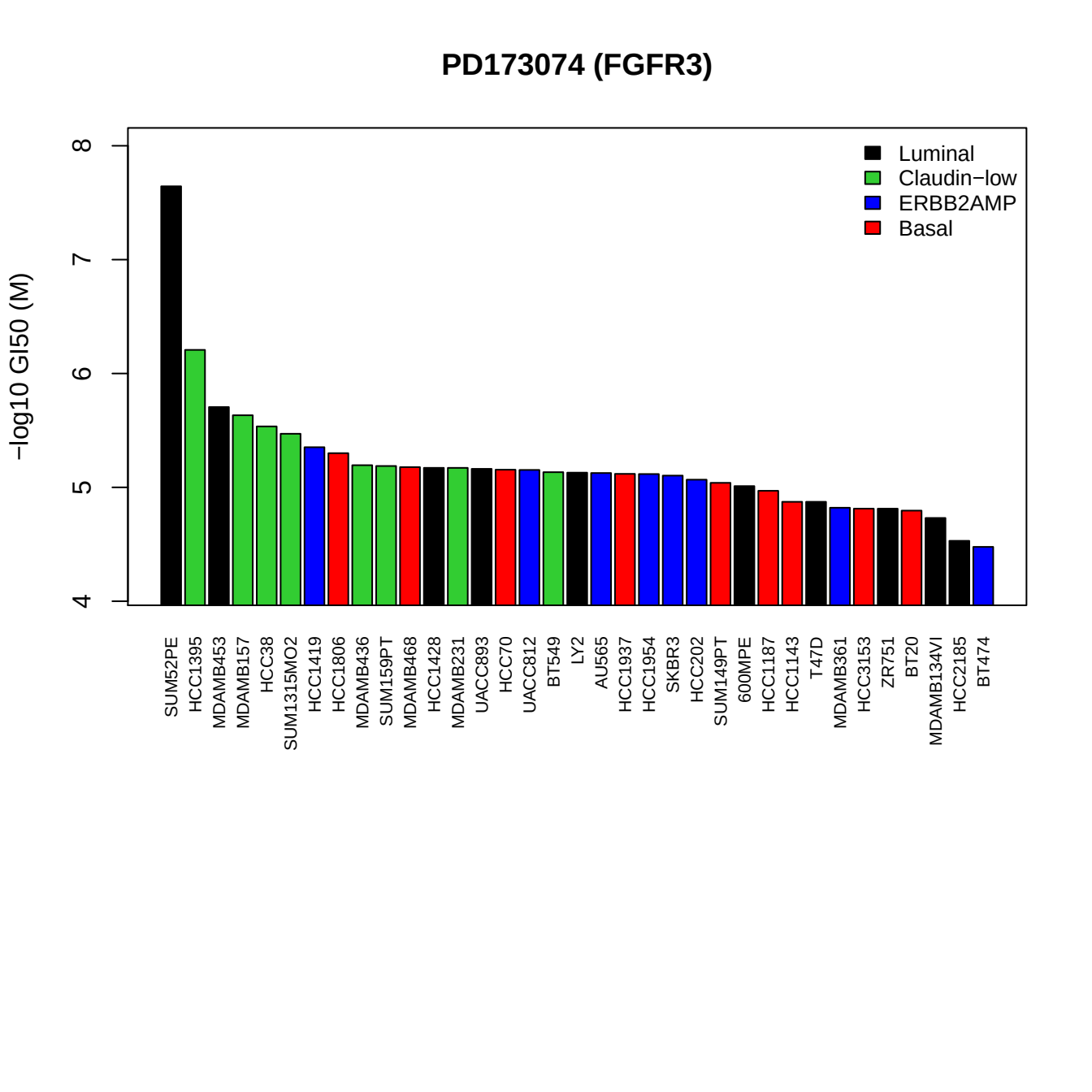
PD173074 (FGFR3)
−log10 GI50 (M)
4
5
6
7
8
Luminal
Claudin−low
ERBB2AMP
Basal
SUM52PE
HCC1395
MDAMB453
MDAMB157
HCC38
SUM1315MO2
HCC1419
HCC1806
MDAMB436
SUM159PT
MDAMB468
HCC1428
MDAMB231
UACC893
HCC70
UACC812
BT549
LY2
AU565
HCC1937
HCC1954
SKBR3
HCC202
SUM149PT
600MPE
HCC1187
HCC1143
T47D
MDAMB361
HCC3153
ZR751
BT20
MDAMB134VI
HCC2185
BT474

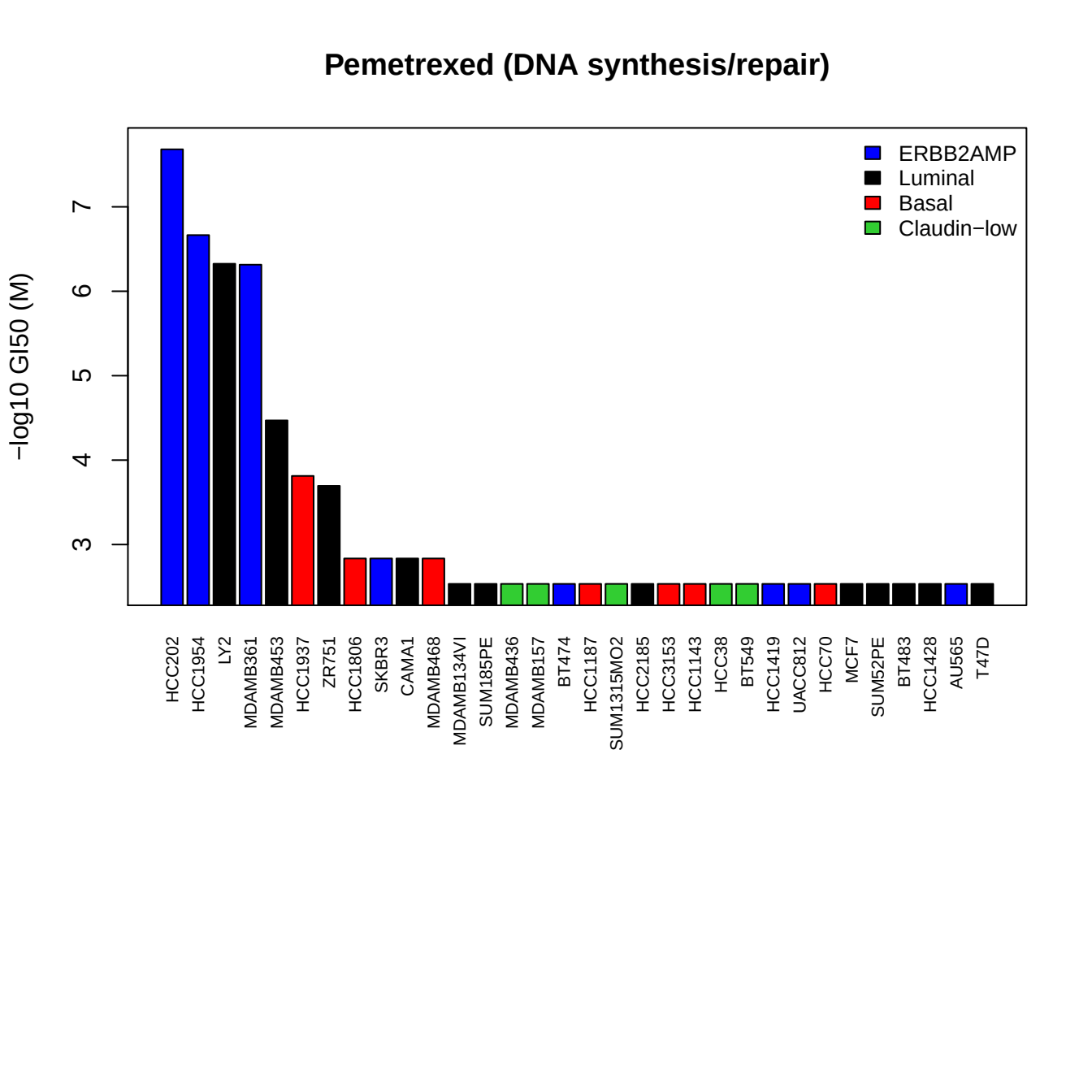
Pemetrexed (DNA synthesis/repair)
−log10 GI50 (M)
3
4
5
6
7
ERBB2AMP
Luminal
Basal
Claudin−low
HCC202
HCC1954
LY2
MDAMB361
MDAMB453
HCC1937
ZR751
HCC1806
SKBR3
CAMA1
MDAMB468
MDAMB134VI
SUM185PE
MDAMB436
MDAMB157
BT474
HCC1187
SUM1315MO2
HCC2185
HCC3153
HCC1143
HCC38
BT549
HCC1419
UACC812
HCC70
MCF7
SUM52PE
BT483
HCC1428
AU565
T47D

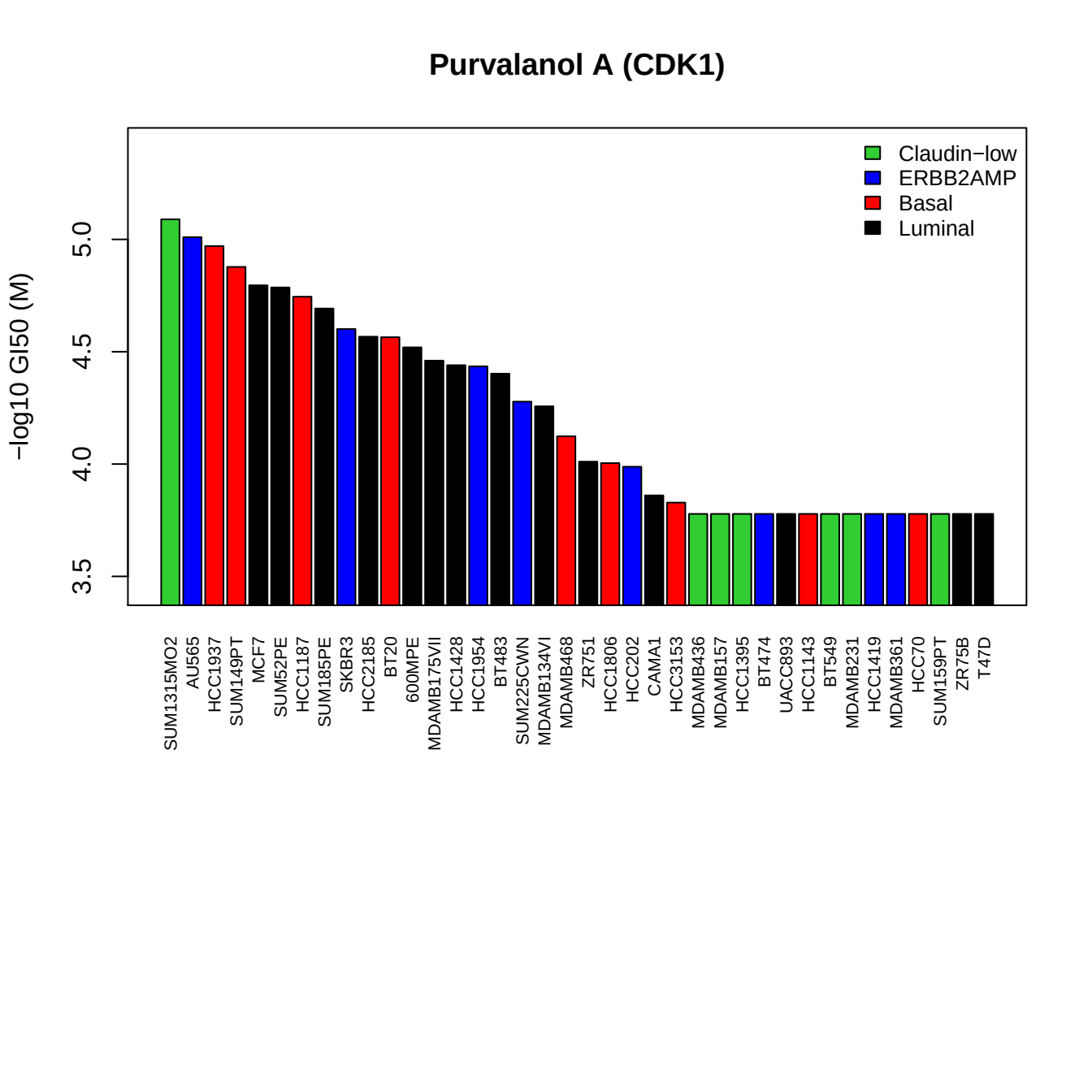
Purvalanol A (CDK1)
−log10 GI50 (M)
3.5
4.0
4.5
5.0
Claudin−low
ERBB2AMP
Basal
Luminal
SUM1315MO2
AU565
HCC1937
SUM149PT
MCF7
SUM52PE
HCC1187
SUM185PE
SKBR3
HCC2185
BT20
600MPE
MDAMB175VII
HCC1428
HCC1954
BT483
SUM225CWN
MDAMB134VI
MDAMB468
ZR751
HCC1806
HCC202
CAMA1
HCC3153
MDAMB436
MDAMB157
HCC1395
BT474
UACC893
HCC1143
BT549
MDAMB231
HCC1419
MDAMB361
HCC70
SUM159PT
ZR75B
T47D

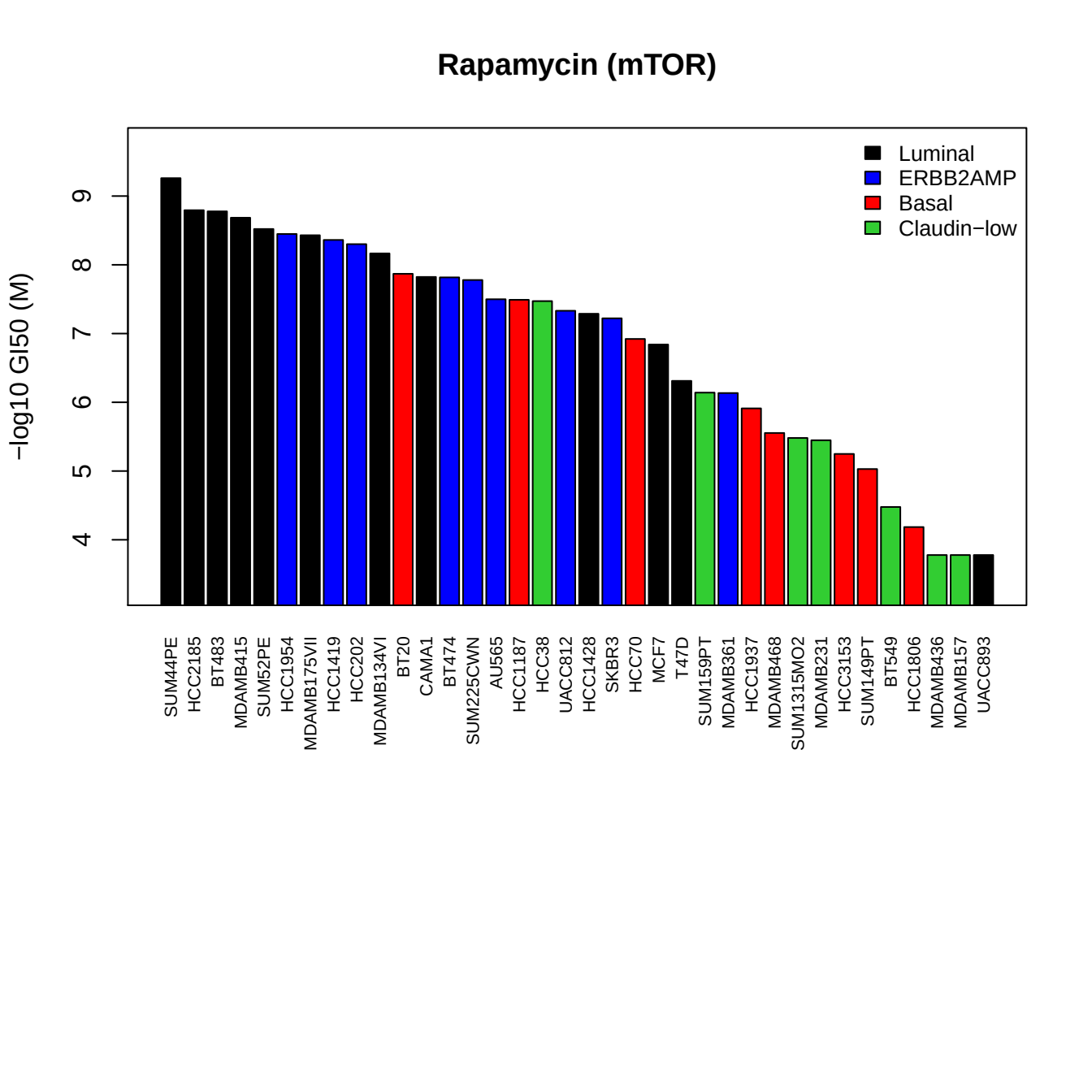
Rapamycin (mTOR)
−log10 GI50 (M)
4
5
6
7
8
9
Luminal
ERBB2AMP
Basal
Claudin−low
SUM44PE
HCC2185
BT483
MDAMB415
SUM52PE
HCC1954
MDAMB175VII
HCC1419
HCC202
MDAMB134VI
BT20
CAMA1
BT474
SUM225CWN
AU565
HCC1187
HCC38
UACC812
HCC1428
SKBR3
HCC70
MCF7
T47D
SUM159PT
MDAMB361
HCC1937
MDAMB468
SUM1315MO2
MDAMB231
HCC3153
SUM149PT
BT549
HCC1806
MDAMB436
MDAMB157
UACC893

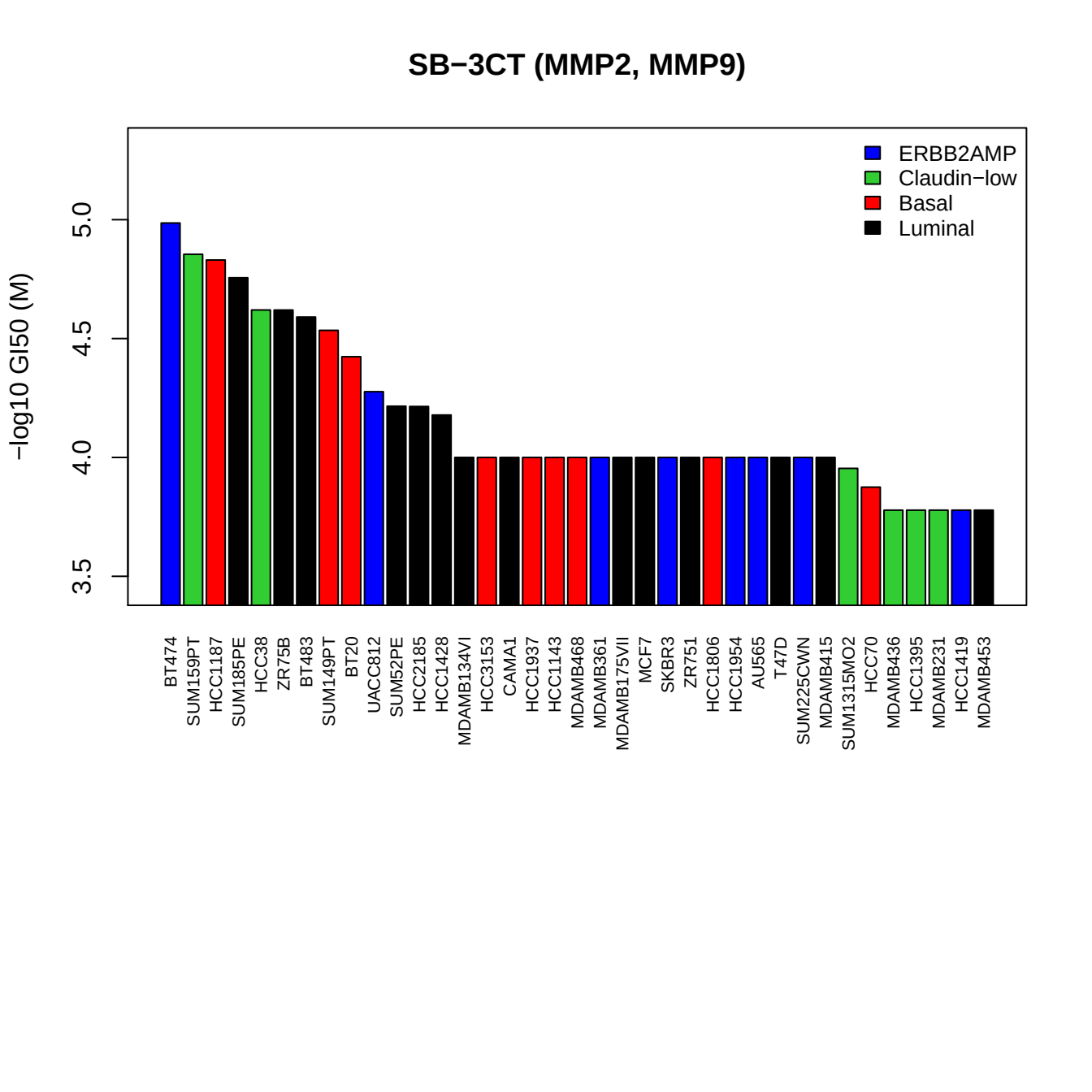
SB−3CT (MMP2, MMP9)
−log10 GI50 (M)
3.5
4.0
4.5
5.0
ERBB2AMP
Claudin−low
Basal
Luminal
BT474
SUM159PT
HCC1187
SUM185PE
HCC38
ZR75B
BT483
SUM149PT
BT20
UACC812
SUM52PE
HCC2185
HCC1428
MDAMB134VI
HCC3153
CAMA1
HCC1937
HCC1143
MDAMB468
MDAMB361
MDAMB175VII
MCF7
SKBR3
ZR751
HCC1806
HCC1954
AU565
T47D
SUM225CWN
MDAMB415
SUM1315MO2
HCC70
MDAMB436
HCC1395
MDAMB231
HCC1419
MDAMB453

Sigma AKT1−2 inhibitor (Akt 1/2)

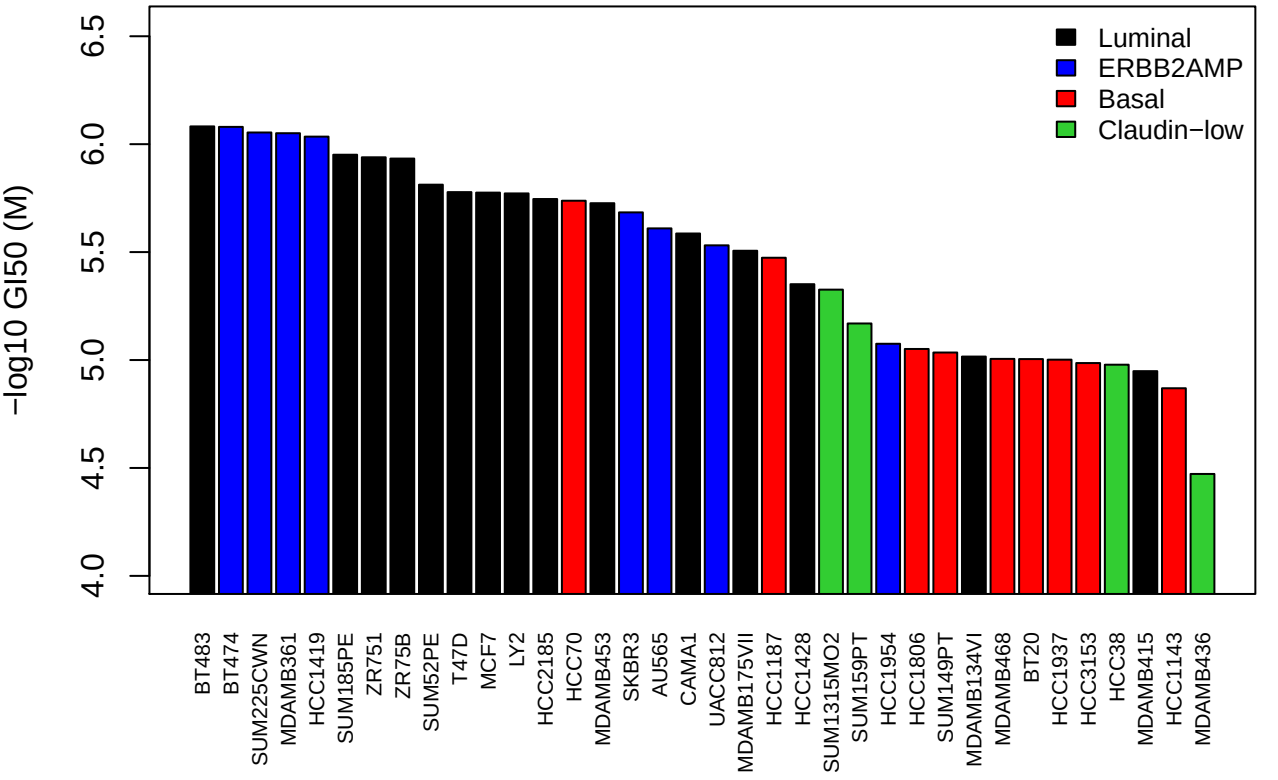

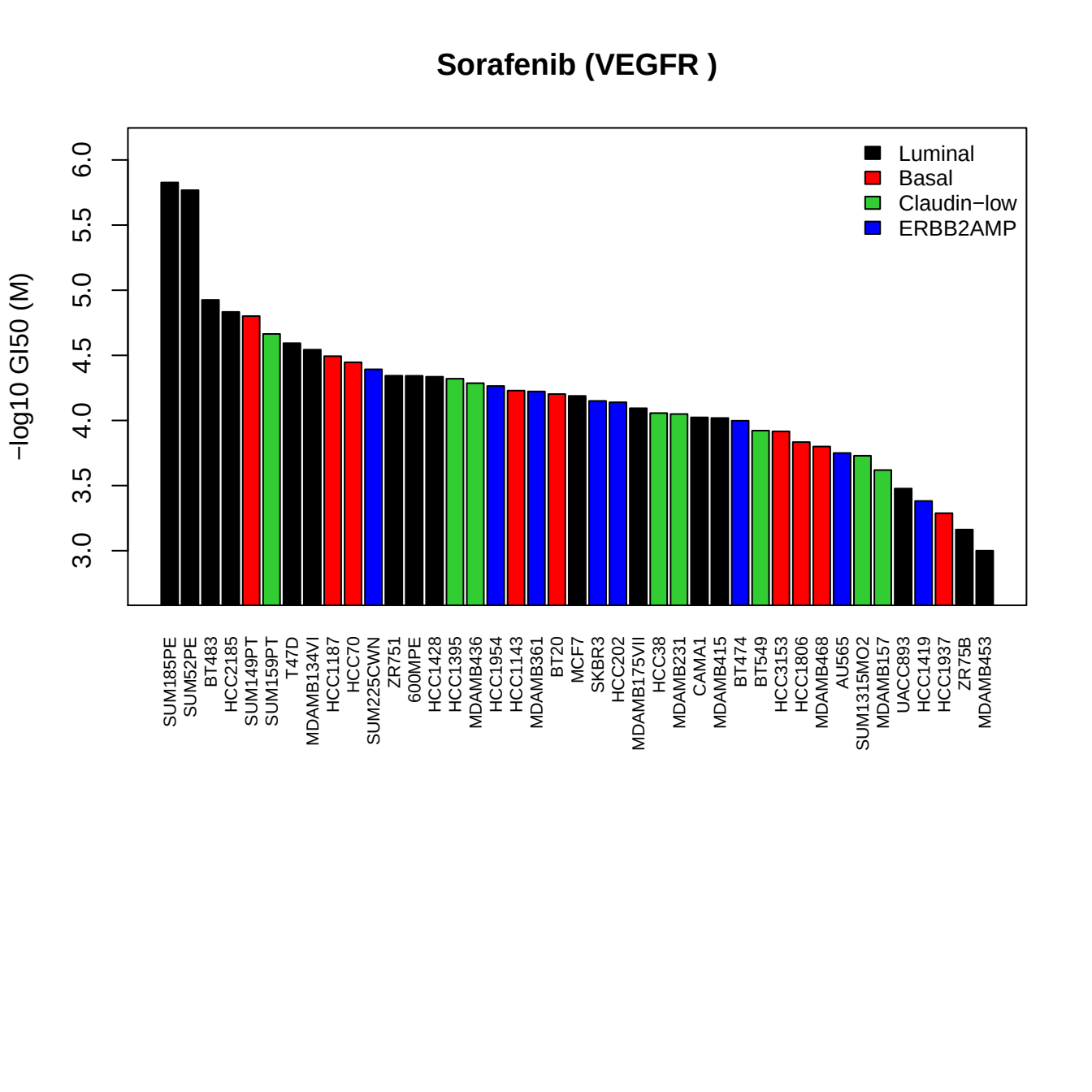
Sorafenib (VEGFR)
−log10 GI50 (M)
3.0
3.5
4.0
4.5
5.0
5.5
6.0
Luminal
Basal
Claudin−low
ERBB2AMP
SUM185PE
SUM52PE
BT483
HCC2185
SUM149PT
SUM159PT
T47D
MDAMB134VI
HCC1187
HCC70
SUM225CWN
ZR751
600MPE
HCC1428
HCC1395
MDAMB436
HCC1954
HCC1143
MDAMB361
BT20
MCF7
SKBR3
HCC202
MDAMB175VII
HCC38
MDAMB231
CAMA1
MDAMB415
BT474
BT549
HCC3153
HCC1806
MDAMB468
AU565
SUM1315MO2
MDAMB157
UACC893
HCC1419
HCC1937
ZR75B
MDAMB453

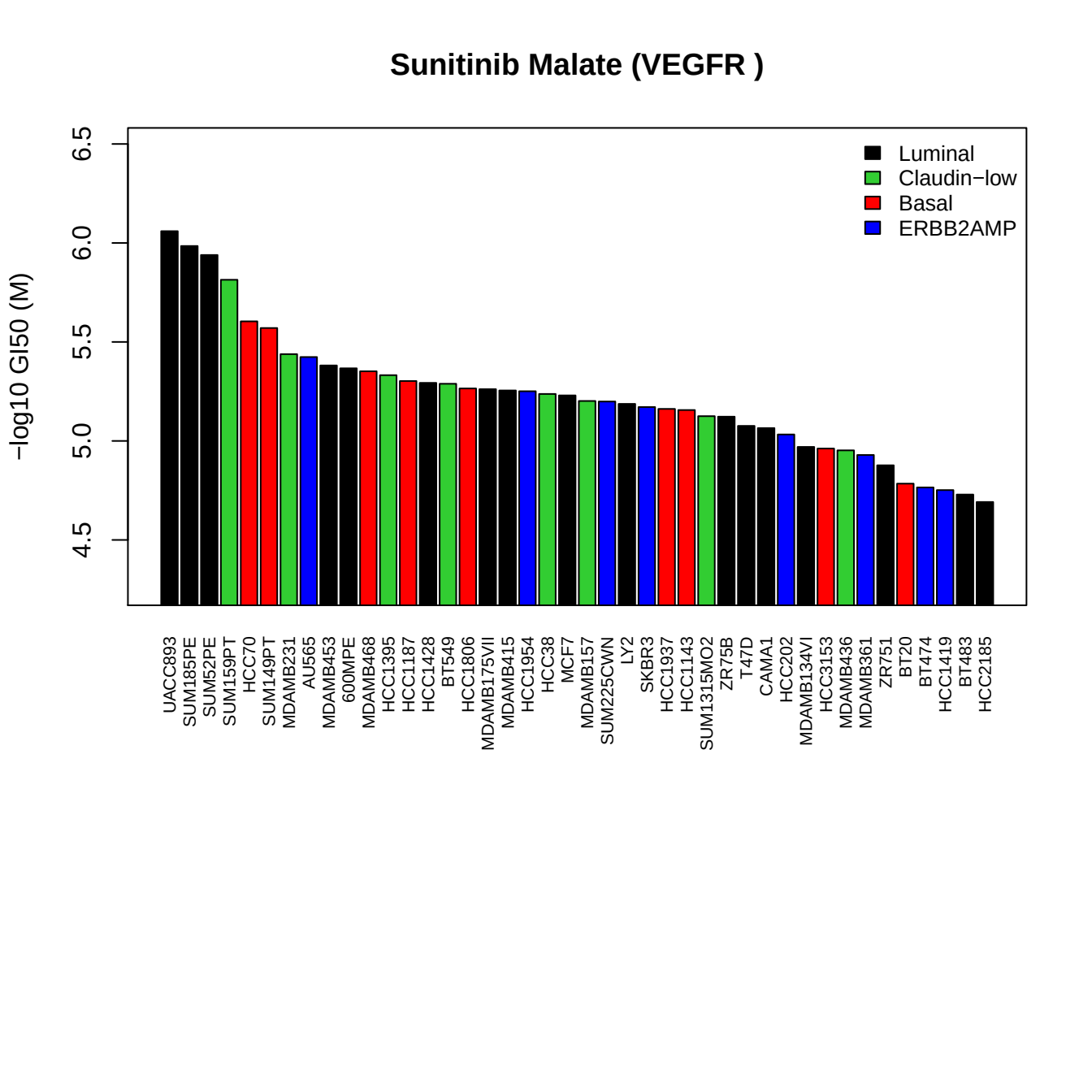
Sunitinib Malate (VEGFR)
−log10 GI50 (M)
4.5
5.0
5.5
6.0
6.5
Luminal
Claudin−low
Basal
ERBB2AMP
UACC893
SUM185PE
SUM52PE
SUM159PT
HCC70
SUM149PT
MDAMB231
AU565
MDAMB453
600MPE
MDAMB468
HCC1395
HCC1187
HCC1428
BT549
HCC1806
MDAMB175VII
MDAMB415
HCC1954
HCC38
MCF7
MDAMB157
SUM225CWN
LY2
SKBR3
HCC1937
HCC1143
SUM1315MO2
ZR75B
T47D
CAMA1
HCC202
MDAMB134VI
HCC3153
MDAMB436
MDAMB361
ZR751
BT20
BT474
HCC1419
BT483
HCC2185

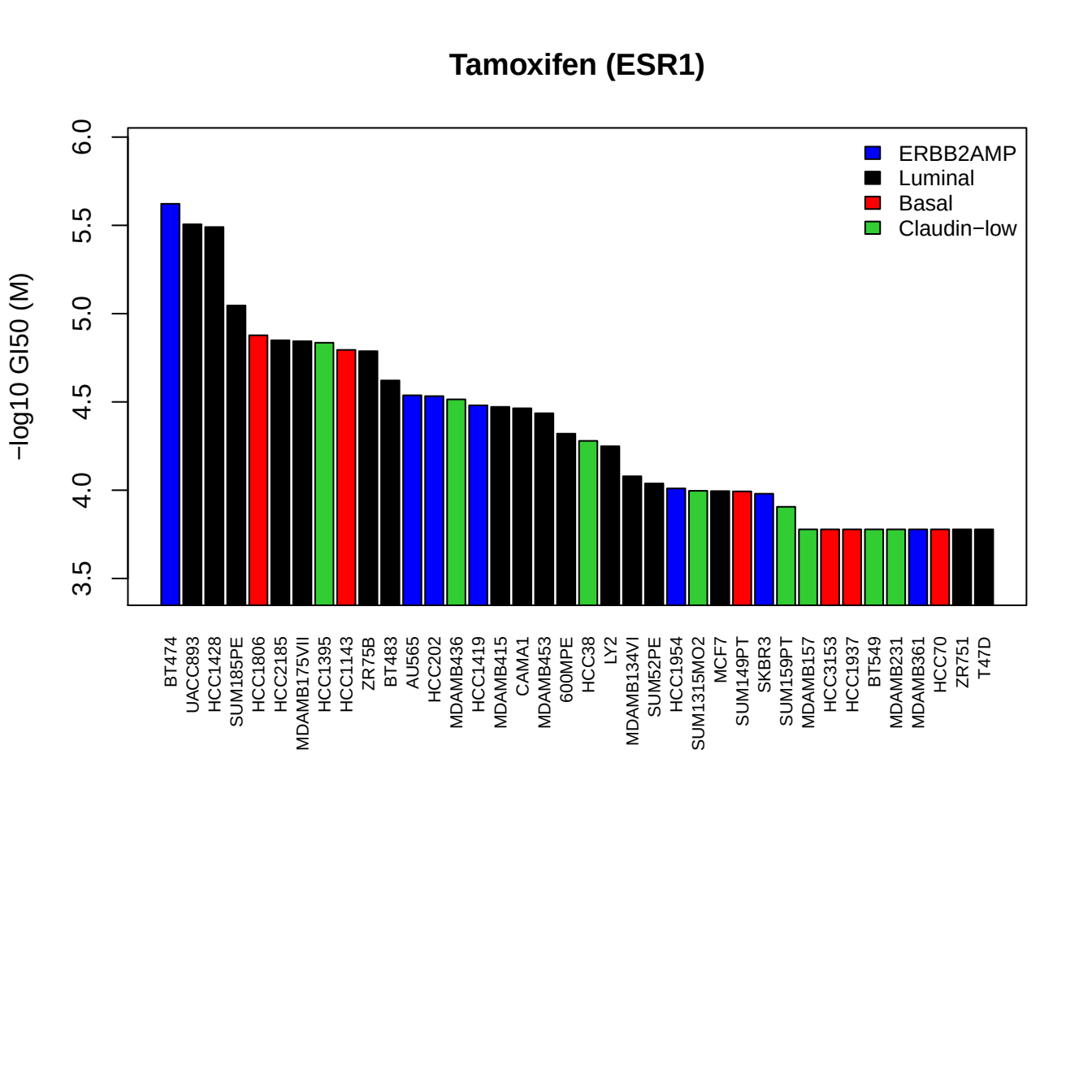
Tamoxifen (ESR1)
−log10 GI50 (M)
6.0
5.5
5.0
4.5
4.0
3.5
ERBB2AMP
Luminal
Basal
Claudin−low
BT474
UACC893
HCC1428
SUM185PE
HCC1806
HCC2185
MDAMB175VII
HCC1395
HCC1143
ZR75B
BT483
AU565
HCC202
MDAMB436
HCC1419
MDAMB415
CAMA1
MDAMB453
600MPE
HCC38
LY2
MDAMB134VI
SUM52PE
HCC1954
SUM1315MO2
MCF7
SUM149PT
SKBR3
SUM159PT
MDAMB157
HCC3153
HCC1937
BT549
MDAMB231
MDAMB361
HCC70
ZR751
T47D

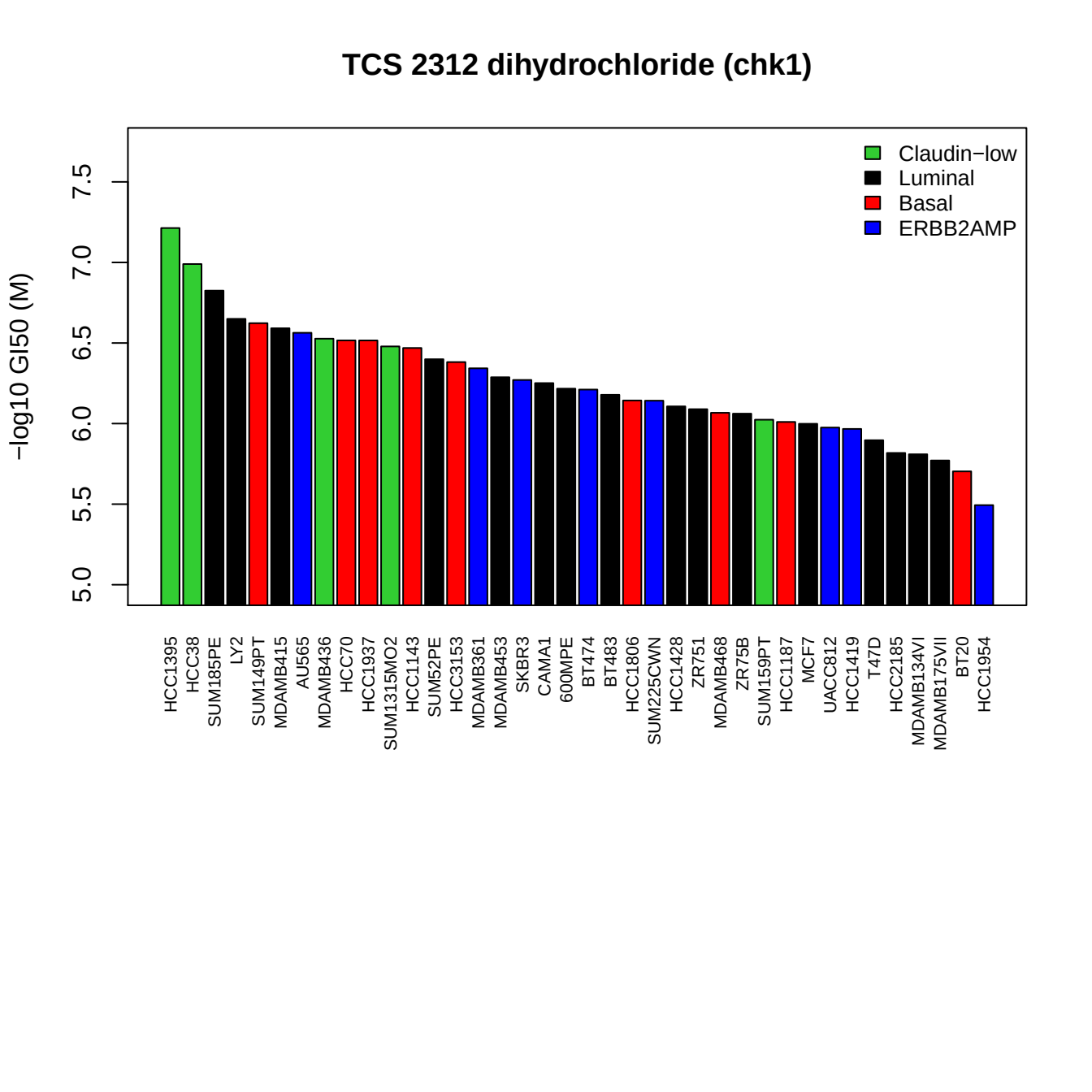
TCS 2312 dihydrochloride (chk1)
−log10 GI50 (M)
5.0
5.5
6.0
6.5
7.0
7.5
Claudin−low
Luminal
Basal
ERBB2AMP
HCC1395
HCC38
SUM185PE
LY2
SUM149PT
MDAMB415
AU565
MDAMB436
HCC70
HCC1937
SUM1315MO2
HCC1143
SUM52PE
HCC3153
MDAMB361
MDAMB453
SKBR3
CAMA1
600MPE
BT474
BT483
HCC1806
SUM225CWN
HCC1428
ZR751
MDAMB468
ZR75B
SUM159PT
HCC1187
MCF7
UACC812
HCC1419
T47D
HCC2185
MDAMB134VI
MDAMB175VII
BT20
HCC1954

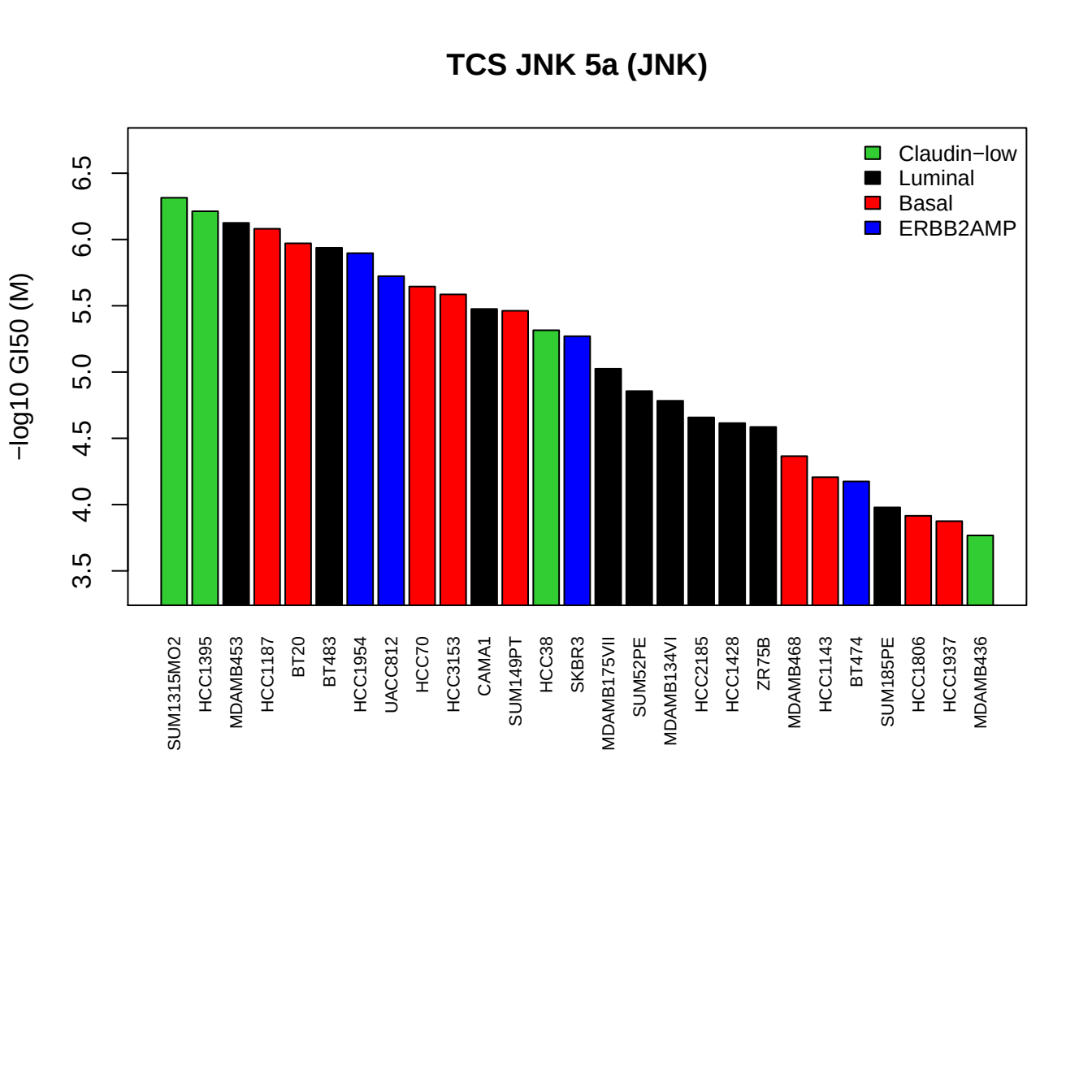
TCS JNK 5a (JNK)
−log10 GI50 (M)
3.5
4.0
4.5
5.0
5.5
6.0
6.5
Claudin−low
Luminal
Basal
ERBB2AMP
SUM1315MO2
HCC1395
MDAMB453
HCC1187
BT20
BT483
HCC1954
UACC812
HCC70
HCC3153
CAMA1
SUM149PT
HCC38
SKBR3
MDAMB175VII
SUM52PE
MDAMB134VI
HCC2185
HCC1428
ZR75B
MDAMB468
HCC1143
BT474
SUM185PE
HCC1806
HCC1937
MDAMB436

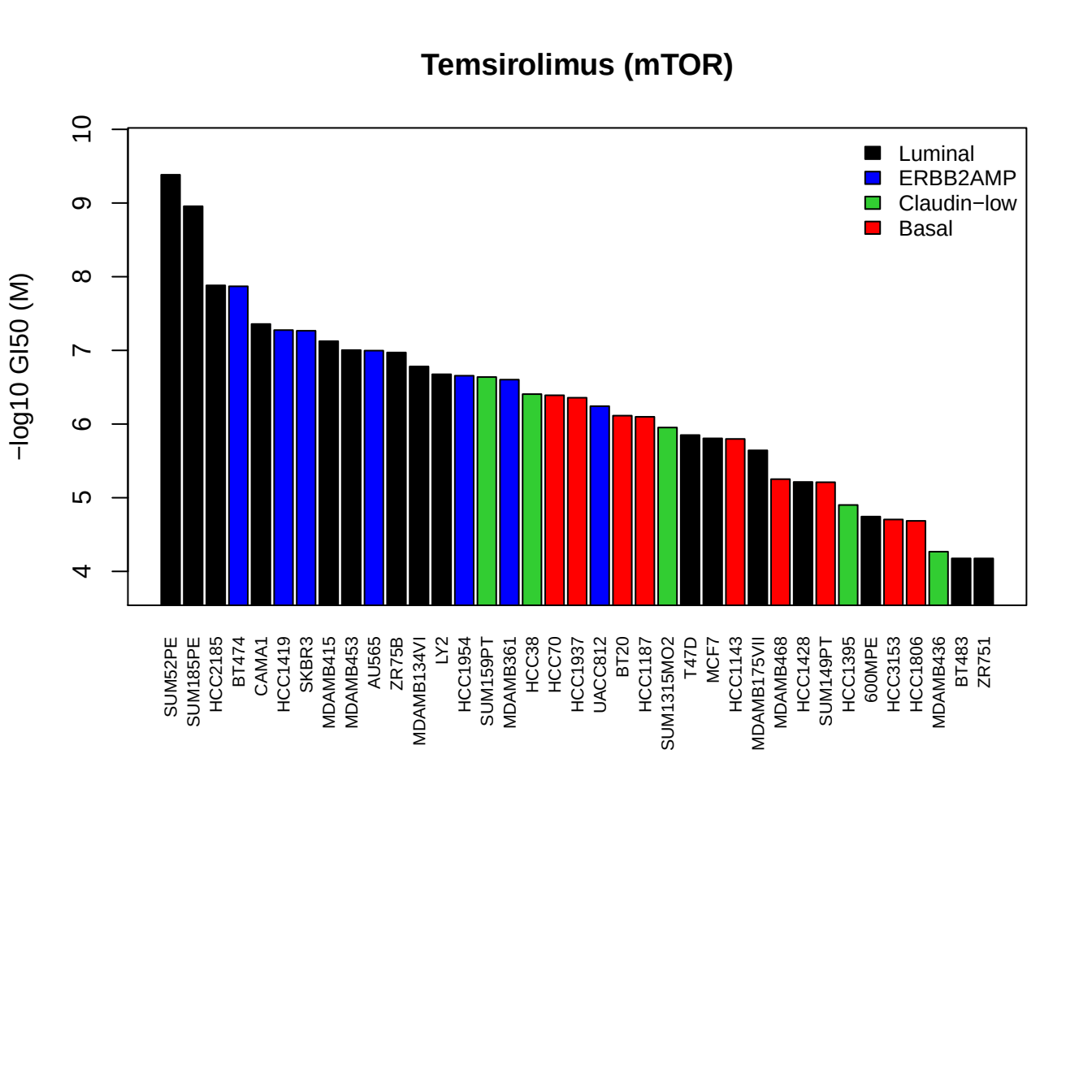
Temsirolimus (mTOR)
−log10 GI50 (M)
4
5
6
7
8
9
10
Luminal
ERBB2AMP
Claudin−low
Basal
SUM52PE
SUM185PE
HCC2185
BT474
CAMA1
HCC1419
SKBR3
MDAMB415
MDAMB453
AU565
ZR75B
MDAMB134VI
LY2
HCC1954
SUM159PT
MDAMB361
HCC38
HCC70
HCC1937
UACC812
BT20
HCC1187
SUM1315MO2
T47D
MCF7
HCC1143
MDAMB175VII
MDAMB468
HCC1428
SUM149PT
HCC1395
600MPE
HCC3153
HCC1806
MDAMB436
BT483
ZR751

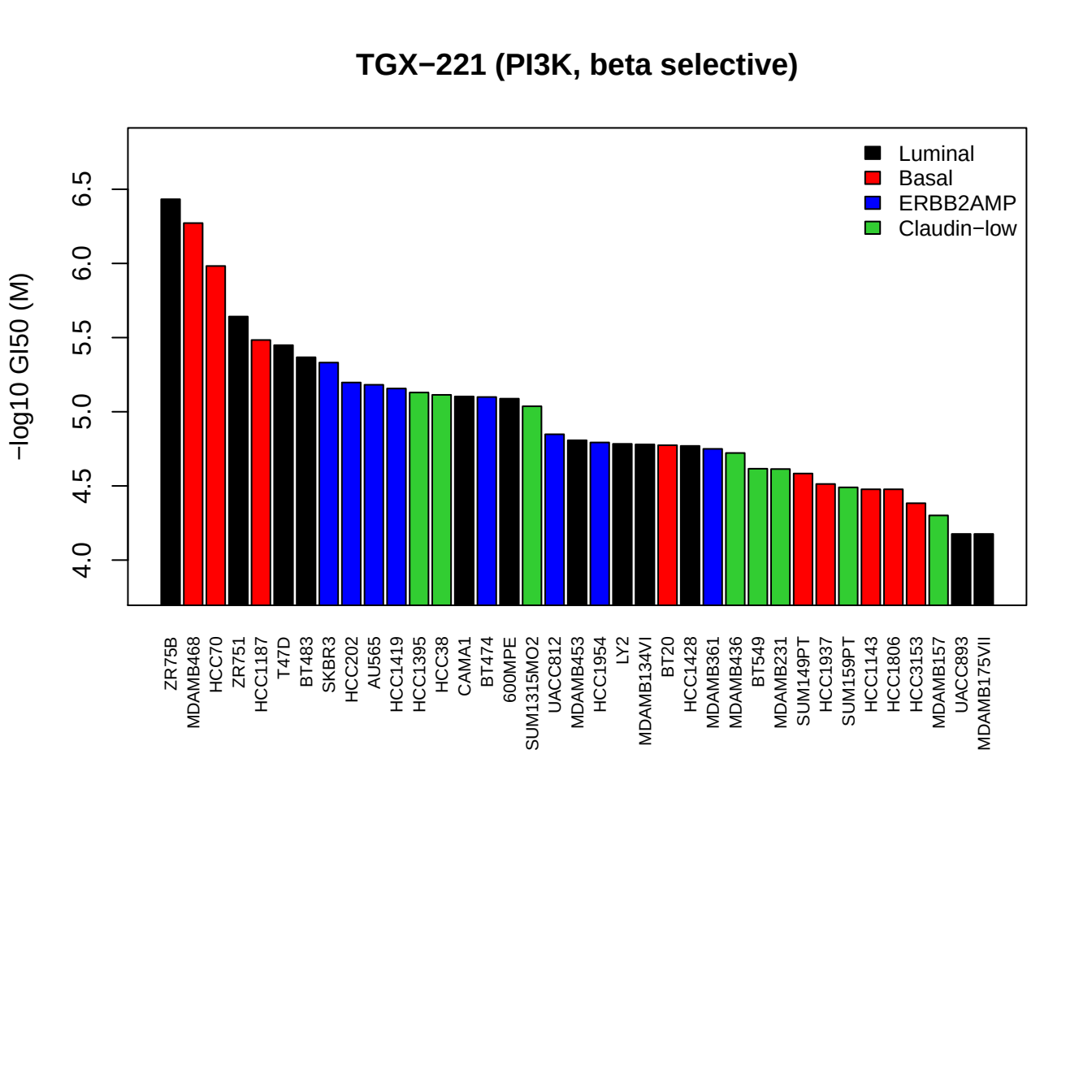
TGX−221 (PI3K, beta selective)
−log10 GI50 (M)
4.0
4.5
5.0
5.5
6.0
6.5
Luminal
Basal
ERBB2AMP
Claudin−low
ZR75B
MDAMB468
HCC70
ZR751
HCC1187
T47D
BT483
SKBR3
HCC202
AU565
HCC1419
HCC1395
HCC38
CAMA1
BT474
600MPE
SUM1315MO2
UACC812
MDAMB453
HCC1954
LY2
MDAMB134VI
BT20
HCC1428
MDAMB361
MDAMB436
BT549
MDAMB231
SUM149PT
HCC1937
SUM159PT
HCC1143
HCC1806
HCC3153
MDAMB157
UACC893
MDAMB175VII

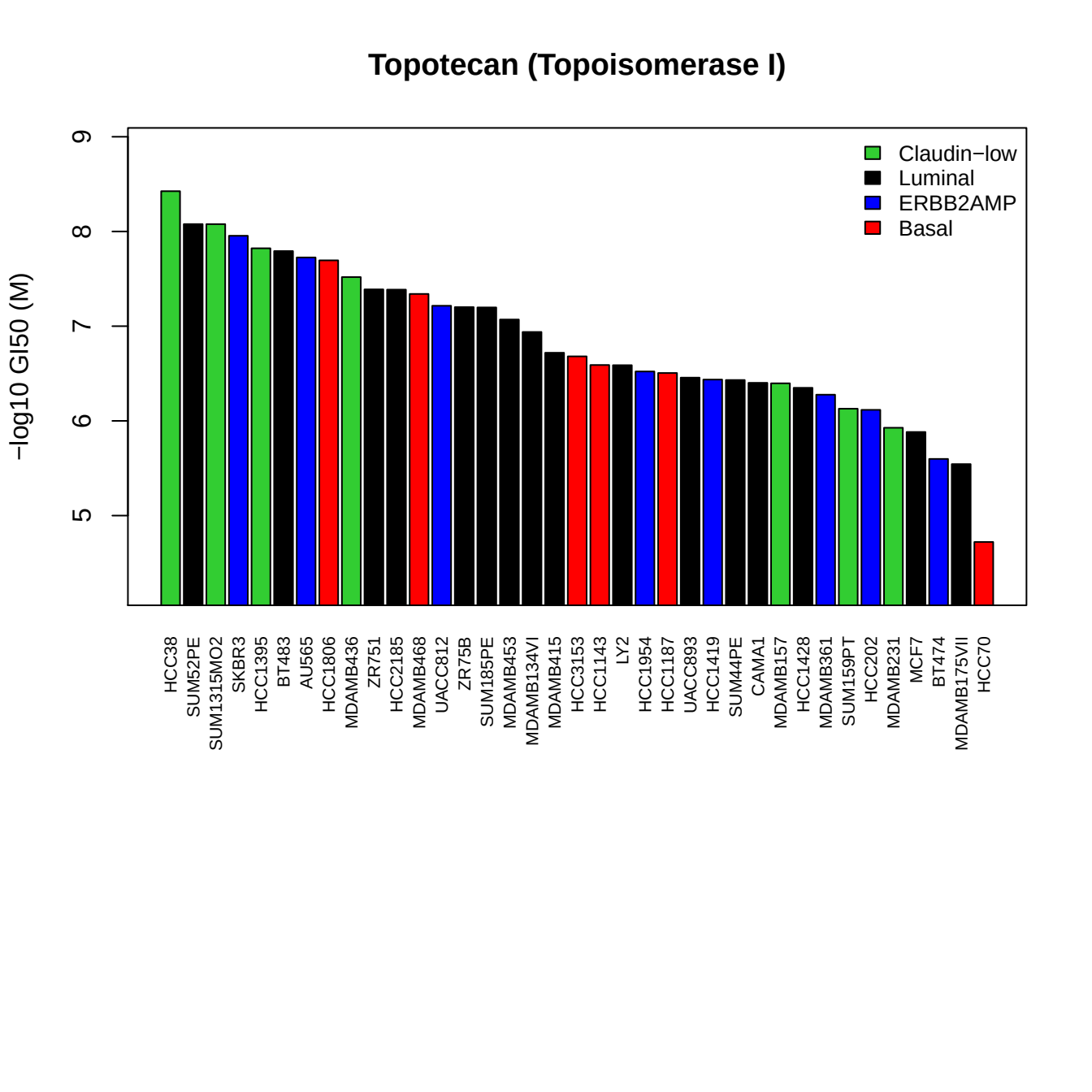
Topotecan (Topoisomerase I)
−log10 GI50 (M)
5
6
7
8
9
Claudin−low
Luminal
ERBB2AMP
Basal
HCC38
SUM52PE
SUM1315MO2
SKBR3
HCC1395
BT483
AU565
HCC1806
MDAMB436
ZR751
HCC2185
MDAMB468
UACC812
ZR75B
SUM185PE
MDAMB453
MDAMB134VI
MDAMB415
HCC3153
HCC1143
LY2
HCC1954
HCC1187
UACC893
HCC1419
SUM44PE
CAMA1
MDAMB157
HCC1428
MDAMB361
SUM159PT
HCC202
MDAMB231
MCF7
BT474
MDAMB175VII
HCC70

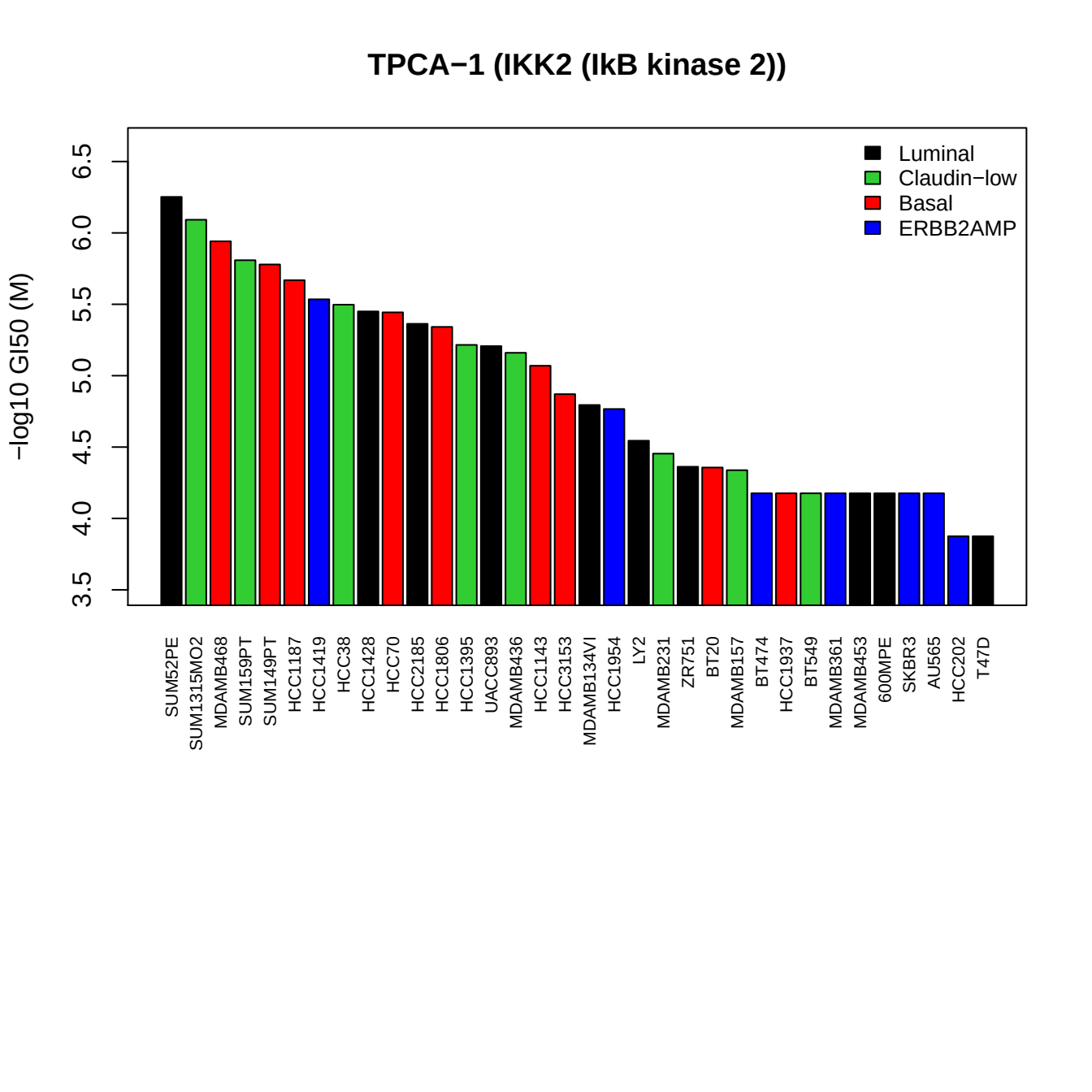
TPCA−1 (IKK2 (IkB kinase 2))
−log10 GI50 (M)
3.5
4.0
4.5
5.0
5.5
6.0
6.5
Luminal
Claudin−low
Basal
ERBB2AMP
SUM52PE
SUM1315MO2
MDAMB468
SUM159PT
SUM149PT
HCC1187
HCC1419
HCC38
HCC1428
HCC70
HCC2185
HCC1806
HCC1395
UACC893
MDAMB436
HCC1143
HCC3153
MDAMB134VI
HCC1954
LY2
MDAMB231
ZR751
BT20
MDAMB157
BT474
HCC1937
BT549
MDAMB361
MDAMB453
600MPE
SKBR3
AU565
HCC202
T47D

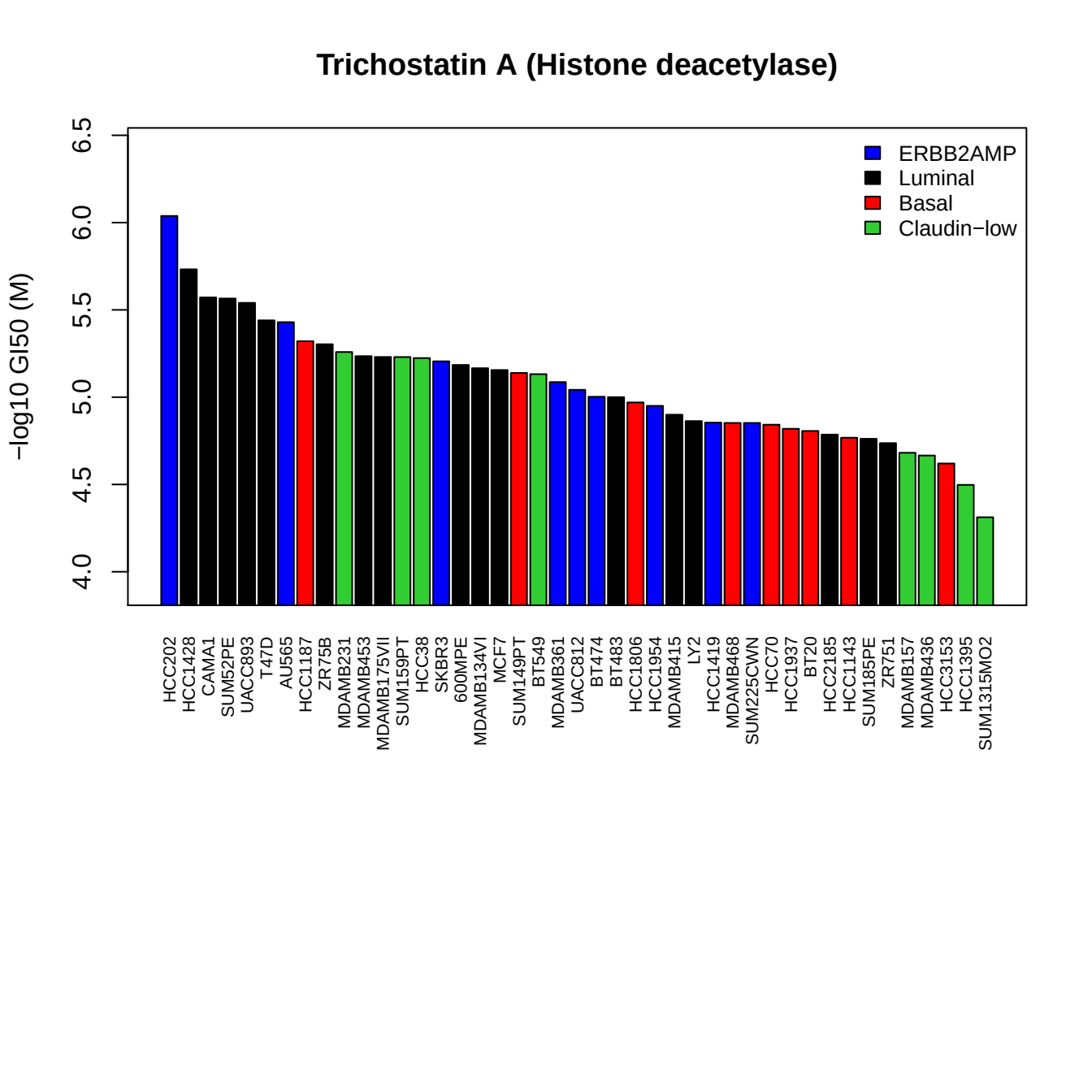
Trichostatin A (Histone deacetylase)
−log10 GI50 (M)
4.0
4.5
5.0
5.5
6.0
6.5
ERBB2AMP
Luminal
Basal
Claudin−low
HCC202
HCC1428
CAMA1
SUM52PE
UACC893
T47D
AU565
HCC1187
ZR75B
MDAMB231
MDAMB453
MDAMB175VII
SUM159PT
HCC38
SKBR3
600MPE
MDAMB134VI
MCF7
SUM149PT
BT549
MDAMB361
UACC812
BT474
BT483
HCC1806
HCC1954
MDAMB415
LY2
HCC1419
MDAMB468
SUM225CWN
HCC70
HCC1937
BT20
HCC2185
HCC1143
SUM185PE
ZR751
MDAMB157
MDAMB436
HCC3153
HCC1395
SUM1315MO2

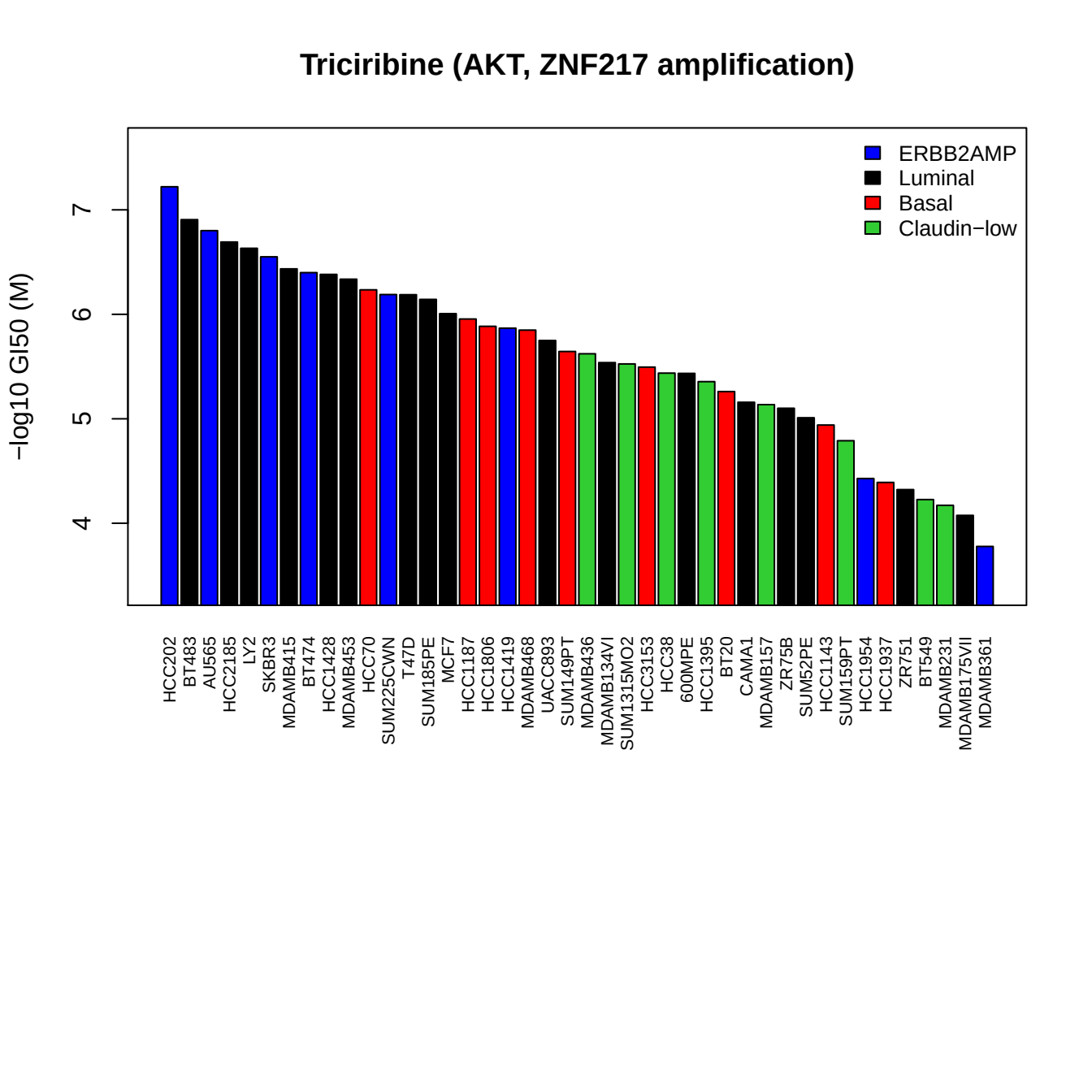
Triciribine (AKT, ZNF217 amplification)
−log10 GI50 (M)
4
5
6
7
ERBB2AMP
Luminal
Basal
Claudin−low
HCC202
BT483
AU565
HCC2185
LY2
SKBR3
MDAMB415
BT474
HCC1428
MDAMB453
HCC70
SUM225CWN
T47D
SUM185PE
MCF7
HCC1187
HCC1806
HCC1419
MDAMB468
UACC893
SUM149PT
MDAMB436
MDAMB134VI
SUM1315MO2
HCC3153
HCC38
600MPE
HCC1395
BT20
CAMA1
MDAMB157
ZR75B
SUM52PE
HCC1143
SUM159PT
HCC1954
HCC1937
ZR751
BT549
MDAMB231
MDAMB175VII
MDAMB361

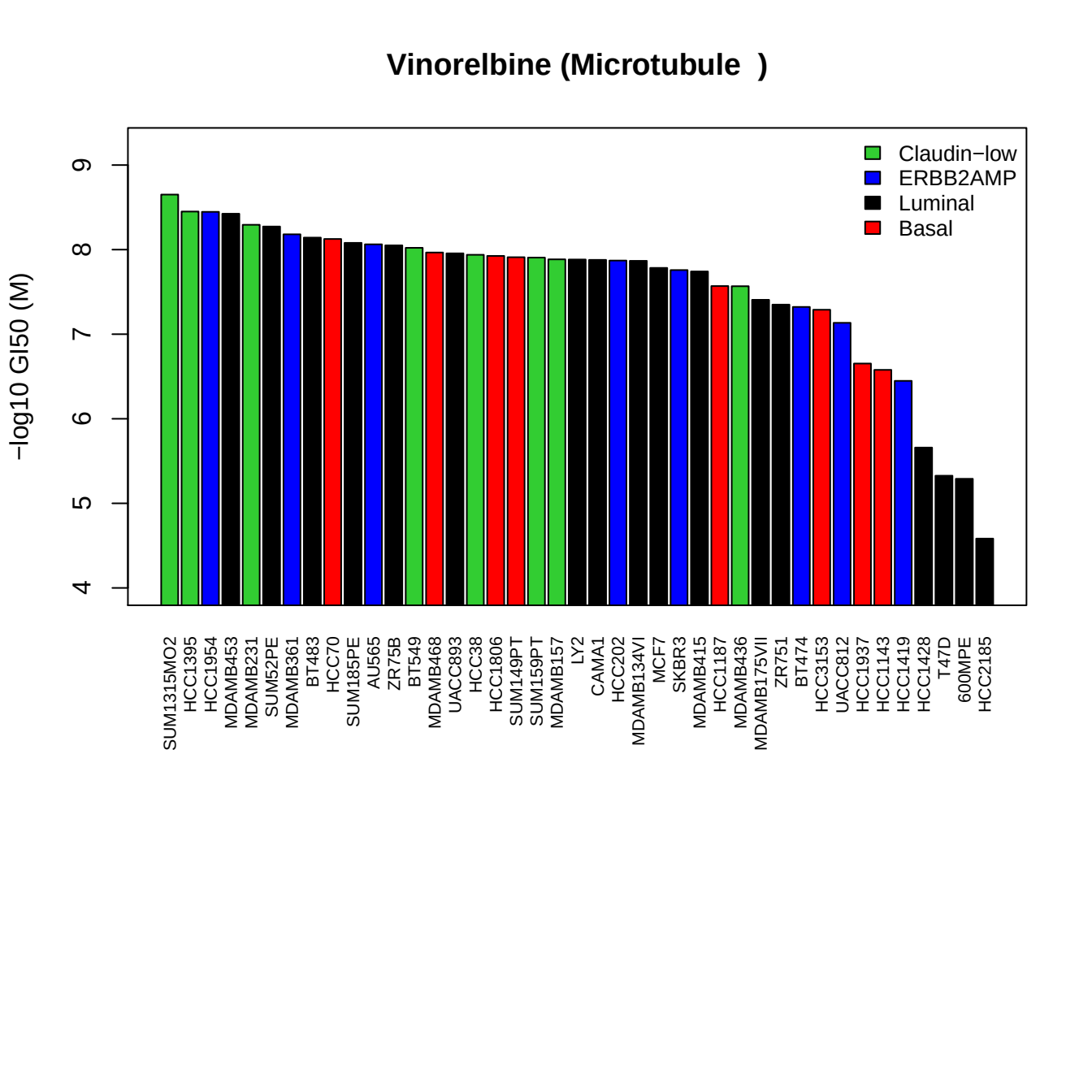
Vinorelbine (Microtubule)
−log10 GI50 (M)
4
5
6
7
8
9
Claudin−low
ERBB2AMP
Luminal
Basal
SUM1315MO2
HCC1395
HCC1954
MDAMB453
MDAMB231
SUM52PE
MDAMB361
BT483
HCC70
SUM185PE
AU565
ZR75B
BT549
MDAMB468
UACC893
HCC38
HCC1806
SUM149PT
SUM159PT
MDAMB157
LY2
CAMA1
HCC202
MDAMB134VI
MCF7
SKBR3
MDAMB415
HCC1187
MDAMB436
MDAMB175VII
ZR751
BT474
HCC3153
UACC812
HCC1937
HCC1143
HCC1419
HCC1428
T47D
600MPE
HCC2185

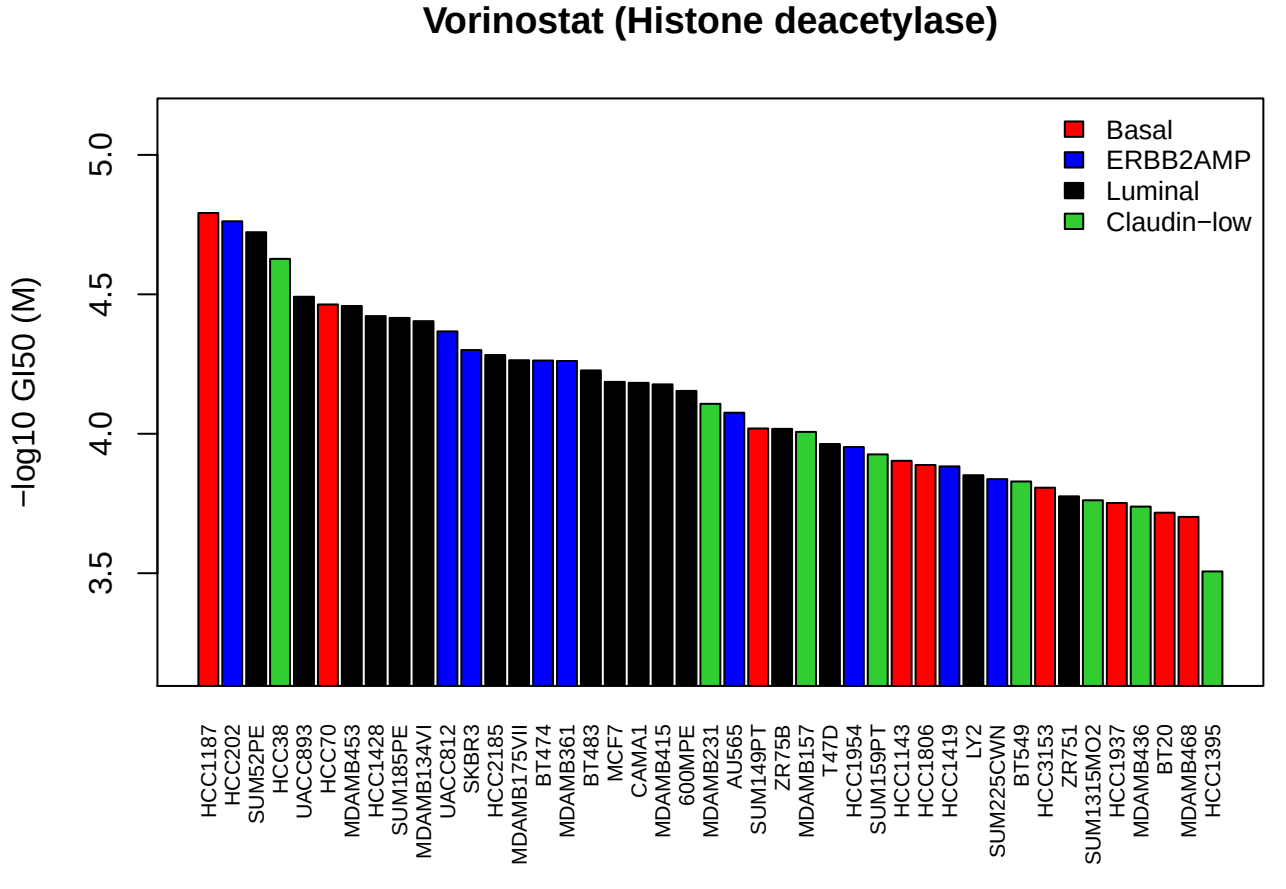
Vorinostat (Histone deacetylase)
−log10 GI50 (M)
5.0
4.5
4.0
3.5
Basal
ERBB2AMP
Luminal
Claudin−low
HCC1187
HCC202
SUM52PE
HCC38
UACC893
HCC70
MDAMB453
HCC1428
SUM185PE
MDAMB134VI
UACC812
SKBR3
HCC2185
MDAMB175VII
BT474
MDAMB361
BT483
MCF7
CAMA1
MDAMB415
600MPE
MDAMB231
AU565
SUM149PT
ZR75B
MDAMB157
T47D
HCC1954
SUM159PT
HCC1143
HCC1806
HCC1419
LY2
SUM225CWN
BT549
HCC3153
ZR751
SUM1315MO2
HCC1937
MDAMB436
BT20
MDAMB468
HCC1395

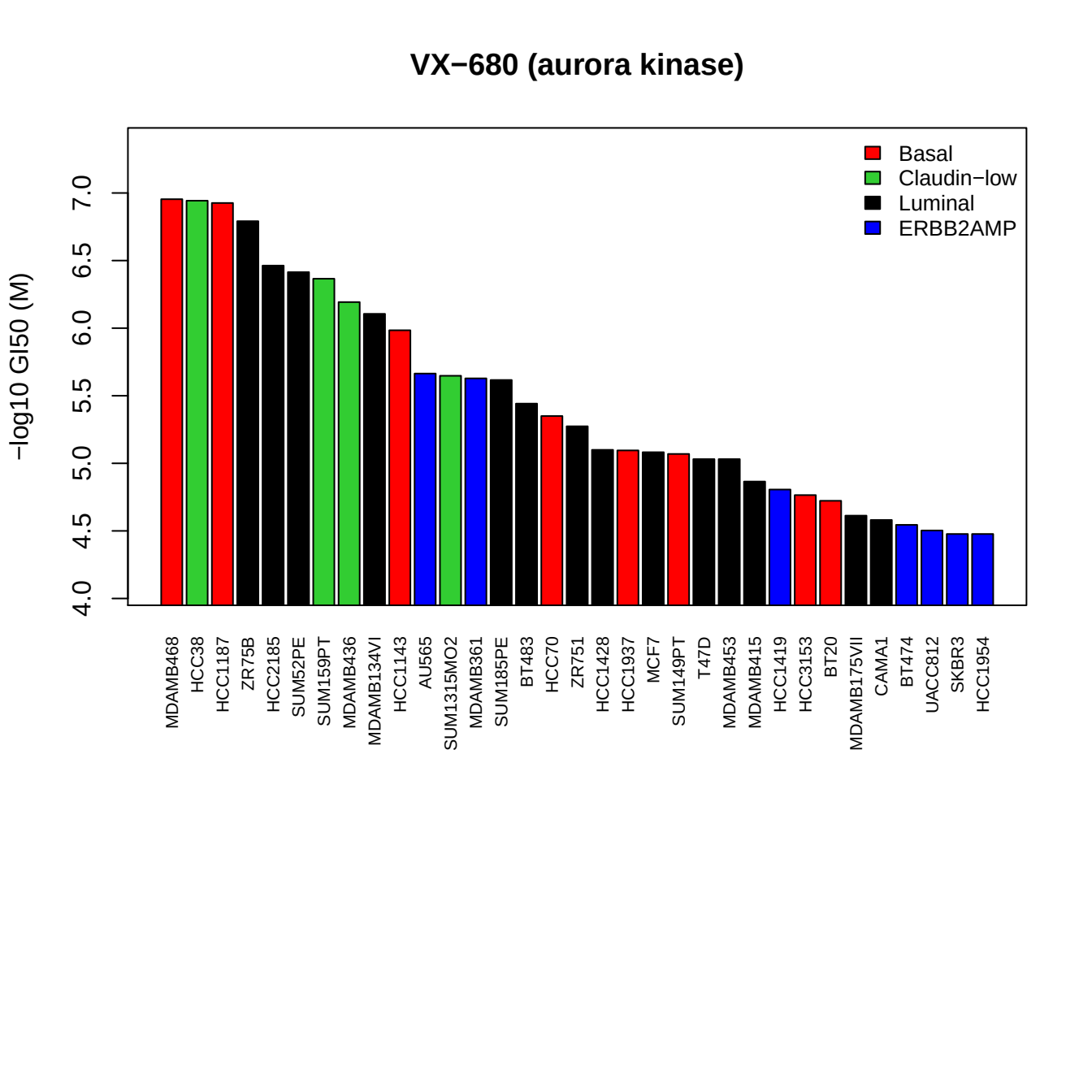
VX−680 (aurora kinase)
−log10 GI50 (M)
4.0
4.5
5.0
5.5
6.0
6.5
7.0
Basal
Claudin−low
Luminal
ERBB2AMP
MDAMB468
HCC38
HCC1187
ZR75B
HCC2185
SUM52PE
SUM159PT
MDAMB436
MDAMB134VI
HCC1143
AU565
SUM1315MO2
MDAMB361
SUM185PE
BT483
HCC70
ZR751
HCC1428
HCC1937
MCF7
SUM149PT
T47D
MDAMB453
MDAMB415
HCC1419
HCC3153
BT20
MDAMB175VII
CAMA1
BT474
UACC812
SKBR3
HCC1954

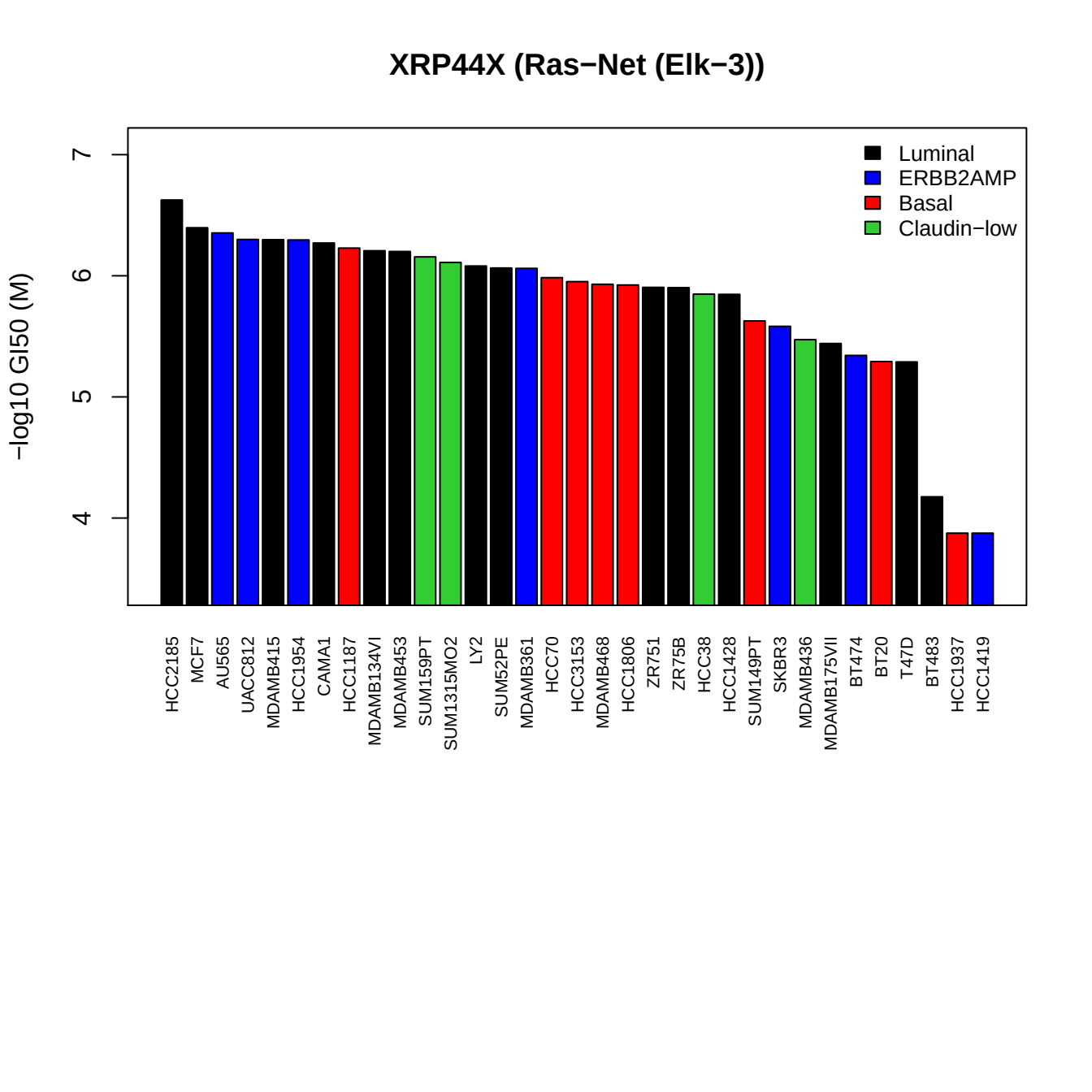
XRP44X (Ras−Net (Elk−3))
−log10 GI50 (M)
4
5
6
7
Luminal
ERBB2AMP
Basal
Claudin−low
HCC2185
MCF7
AU565
UACC812
MDAMB415
HCC1954
CAMA1
HCC1187
MDAMB134VI
MDAMB453
SUM159PT
SUM1315MO2
LY2
SUM52PE
MDAMB361
HCC70
HCC3153
MDAMB468
HCC1806
ZR751
ZR75B
HCC38
HCC1428
SUM149PT
SKBR3
MDAMB436
MDAMB175VII
BT474
BT20
T47D
BT483
HCC1937
HCC1419

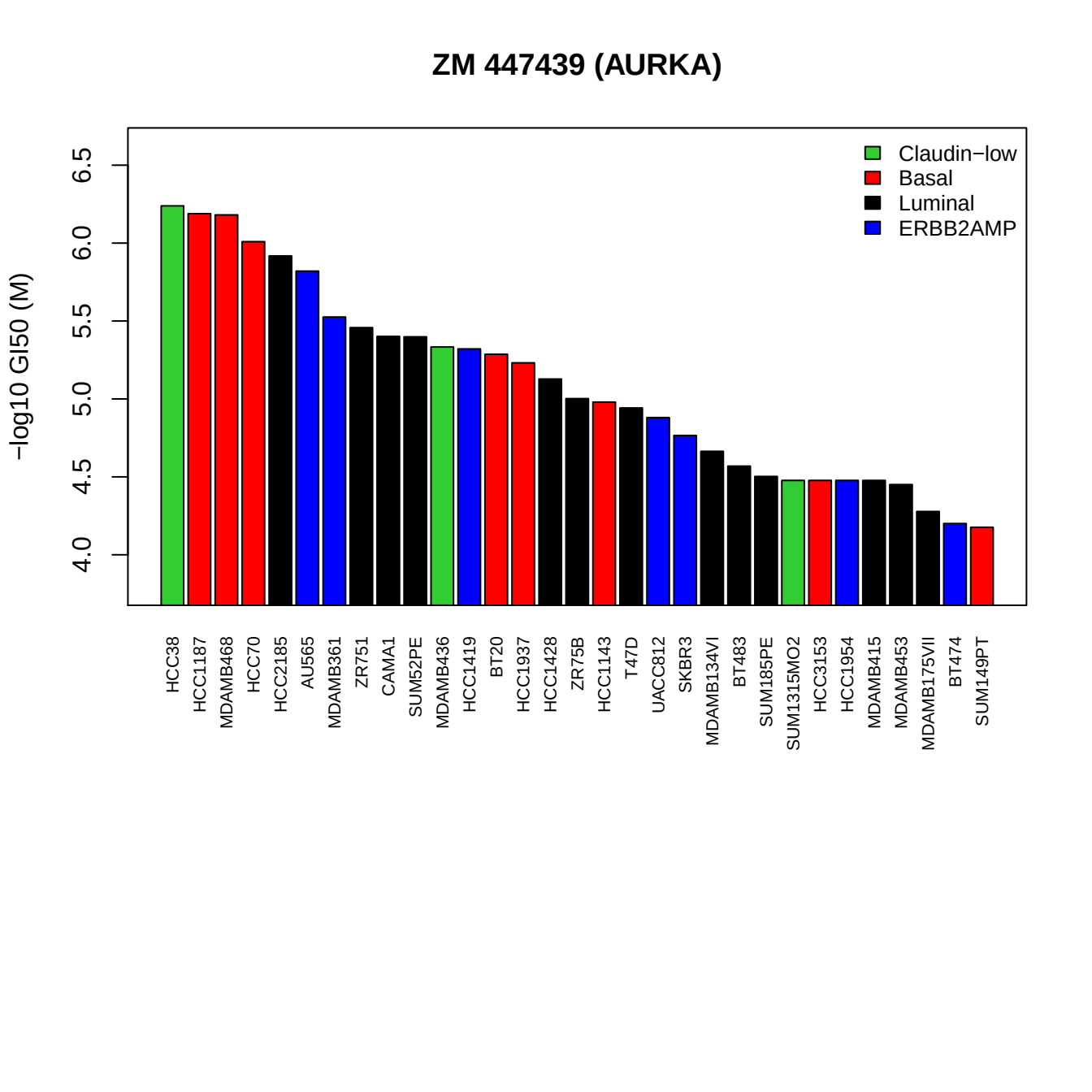
ZM 447439 (AURKA)
−log10 GI50 (M)
4.0
4.5
5.0
5.5
6.0
6.5
Claudin−low
Basal
Luminal
ERBB2AMP
HCC38
HCC1187
MDAMB468
HCC70
HCC2185
AU565
MDAMB361
ZR751
CAMA1
SUM52PE
MDAMB436
HCC1419
BT20
HCC1937
HCC1428
ZR75B
HCC1143
T47D
UACC812
SKBR3
MDAMB134VI
BT483
SUM185PE
SUM1315MO2
HCC3153
HCC1954
MDAMB415
MDAMB453
MDAMB175VII
BT474
SUM149PT